Dissertation

submitted to the

Combined Faculties for the Natural Sciences and for Mathematics

of the Ruperto-Carola University of Heidelberg, Germany

for the degree of

Doctor of Natural Sciences

presented by

MD Ieva Didrihsone

born in Riga, Latvia

Oral-examination:

S100A1 from Damaged Cardiomyocytes Elicits a Chemoattractant Cardiac Fibroblast Phenotype

Referees: Prof. Dr. Gudrun Rappold

Prof. Dr. Patrick Most

Table of Contents

1 Abbreviations and Symbols

~	Approximately
°C	Degree Celsius
Δ	Difference
∞	Infinity
ACM	Adult rat cardiomyocyte
AngII	Angiotensin II
ANOVA	Analysis of variance
ATP	Adenosine triphosphate
Bambi	BMP and activin membrane-bound inhibitor homolog
c	Molar concentration
CCL2	C-C motif chemokine 2
cDNA	Complementary deoxyribonucleic acid
DAMP	Damage associated molecular pattern
DMEM	Dulbecco's Modified Eagle's Medium
ECM	Extracellular matrix
ERK1/2	Extracellular signal-regulated kinases 1 and 2
FCS	Fetal calf serum
FDR	False discovery rate
g	Gram; also acceleration of gravity on Earth
GSEA	Gene set enrichment analysis
h	Hour
H/R	Hypoxia/reoxygenation
HMGB1	High mobility group box 1
i.p.	Intraperitoneal
iBAQ	Intensity based absolute quantification
IL	Interleukin
I.U.	International unit
kDa	Kilodalton
L	Liter
LC-MS/MS	Liquid chromatography-tandem mass spectrometry
LDH	Lactate dehydrogenase
LPS	Lipopolysaccharide
M	Molar (mol/L); also molar mass (g/mol)
m	Meter
MI	Myocardial infarction
min	Minute
MMP	Matrix metalloproteinase
mol	Mole
mRNA	Messenger RNA
MyD88	Myeloid differentiation primary response protein 88
n	Number of biological replicates
NFκB	Nuclear factor kappa-light chain enhancer of activated B cells
Ø	Diameter
OD	Optical density
P	Passage
P/S	Penicillin-streptomycin

PAMP	Pathogen associated molecular pattern
PBS	Dulbecco's phosphate buffered saline
PCA	Principal component analysis
pH	Negative decimal logarithm of the hydrogen ion concentration
PRR	Pattern recognition receptor
qPCR	Quantitative polymerase chain reaction
RAGE	Receptor for advanced glycation end products
RNA	Ribonucleic acid
ROS	Reactive oxygen species
Scr	Scramble control
SEM	Standard error of the mean
siRNA	Small interfering RNA
TGFβ	Transforming growth factor beta
TIMP	Tissue inhibitor of metalloproteinases
TLR	Toll-like receptor
TNFα	Tumor necrosis factor alpha
TRIF	Toll/interleukin-1 receptor domain containing adaptor protein inducing interferon beta
αSMA	Alpha smooth muscle actin

Prefixes

c	centi-10^{-2}
m	milli-10^{-3}
µ	micro-10^{-6}
n	nano-10^{-9}
p	pico-10^{-12}

2 Summary

Despite advancement of therapeutic strategies, myocardial infarction (MI) and subsequent heart failure are still the leading causes of death and disability worldwide. Development of new therapeutic approaches is hampered by insufficient knowledge of the cellular and molecular mechanisms underlying myocardial repair. S100A1 is a Ca^{2+} governing protein in cardiomyocytes. When released upon MI, S100A1 targets neighboring cardiac fibroblasts and is thereby essential for preserving the left ventricular function. The aim of this study was to systematically assess the phenotype of cardiac fibroblasts in response to extracellular S100A1 by comprehensive gene expression and protein profile analysis.

In order to mimic the ischemic myocardium, adult rat cardiac fibroblasts were exposed to extracellular S100A1. Using RNA microarray technology, a time-resolved transcriptome analysis revealed a rapid activation of gene sets involved in chemoattractance alongside downregulation of pro-fibrotic genes. Since the dominant functional changes comprised secreted proteins, a complete secretome analysis of the cardiac fibroblast supernatant was performed by mass spectrometry. On protein level, enrichment analysis highlighted chemotaxis, chemokine receptor binding, and chemokine activity as the predominantly increased categories upon exposure to S100A1. Chemoattractants formed the most abundantly secreted group of proteins in S100A1-treated cardiac fibroblasts, with CCL2 showing the highest quantity. A prominent early-onset increase of CCL2 expression and secretion in response to S100A1 was confirmed by qPCR and ELISA. S100A1-induced CCL2 expression increase was abolished by chemical inhibition and siRNA knockdown of TLR4.

This study demonstrates for the first time a rapid transformation of cardiac fibroblasts into a chemoattractant phenotype upon exposure to S100A1 from damaged cardiomyocytes. These results suggest a novel role for cardiac fibroblasts as the initial link between ischemic injury and the influx of inflammatory cells in the process of myocardial repair.

3 Zusammenfassung

Trotz moderner Therapiemöglichkeiten stellen Myokardinfarkt und nachfolgende Herzinsuffizienz weltweit noch immer die häufigsten Ursachen von Tod und Invalidität dar. Die Entwicklung neuer Therapieansätze verlangt eine Entschlüsselung der zellulären und molekularen Mechanismen, die der Infarktheilung zugrunde liegen. S100A1 ist ein zentraler Regulator des Ca^{2+} Stoffwechsels in Kardiomyozyten. Bei Myokardinfarkt freigesetztes S100A1 verändert benachbarte kardiale Fibroblasten und ist dadurch wesentlich am Erhalt der linksventrikulären Pumpfunktion beteiligt. Ziel der vorliegenden Studie war die systematische Charakterisierung des S100A1-induzierten Phänotyps kardialer Fibroblasten mittels vollständiger Analyse von Genexpressions- und Proteinprofil.

Um die Situation im ischämischen Myokard zu imitieren, wurden aus adulten Rattenherzen isolierte kardiale Fibroblasten mit extrazellulärem S100A1 stimuliert. Eine serielle Transkriptom-Analyse mittels RNA Microarray zeigte eine schnelle Aktivierung von Genen, die mit der Freisetzung von Chemokinen in Verbindung stehen. Gleichzeitig war eine verminderte Expression von pro-fibrotischen Faktoren zu beobachten. Da die beobachteten Veränderungen im Genexpressionsmuster überwiegend sezernierte Proteine betrafen, wurde eine Sekretom-Analyse des Überstands kardialer Fibroblasten mittels Massenspektrometrie durchgeführt. Auf Proteinebene wurden mittels Enrichment Analysis "chemotaxis", "chemokine receptor binding" und "chemokine activity" als die bestimmenden Merkmale von S100A1-stimulierten kardialen Fibroblasten charakterisiert. Unter den sezernierten Proteinen stellten Chemokine hierbei die quantitativ größte Gruppe dar, wobei CCL2 die höchste Abundanz aufwies. Eine frühe und deutliche Überexpression und Sekretion von CCL2 als Reaktion auf S100A1 wurde durch qPCR und ELISA bestätigt. Die S100A1-induzierte CCL2 Produktion kardialer Fibroblasten konnte durch chemische Inhibition und siRNA Knockdown von TLR4 gehemmt werden.

Diese Studie zeigt erstmals eine rasche Transformation kardialer Fibroblasten in einen chemotaktischen Phänotyp nach Stimulation durch S100A1 aus geschädigten Kardiomyozyten. Diese Ergebnisse deuten darauf hin, dass kardialen Fibroblasten beim Myokardinfarkt eine neue Funktion als initiale Verknüpfung zwischen ischämischer Schädigung und Immunzellinfiltration zukommen könnte.

4 Introduction

4.1 Myocardial Infarction

4.1.1 Definition and Epidemiology

Myocardial infarction is defined as myocardial necrosis due to acute myocardial ischemia [1]. There are two major types of myocardial infarction representing different causal mechanisms. The main cause of necrotic injury in the heart (type I myocardial infarction) is the blockage of a coronary blood vessel by a thrombus due to the rupture of an atherosclerotic plaque. Alternatively, type II myocardial infarction occurs in response to an acute imbalance of myocardial demand and supply for oxygen, which can be caused by endothelial dysfunction, tachy- or bradycardia, severe hypo- or hypertension, vasospasm, or respiratory failure [1].

Clinically, myocardial infarction is characterized by typical ischemic chest pain symptoms, electrocardiographic abnormalities, imaging technique findings, such as segmental ventricular akinesia in echocardiography, and by the detection of raise and/or fall of heart necrosis biomarkers in blood plasma, particularly cardiac troponin I or T [1–4]. The results of clinical and laboratory findings have to be interpreted together, thereby ensuring accurate differentiation between acute ischemic myocardial necrosis and myocardial damage due to other conditions, such as sepsis, heart failure or illicit drug use, which require a different therapeutic strategy [5,6].

According to the World Health Organization, coronary heart disease and acute myocardial infarction are the leading causes of death and disability worldwide [7]. The major complication after myocardial infarction is chronic heart failure affecting 16% of men and 22% of women within 5 years after myocardial infarction [8]. Heart failure has a negative prognosis for the patients with 50% mortality within 5 years and limited therapeutic options [9]. Factors, which favor the development of heart failure after MI, include larger size of initial infarction and improper healing thereafter [10]. Since the major cause of myocardial infarction is thrombotic occlusion of coronary arteries [11], the central therapeutic strategy is the timely recanalization of the culprit artery [2,3]. Since the extensive introduction of coronary care units and reperfusion therapies, the short term in-hospital mortality of MI patients has decreased from 30% in the mid of 20 century to 6% in 2006 [12,13]. Moreover, the success of reperfusion therapy has been attributed to 28% reduction in the incidence of subsequent heart failure [14] by limiting the extent of cardiomyocyte death and thus the size of myocardial infarction [15].

4.1.2 Cardiac Repair after Infarction

Myocardial infarction is followed by a fine-tuned healing cascade which is triggered by ischemic cardiomyocyte death (Figure 1) [10]. Since adult cardiomyocytes possess very limited regenerative capacity, the necrotic area is replaced with a durable scar in order to ensure cardiac function [16–18].

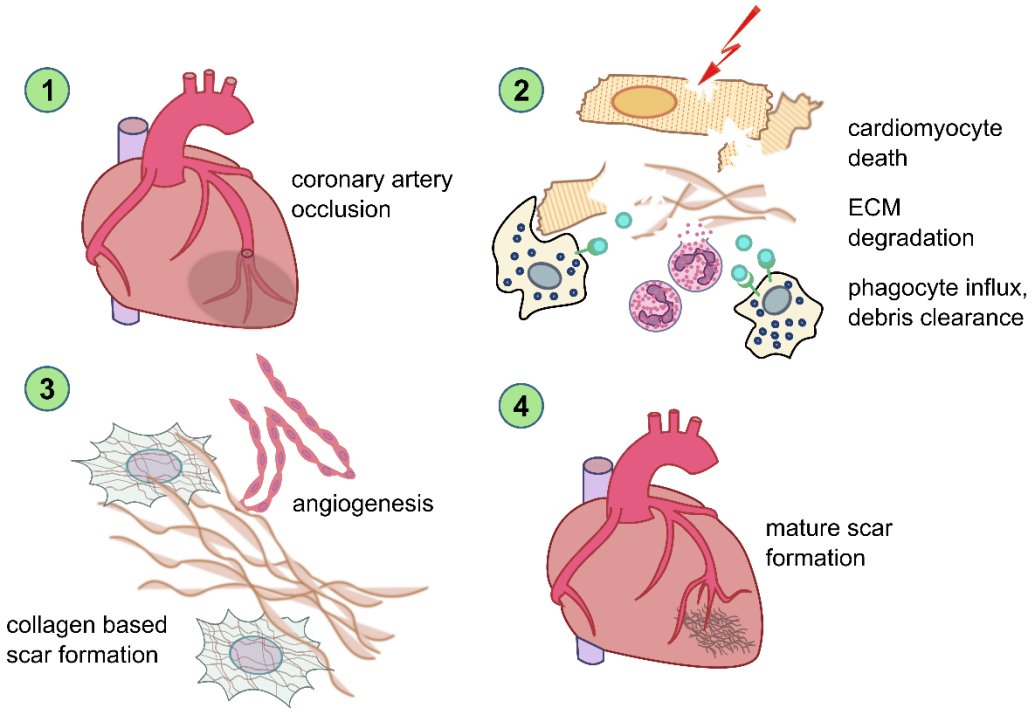

Figure 1: Healing cascade after myocardial infarction.

(1) Coronary blood vessel obstruction is the initial phase of myocardial infarction (not the case in type II - mentioned earlier in the text). (2) Subsequent cardiomyocyte death triggers inflammatory cell influx, which is facilitated by the degradation of extracellular matrix (ECM). Neutrophils and macrophages collectively clear the cellular debris. (3) Myofibroblasts synthesize a collagen-based matrix and angiogenesis ensures the restoration of the blood flow within the newly formed scar. (4) A mature scar with crosslinked matrix and low amount of persistent myofibroblasts is formed.

Early studies of temporal coronary artery occlusion, which were performed in dogs, revealed that 40 min of ischemia result in a macroscopically visible subendocardial necrosis [19]. During the initial phase after myocardial infarction cellular debris is removed by inflammatory cells. They also trigger the transition to the scar formation phase, during which myofibroblasts fill the necrotic area with a collagen-based matrix and angiogenesis ensures the vascularization of the newly formed scar. In the final phase, the provisional scar is transformed into a tightly crosslinked type I collagen-based scar (Figure 1).

4.1.2.1 Inflammation

Cardiomyocyte injury triggers a rapid infiltration of inflammatory cells [20], which is facilitated by extracellular matrix degradation [21] and increased vascular permeability [22]. The majority of infiltrating inflammatory cell types are neutrophils and inflammatory and reparative monocytes that further differentiate into macrophages [23]. Inflammatory monocytes become M1 macrophages and, in later stages, also M2 macrophages, whereas reparative monocytes are considered to give rise only to M2 macrophages [24–26]. In mice, inflammatory cells are reported to infiltrate the infarction area within the first minutes after the occlusion of a coronary blood vessel. Although the first infiltrating population is patrolling monocytes from the vasculature [27], the following neutrophil influx forms the dominant cell population within the infarct in the first 24 hours [28]. Thereafter, inflammatory and reparative monocytes numbers peak on day 3 and 5, respectively [24].

The sequential influx, differentiation and activity of inflammatory cells lead to clearance of the infarction site from cellular debris and activation of scar formation. Neutrophils produce a vast amount of extracellular matrix degrading proteins and reactive oxygen species that participate in pro-angiogenic and pro-fibrotic processes [29–31]. Neutrophils also secrete α-defensin that acts as a monocyte chemoattractant [32] and lipocalin that, in turn, promotes macrophage polarization into an M2c phenotype, which has the highest efferocytotic (cellular debris clearance) activity [33,34]. The subsequently differentiated M1 macrophages participate in cellular debris efferocytosis [28] and engulf apoptotic neutrophils [35], thus contributing to the restriction of the acute inflammatory phase [36]. The engulfment of apoptotic neutrophils triggers macrophage polarization towards an M2 phenotype [37], which is known to resolve inflammation and to initiate the scar formation phase by promoting angiogenesis and myofibroblast accumulation [25,38].

Early attempts to improve the outcome of myocardial infarction by broadly suppressing the inflammatory response with glucocorticoids or nonsteroidal anti-inflammatory drugs have provided no benefits. Although the initial experiments in dogs showed that glucocorticoids reduce the myocardial necrosis following infarction [39], subsequent experiments indicated dose-dependent scar thinning [40], thereby increasing the risk of ventricular aneurysm formation or rupture. The initial trials of glucocorticoids in patients with myocardial infarction indicated conflicting outcomes [41], but larger randomized clinical trials showed no survival benefits [42]. Similarly, nonsteroidal anti-inflammatory drugs initially were shown to reduce the infarcted area, presumably, by reducing the rate of necrosis. In dogs, treatment with ibuprofen reduced the size of infarct without affecting blood flow or oxygen demand [43]. However, further experiments showed that ibuprofen administration after

myocardial infarction is also associated with scar thinning [44]. In humans, indomethacin or ibuprofen administration resulted in infarct scar thinning [45] and was suggested to be associated with ventricular rupture after myocardial infarction [46]. Since broad suppression of inflammatory response has failed to be beneficial, the ongoing search for new therapeutic approaches is focusing on targeted immunomodulatory strategies in order to improve infarct healing.

4.1.2.2 Scar Formation

During the inflammatory phase the original extracellular matrix is degraded in order to facilitate inflammatory cell traffic. To ensure the integrity of the heart wall during this phase a provisional matrix is formed. The initial plasma fibrin based structure is replaced by a more durable cellular-based fibronectin and hyaluronan matrix [47]. Cellular debris removal is accompanied by the infiltration of myofibroblasts, which start to extensively produce extracellular matrix proteins. Myofibroblasts also contract the newly formed collagen matrix, thus reducing the area and strengthening the durability of the scar [48,49]. Scar maturation is characterized by the replacement of initial type III collagen with type I collagen, crosslinking of collagen fibers and clearance of the initially excessive amount of myofibroblasts [49,50]. Finally, the mature scar represents a vascularized tissue consisting mainly of a collagen based matrix with a small portion of cellular components, such as myofibroblasts, smooth muscle cells and residual cardiomyocytes [51,52].

4.1.3 Therapeutic Implications

Although each of the above described phases and cellular components are necessary for the appropriate healing of myocardial infarction, they may lead to exaggerated expansion of the initial injury and adverse cardiac remodeling when spatially and timely unrestricted [10]. Uncontrolled neutrophil activation, for instance, leads to thinning of the infarct wall and consequently systolic heart failure [10,53]. Moreover, unlimited myofibroblast activation causes heart wall stiffening and diastolic heart failure [10,54].

For the further reduction of long term adverse outcome after myocardial infarction, the development of new therapeutic strategies is needed. Therapeutic targeting of the subsequent healing process holds a great potential for the prevention of post-infarction complications. However, current attempts to introduce such modulatory therapeutic interventions have failed [55], thus substantiating the need for a deeper understanding of the underlying molecular mechanisms.

4.2 Danger Associated Molecule Patterns (DAMPs)

4.2.1 Definition

It has long been known that ischemically damaged myocardium elicits a strong inflammatory reaction [56]. Historically, the mechanism, which links myocardial injury to activation of the immune system, was strongly debated because of the paradigm that the immune system is evolved to protect the host against external pathogens. In 1994, Polly Matzinger first described a concept which postulated that “the immune system does not care about self and non-self, that its primary driving force is the need to detect and protect against danger” (Figure 2) [57].

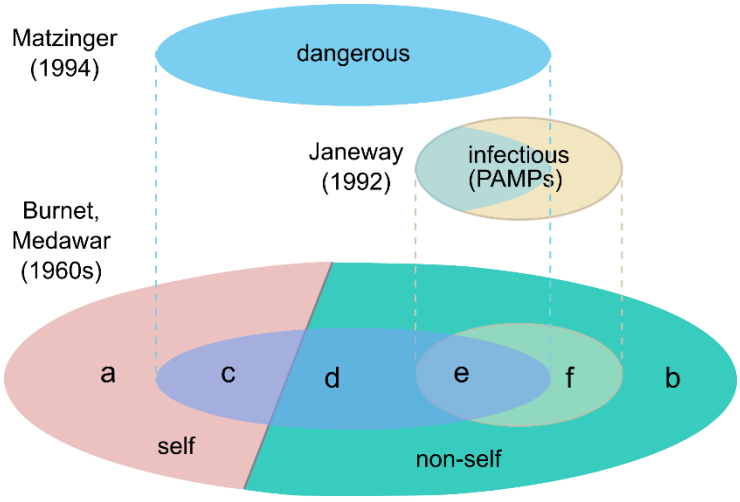

		a	b	c	d	e	f
Responses to each set predicted by:	SNS	-	+	-	+	+	+
	INS	-	-	-	-	+	+
	Danger	-	-	+	+	+	-

Figure 2: Models for discrimination of antigens that elicit an immune response.

The historically oldest model, how the immune response discriminates immunogenic versus non-immunogenic substances, proposes recognition of self (set a) versus non-self (set b). Janeway offered a refined version, saying that the immune system recognizes specific patterns of non-self antigens, so called pathogen-associated molecular patterns (PAMPs) (set e+f). Matzinger proposed a model, where an immunogenic response is elicited by substances that induce stress or inappropriate cell death. Part of this group are self-antigens, which are mutations or molecules that are normally hidden from immune system (set c), environmental toxins (set d) and pathogens (set e). Set f is microorganisms that have PAMPs, but which are harmless (symbiotic bacteria).
(SNS- self versus non-self; INS- infectious non-self)
Taken from [58] with modifications.

Matzinger’s model stated that an immune response can be triggered by self-molecules, which are exposed to immune system upon the tissue injury, in order to clear the debris

and prevent further injury. Thereby, the model offered a hypothesis for how the immune system might be activated in response to sterile injury, such as myocardial infarction. In line with this concept, Seong and Matzinger first used the term “damage associated molecular pattern” (DAMP) in 2004, describing immunogenic properties of hydrophobic portions of molecules, irrespective of their origin from pathogens or the organism itself [59].

In 2005, Joost Oppenheim and De Yang proposed a classification where all DAMPs are divided into two groups: 1) pathogen-associated molecular patterns (PAMPs), representing molecules of microbial or viral origin, which elicit an immunogenic response, and 2) alarmins, endogenous molecules that signal tissue injury (Figure 3A) [60,61]. To date, two additional modifications of this concept are commonly used. They employ the term “DAMP” strictly for endogenous self-derived immunogens, whereas pathogen-derived immunogens (PAMPs) are separate. In the first one, DAMPs are further divided into three subcategories. The first subgroup covers intracellular proteins, which are passively released from dying cells. The second subcategory encompasses damaged or modified extracellular matrix fragments. The third subcategory are alarmins, which denote cytokine-like molecules that are stored in cells and released upon cellular stress or lysis (Figure 3B) [62,63]. The second classification uses DAMPs and alarmins as synonyms [64,65] (Figure 3C).

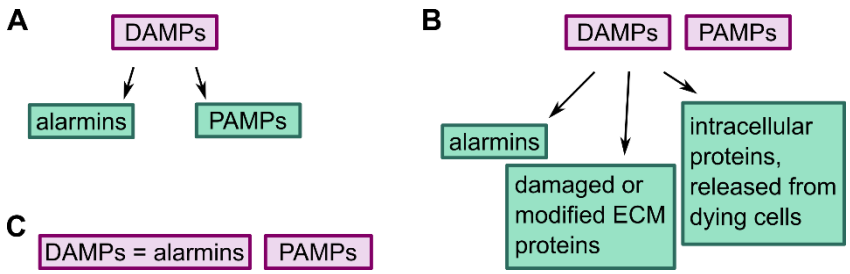

Figure 3: Three different classifications of antigens according to their origin.

(A) Oppenheim’s and Yang’s classification uses DAMPs as an umbrella term for PAMPs (immunogens from bacteria and viruses) and alarmins (endogenous danger signals) [60]. (B) DAMPs are used as an umbrella term for passively released intracellular proteins, modified or damaged extracellular matrix, or alarmins (cytokine-like proteins, which are stored in cells and quickly released upon cellular stress) [62,63]. (C) DAMPs and alarmins are used as synonyms [64,66].
(DAMP- damage associated molecular pattern, PAMP- pathogen associated molecular pattern, ECM- extracellular matrix)

Since there is no unified nomenclature, immunogenic molecules that signal tissue damage after myocardial infarction will be denoted as "DAMPs" in this thesis.

4.2.2 Pattern Recognition Receptors (PRRs)

DAMPs signal through pattern recognition receptors (PRRs), expressed by immune cells, like dendritic cells and macrophages, and non-immune cells, such as fibroblasts, smooth muscle cells and endothelial cells [67–70]. PRRs can be localized on the extracellular membrane as well as in the intracellular compartment [71]. On the extracellular membrane are localized groups of toll-like receptors (TLR), C-type lectin receptors (CLR) and various ungrouped receptors, like the receptor for advanced glycation end products (RAGE) or interleukin 1 receptors (IL1R). In the intracellular compartment, danger molecules are captured by nucleotide-binding oligomerization domain (NOD)-like receptors (NLRs) and retinoic acid-inducible gene (RIG)-I-like receptors (RLRs) [62,67,71].

4.2.3 Toll-Like Receptor 4 (TLR4)

TLR4 is the most abundant toll-like receptor in the heart [72]. It can capture ligands both at the cell surface level or from endosomes [73,74]. The signal transduction is ensured via two pathways that are determined by different recruited adaptor proteins: MyD88 and TRIF [75]. At the plasma membrane TLR4 triggers activation of the MyD88-dependent pathway that leads to an increase of inflammatory cytokine production [76]. TRIF-dependent pathway is activated upon endocytosis of TLR4. It further induces inflammatory cytokine and type I interferon production [76,77]. It has been suggested that endosomal acidification is essential for the ligand binding and recruitment of TRIF adaptor protein to TLR4 in endosomes [78]. Moreover, stimulation of TLR4 augments the TGFβ-mediated fibrotic response in murine and human skin fibroblasts [79]. In murine hepatic stellate cells, the TLR4-triggered fibrotic response has been reported to be mediated via MyD88 by enhancing TGFβ signaling through downregulation of its pseudoreceptor Bambi [80].

In the setting of myocardial infarction, TLR4 stimulation has been demonstrated to have divergent effects. Lipopolysaccharides (LPS) are classical ligands for TLR4 [67]. Pretreatment of rats with LPS has been reported to reduce the size of infarction and subsequent cardiac dysfunction after ischemia/reperfusion [81]. In ischemia/reperfusion of isolated rat hearts, the protective properties of LPS become apparent after 12 hours of pretreatment. The beneficial effect is abrogated by the protein synthesis inhibitor cycloheximide [82], thus indicating cardioprotective properties for the proteins that are produced upon the stimulation with LPS. On the other hand, TLR4 deficiency improves cardiac function without affecting infarct size, reduces inflammatory cytokine expression and interstitial fibrosis in remote myocardium after permanent coronary ligation in mice [83]. In an ischemia/reperfusion model, TLR4 deficiency reduces the size of infarct and

inflammatory cytokine expression [84,85], however, without improving cardiac function [85].

MyD88 serves as a downstream adaptor protein for interleukin 1 and 18 and all toll-like receptors, except TLR3 [86–88]. Interestingly, induction of ischemia/reperfusion in MyD88-deficient mice results in decreased size of infarction, improved cardiac function and attenuated neutrophil recruitment in comparison to wild type controls. However, MyD88 deficiency has no impact on infarct size or cardiac function when ischemia/reperfusion is induced in isolated hearts [89]. Impeded recruitment of neutrophils and decreased size of myocardial infarction after ischemia/reperfusion can be influenced by MyD88 deficiency in the bone marrow [90], pointing out the differences between local cardiac PRR and systemic PRR signaling.

4.2.4 DAMPs after Myocardial Infarction

Recognition of DAMPs by PRRs represents the initial signaling event of tissue damage after myocardial infarction [91]. Several groups of DAMPs have been demonstrated to contribute to myocardial inflammation in the infarcted heart, including S100 proteins, heat shock proteins, high mobility group box 1 protein (HMBG1) and interleukin 1α [91,92]. DAMPs often do not display receptor specificity, so that one molecule can bind several PRRs. For example, HMGB1 signals through TLR4 [93], but also through TLR2 [94], TLR9 [95] and RAGE [96]; S100A8/9 binds to TLR4 [97], but also to RAGE [98].

HMGB1 is one of the best characterized DAMPs and therefore often referred to as a prototype [99]. HMGB1 is a nuclear non-histone DNA binding protein. In the nucleus it is involved in gene transcription and DNA stabilization [92]. It is released from necrotic cells, but not from apoptotic cells, and elicits a pro-inflammatory response [100]. Additionally, HMGB1 has been reported to be secreted from murine macrophages and human monocytes upon exposure to LPS [101,102]. When directly injected into the heart, HMGB1 triggers inflammatory cell infiltration, which is abrogated in TLR4 deficient mice [63]. The pro-inflammatory activity of HMGB1 depends on the extracellular redox milieu. It loses its cytokine activity upon oxidation of its cysteine residues [103]. In the setting of a myocardial infarction, HMGB1 has been reported to have opposing effects. After permanent coronary artery ligation, heightened HMGB1 release from HMGB1 overexpressing mice leads to smaller infarct size, improved cardiac function and increased vascularization [104]. In the model of ischemia/reperfusion, however, inhibition of HMGB1 reduces infarct size and improves cardiac function. The detrimental effect of HMGB1 is mediated in a RAGE-dependent manner [96].

S100A1 has recently been described as a cardiovascular DAMP, which is rapidly released from cardiomyocytes upon myocardial infarction [64,105]. When directly injected in the heart, S100A1 elicits increase of pro-inflammatory ICAM1 and anti-inflammatory thrombospondin 2 expression, simultaneously suppressing collagen 1 expression. In the model of ischemia/reperfusion in mice, the inhibition of extracellular S100A1 leads to increased infarct size and worsened cardiac function. Of note, TLR4 has been identified as a receptor for extracellular S100A1 without any evidence of parallel signaling through RAGE [64].

The initial alarming about myocardial injury is ensured by DAMPs that bind to pattern-recognition receptors. Targeting the DAMPs/PRR system, *in vivo* experiments in rodents have so far revealed divergent effects on the healing cascade after myocardial infarction. Further studies are required in order to delineate the effect of diverse DAMPs/PRRs on myocardial and immune cells and the resulting impact on myocardial infarct healing.

4.3 Cardiac Fibroblasts

Fibroblasts are commonly defined as cells of mesenchymal origin that produce extracellular matrix proteins, including interstitial collagens, fibronectin and laminin [106,107]. They are widely distributed throughout the complete organism and have diverse transcriptional profiles that depend on the organ of origin [108].

Cardiac fibroblasts are among the most numerous cell types within the heart [109,110]. Together with endothelial cells, fibroblasts form the majority of the non-myocyte fraction within the myocardium [111,112]. Fibroblasts are embedded in a collagen-based network that surrounds cardiomyocytes [110]. Cell-matrix organization and fibroblast content differs among different regions of the heart [107]. In the ventricles cardiomyocytes are organized in layers, which are enveloped by connective tissue and fibroblast sheets [113]. In the sinoatrial node, the pacemaker region of the heart, fibroblasts are more abundant, and the cell-matrix network is less organized than in the ventricles [107]. Besides surrounding pacemaker myocytes, fibroblasts also form islands of themselves [114].

Under physiological conditions fibroblasts ensure the structural integrity of the heart by governing extracellular matrix turnover [109]. In addition to its structural role, connective tissue, which is produced by fibroblasts, also serves as an electrical insulator [115], thereby maintaining the electrical properties of the myocardium. Fibroblasts are known to express several gap-junction proteins, like connexin 40, 43 and 45 [109], although the precise role of fibroblasts in the electrical coupling of myocardium has yet to be defined [116]. Due to their close proximity to cardiomyocytes [117] and lower vulnerability to

injurious factors [118], fibroblasts are often referred to as “sentinel cells" of the myocardium [106].

4.3.1 Cardiac Fibroblasts in Myocardial Infarction

Cardiac fibroblasts actively participate in the healing process after myocardial infarction. To date, the best described form of cardiac fibroblast activation upon myocardial infarction is their transform into a myofibroblast phenotype, which ensures scar tissue formation [119,120]. In mice, myofibroblasts appear on day 4 after infarction and peak on day 7 [23]. In electron micrographs of the myocardium, cardiac fibroblasts are elongated cells with sheet-like extensions, whereas myofibroblasts are notably larger cells with multiple membrane processes and a high amount of exocytotic vesicles [116,117]. A classical marker for myofibroblasts is α smooth muscle actin (αSMA) [121]. The current model of fibroblast activation includes the transformation into a proto-myofibroblast, which further transforms into a mature myofibroblast (Figure 4) [48,106,122].

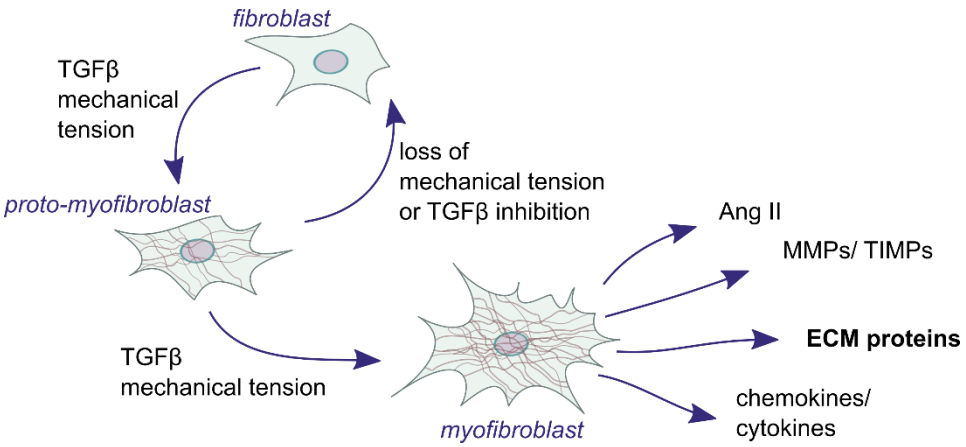

Figure 4: *In vitro* differentiation of cardiac myofibroblasts.

Mechanical tension and TGFβ initiate the fibroblast transformation into αSMA expressing proto-myofibroblasts. Further stimulation with TGFβ and/or retained mechanical tension results in the formation of fully differentiated myofibroblasts, which express high amounts of αSMA. Myofibroblasts produce various cytokines/chemokines, MMPs/TIMPs and AngII. Nonetheless, their most distinct feature is the prominent production of extracellular proteins, in particular collagens. Withdrawal of activating stimuli results in proto-myofibroblast de-differentiation into fibroblasts. In contrast, myofibroblasts are terminally differentiated cells that cannot convert back to proto-myofibroblasts or fibroblasts.

(αSMA- alpha smooth muscle actin, TGFβ- transforming growth factor beta, AngII- angiotensin II, MMP- matrix metalloproteinase, TIMP- tissue inhibitor of metalloproteinase, ECM- extracellular matrix)

Adapted from [48,106,122].

In 2014, Driesen and colleagues demonstrated the course of cardiac fibroblast differentiation into myofibroblasts in a cell culture model. Cardiac fibroblasts transformed into proto-myofibroblasts upon mechanical tension and/or TGFβ stimulation. Fibroblasts

were αSMA negative and possessed high proliferative capacity, whereas proto-myofibroblasts were αSMA positive with a decreased proliferative capacity. Further TGFβ stimulation and maintained mechanical tension resulted in mature myofibroblast formation that was characterized by prominent αSMA staining and the lack of proliferative capacity. With removal or blocking of the activating stimuli proto-myofibroblasts but not myofibroblasts were able to de-differentiate back to fibroblasts. On the protein level, myofibroblasts were secreting an increased amount of collagen, tissue inhibitor of metalloproteinases 1 (TIMP1), and chemoattractant CCL2. In contrast, fibroblasts were characterized by a prominent secretion of interleukin 10 (IL10). Proto-myofibroblasts secreted more collagens than fibroblasts, but less than myofibroblasts. Importantly, cardiac fibroblasts, grown in stiff plastic cell culture dishes and in serum enriched medium, developed a proto-myofibroblast phenotype spontaneously, resulting from mechanical tension from the plastic surface and the presence of TGFβ in fetal calf serum [122].

TGFβ elicits fibroblast differentiation into myofibroblasts, which produce various cytokines and a high amount of collagens [106,122–124]. In a model of dermal fibroblast and keratinocyte co-culture, keratinocyte-derived interleukin 1 (IL1) has been shown to inhibit TGFβ-mediated formation of myofibroblasts by activating nuclear factor κB (NFκB) transcription factors in fibroblasts. Although a notable amount of TGFβ has been found after 24 hours of co-culture, the myofibroblast phenotype was not observed before day 4 [125].

In the setting of myocardial infarction, IL1 is reported to be involved in the initiation and amplification of the inflammatory response [126]. In cell culture, IL1β is able to inhibit and reverse cardiac fibroblast differentiation into proto-myofibroblasts. This has been suggested as a potential endogenous control mechanism for the restriction of premature activation of myofibroblast differentiation after myocardial infarction *in vivo* [127–129]. Interestingly, IL1 also induces an increase in the production of inflammatory adhesion molecules and chemokines in cardiac fibroblasts [130,131].

4.3.2 DAMPs and Cardiac Fibroblasts

The signaling of sterile tissue injury is ensured by DAMPs that are sensed by various cell types, resulting in the initiation of an inflammatory response. Stimulation with HMGB1 induces the expression of pro-inflammatory cytokines in cardiac fibroblasts and, to a lesser extent, also in myofibroblasts, thus demonstrating cardiac fibroblasts as potential sensors of DAMPs and active participants in the inflammatory phase. HMGB1 does not trigger fibroblast transformation into myofibroblasts. Notably, fibroblasts express significantly

more RAGE, which is one of the receptors for HMGB1, than myofibroblasts [132]. When treated with S100A8/9 [133], the most significantly upregulated function in cardiac fibroblasts is chemokine activity, as assessed by transcriptome analysis [134].

In conclusion, cardiac fibroblasts have been shown to be critically involved in the scar formation phase after infarction. Additionally, fibroblast phenotype modulation by DAMPs seems to represent a key event for the initiation of an inflammatory reaction. Further research will have to reveal how the immune response after infarction is modulated by DAMP-stimulated cardiac fibroblasts.

4.4 S100A1

S100A1 is a member of the S100 protein family that consists of small (9-13 kDa) Ca^{2+} binding proteins, which participate in various intracellular activities [135,136]. Members of the S100 protein family have been reported to have cytokine-like functions in extracellular space, although it is not clear, if they can be actively secreted or only passively released from damaged cells [137,138]. Homodimers are the preferential form of oligomerization for S100 proteins [135]. The homodimer of S100A1 can bind four Ca^{2+} ions. This leads to the exposure of a hydrophobic pocket that represents a binding site for target proteins [139,140] (Figure 5).

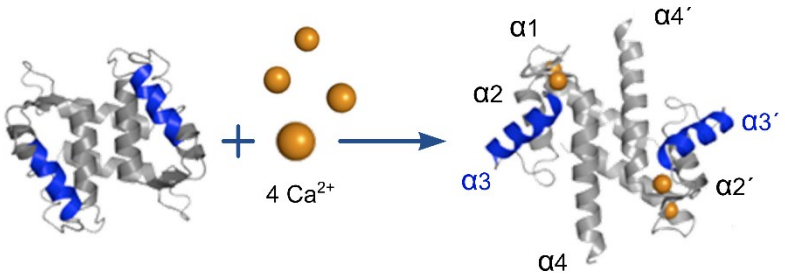

Figure 5: Conformational changes of S100A1 upon Ca^{2+} binding.

The binding of Ca^{2+} results in conformational changes of the S100A1 dimer. It opens a hydrophobic pocket that interacts with target proteins. α3 and α3' helices (blue) rotate 90°, exposing highly bioactive hydrophobic residues on α3 and α4 helix and α3' and α4' helix, as well as on the hinge region between α2 and α3 helices and between α2' and α3' helices.
Taken from [140] with modifications.

S100A1 protein is most abundant in muscle tissues, with the highest amounts found in the heart. In lower quantity, it is also found in other organs, like brain, kidneys and skin [141]. In the heart, S100A1 is mainly localized in the left ventricle, predominantly in cardiomyocytes. So far, no S100A1 expression has been detected in cardiac fibroblasts [64,142,143].

4.4.1 S100A1 in Cardiomyocytes

S100A1 is involved in all major intracellular Ca^{2+} handling events within cardiomyocytes. It interacts with proteins of sarcoplasmic reticulum, myofilaments, and mitochondria (Figure 6).

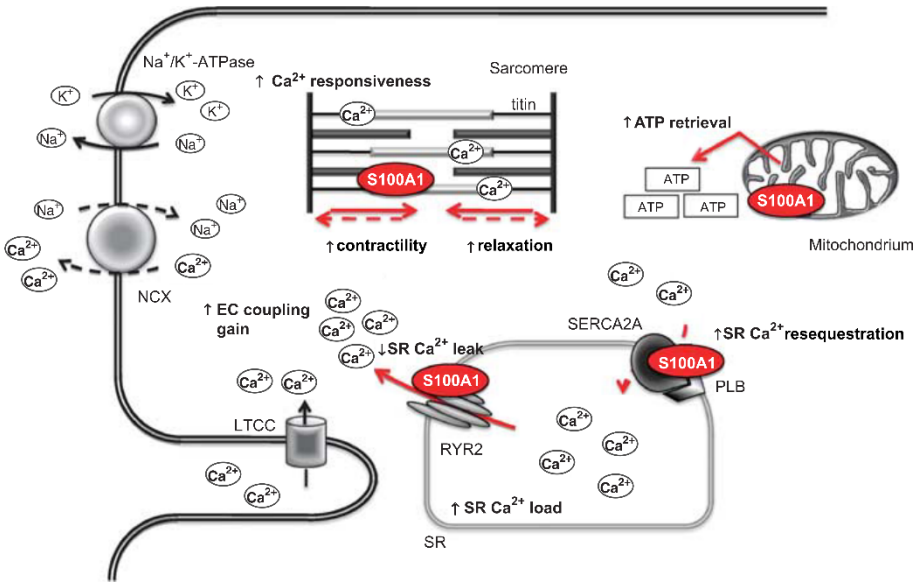

Figure 6: Target structures and functions of S100A1 in cardiomyocytes.

During diastole, S100A1 increases sarcoplasmic reticulum Ca^{2+} load by enhancing SERCA2A-mediated Ca^{2+} uptake from the cytosol and by preventing Ca^{2+} leakage through RYR2. S100A1 also decreases the stiffness of the sarcomere protein titin, thereby facilitating diastolic relaxation. Within the mitochondria S100A1 enhances ATP production.
(LTCC-L-type calcium channel, NCX-sodium-calcium exchanger, ATP-adenosine triphosphate, SR-sarcoplasmic reticulum, SERCA2A-sarcoplasmatic reticulum Ca^{2+} ATPase 2a, PLB-phospholamban, RYR2-ryanodine receptor 2, EC coupling-excitation-contraction coupling)
Taken from [144] with modifications.

S100A1 binds to sarcoplasmic reticulum Ca^{2+} ATPase 2a (SERCA2A) and enhances its capacity to transfer Ca^{2+} from cytosol to the sarcoplasmic reticulum [145]. During diastole, the binding of S100A1 to RYR2 protects from arrhythmogenic Ca^{2+} leakage from the sarcoplasmic reticulum [146,147]. S100A1 also improves mitochondrial ATP production [148] and reduces passive stiffness of titin [149]. The execution of various S100A1 dependant processes in myocardium is ensured with the total amount of approximately 2 µg/mg of S100A1 protein within the heart [141].

4.4.2 Extracellular S100A1

The effect of extracellular S100A1 has been investigated in neuronal, pulmonary, and cardiovascular systems [135,150–152]. Chicks that received an intracerebral injection of S100A1-neutralizing antibody developed amnestic disorders, as measured by the

decreased retention of an aversive experience [153]. In mouse neuroblastoma cells, extracellular S100A1 activates NFκB and enhances neurite outgrowth in a RAGE dependant manner [154]. In the same setting, S100A1 displayed toxic effects in concentrations higher than 1 µM [154]. A mixture of S100A1 and S100B was shown to induce apoptosis in the undifferentiated neural cell line P12, which is derived from the rat pheochromocytoma [155,156]. Recently it has been demonstrated that extracellular S100A1 is internalized by lung endothelial cells, where it interacts with endothelial nitric oxide synthase (eNOS), resulting in protection against TNFα induced apoptosis [151]. In neonatal cardiomyocytes, 2-deoxyglucose induced apoptosis is limited by extracellular S100A1 [157].

Upon myocardial infarction, S100A1 is rapidly depleted from human cardiomyocytes [105] and can be detected in the serum [64,141,158]. Although the kinetics of S100A1 serum levels resemble the time course of cardiac troponins [159], the diagnostic value of S100A1 is limited by its non-cardiomyocyte specific expression pattern, since elevated serum values can also be found in skeletal muscle disorders [141].

Most recently, extracellular S100A1 has been reported to be involved in the healing process after myocardial infarction. Systemic S100A1 inhibition with a neutralizing antibody results in larger size of infarction and worsened cardiac function after ischemia/reperfusion injury [64].

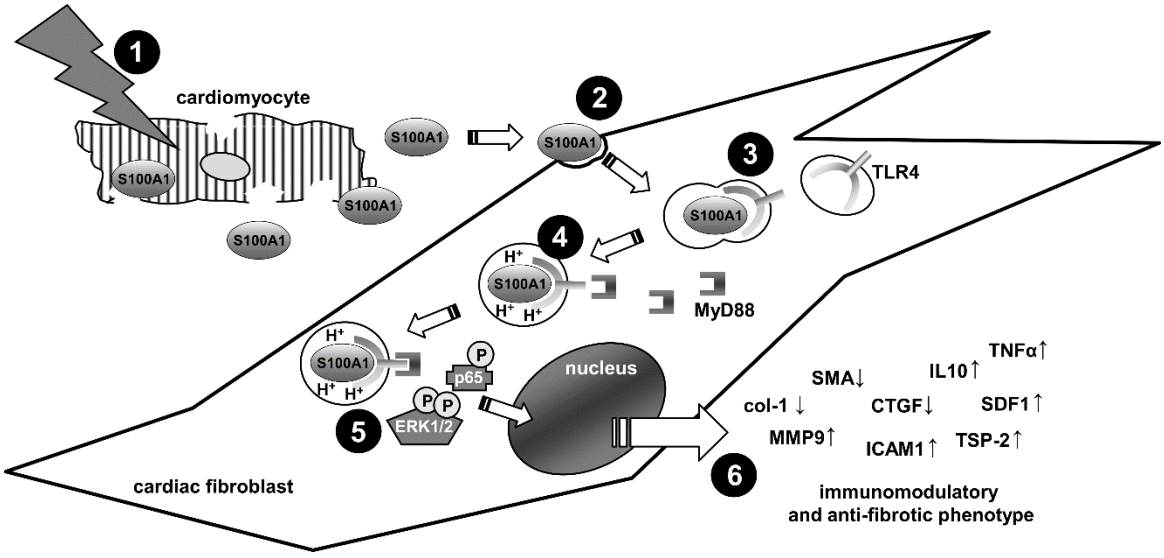

Figure 7: Extracellular S100A1 effect on cardiac fibroblasts.

(1) Upon myocardial infarction S100A1 is released from damaged cardiomyocytes. (2) Neighboring cardiac fibroblasts take extracellular S100A1 up by macropinocytosis. (3) and (4) Internalized S100A1 binds to TLR4 in acidic endosomes and signals in a MyD88-dependent manner. (5) Stimulation with S100A1 elicits ERK1/2 and NFκB activation. (6) S100A1-induced signal transduction resulted in significant gene expression changes on mRNA and protein level.
(TLR4- toll-like receptor 4, MyD88- myeloid differentiation primary response protein 88, ERK1/2- extracellular signal-related kinase 1/2, p65- nuclear factor κ B p65 subunit, col-1 – collagen 1, SMA- α smooth muscle actin, CTGF- connective tissue growth factor, MMP9- matrix metalloproteinase 9, IL10- interleukin 10, ICAM1- intercellular adhesion molecule 1, TNFα- tumor necrosis factor alpha, SDF1- stromal cell derived factor 1, TSP-2 - thrombospondin 2)
Taken from [64] with modifications.

It has been shown that S100A1 that is released from damaged cardiomyocytes is taken up by neighboring cardiac fibroblasts (Figure 7) [64]. In detail, S100A1 is immediately internalized in cardiac fibroblasts by macropinocytosis. Importantly, neither endothelial cells, smooth muscle cells, nor adult cardiomyocytes internalize extracellular S100A1. In cardiac fibroblasts, S100A1 binds to TLR4 in acidic endosomes and recruits cytoplasmic MyD88, resulting in activation of extracellular signal-related kinase 1/2 (ERK1/2) and NFκB transcription factors. On the level of gene expression, S100A1 triggers downregulation of αSMA and collagen 1, simultaneously increasing anti-inflammatory protein IL10 [160] and thrombospondin 2 (TSP2) [161], as well as inflammatory protein ICAM1 [162], stromal cell derived factor 1 (SDF1) [163] and TNFα [164] expression. Interestingly, administration of S100A1-neutralizing antibody prior ischemia/reperfusion injury results in abrogated expression increase of IL10 and ICAM1 that is accompanied with delayed TNFα expression increase.

In summary, S100A1 is released from damaged cardiomyocytes upon myocardial infarction. Following rapid internalization, S100A1 activates a TLR4-MyD88-dependent

signal transduction cascade in cardiac fibroblasts, leading to decreased profibrotic markers, such as αSMA and col-1, and increased expression of immunomodulatory markers, for example, ICAM1, TNFα and IL10.

4.5 Aims of the Study

In myocardial infarction, cardiac fibroblasts have traditionally been linked with the phase of scar formation, during which they transform into myofibroblasts and extensively produce extracellular matrix proteins. However, there is growing evidence that fibroblasts rapidly respond to infarction-related DAMPs, suggesting an active role in the inflammatory phase after myocardial infarction. S100A1 has been shown to be released into the interstitial space from ischemic cardiomyocytes and rapidly internalized by cardiac fibroblasts. In a cell culture model, extracellular S100A1 initiates a distinct signal transduction cascade, resulting in downregulation of αSMA and collagen 1 and increased expression of IL10 and ICAM1. This cardiac fibroblast phenotype might play a key role in the initiation of immune response to myocardial infarction.

Therefore, the aims of this study were:

1) Systematic time-resolved characterization of the gene expression profile of cardiac fibroblasts upon exposure to extracellular S100A1.
2) Comprehensive analysis of the proteomic profile that defines the S100A1-stimulated cardiac fibroblast phenotype.

5 Materials and Methods

5.1 Materials

5.1.1 Equipment and Consumables

Device/ instrument	Manufacturer
C1000 touch thermal cylcer	Bio-Rad
Centrifuges	
Heraeus Megafuge 40R	Thermo Fisher Scientific
Mikro 200 R	Hettich
Rotina 420 R	Hettich
Table top centrifuge	Roth
CFX96 Touch™ Real-Time PCR Detection System	Bio-Rad
Heating circulator	HAAKE
Incubator Heracell 150i with oxygen control	Thermo Fisher Scientific
Laminar flow hood	Thermo Fisher Scientific
Langendorf perfusion apparatus	Custom-made
Magnetic stirrer with hot plate	neoLab
Magnetic stirring bars	neoLab
Microscope IMT-2	Olympus
Microscope IX81S1F-3	Olympus
MyiQ™ Single-Color Real-Time PCR Detection System	Bio-Rad
Neubauer cell counting chamber	Marienfeld-Superior
pH meter	WTW
Pipette controller accu-jet® pro	BRAND
Pipette	Eppendorf
Peristaltic pump	Ismatec
Scale	KERN
Scissors, fine tip forceps, surgical forceps, bulldog clamp	Fine Science Tools, B Braun
Spectrophotometer Multiskan Spectrum	Thermo Fisher Scientific
Spectrophotometer NanoDrop 2000	Thermo Fisher Scientific
Pump for cell culture	NeoLab
Vortex	IKA
Water bath	Memmert

Consumables	Manufacturer
Cell culture 6-well plates	Greiner Bio-One
Cell culture flasks, T75, T175	Sarsted

Clear bottom 96-well plates	Thermo Fisher Scientific
Cell strainer 24mm Netwell™ insert with 440 µm mesh size polyester membrane, sterile	Corning
Amicon Ultra-2 Centrifugal Filter Unit with Ultracel-3 membrane	Merck Millipore
Adhesive seals, optical	Bio-Rad
RNAase clear 0.5, 1.5, 2 mL tubes, PCR plates	nerbe plus
1.5 mL tubes	Sarsted
15, 50 mL tubes	Greiner Bio-One
Plastic Pasteur pipettes	BRAND
Serological pipettes	Greiner Bio-One
Pipette tips with filters	Sarsted
Reagent reservoirs, 50 mL	Corning
Sterile vacuum filtration system Stericup	Merck Millipore
Syringes, needles	BD

5.1.2 Materials for Cell Isolation, Culturing and Stimulation

Chemical	Catalog number	Manufacturer
Butanedione monoxime (BDM)	B0753	Sigma-Aldrich
$CaCl_2 \cdot 2H_2O$	C7902	Sigma-Aldrich
(±) Carnitine hydrochloride	C9500	Sigma-Aldrich
Creatine	C3630	Sigma-Aldrich
EDTA tetrasodium salt $\cdot 2H_2O$	E6511	Sigma-Aldrich
D (+) Glucose	G7021	Sigma-Aldrich
HEPES	H4034	Sigma-Aldrich
KCl	P5405	Sigma-Aldrich
Mercaptopropionylglycin	M6635	Sigma-Aldrich
MgSO4	M2643	Sigma-Aldrich
Na-Pyruvat	P5280	Sigma-Aldrich
Na-Acetate	S5636	Sigma-Aldrich
NaCl	S5886	Sigma-Aldrich
Na-Glutamate	G5889	Sigma-Aldrich
NaHCO3	S5761	Sigma-Aldrich
NaOH	106498	Merck Millipore
Phenol Red sodium salt	P5530	Sigma-Aldrich
Taurine	T8691	Sigma-Aldrich
Water, CHROMASOLV® Plus, for HPLC	34877	Sigma-Aldrich

Medium/ reagent/ additive	Catalog number	Manufacturer
CLI095 (TLR4 inhibitor)	tlrl-cli95	Invivogen
Collagenase, type 2	CLS-2	Worthington

Dulbecco's Modified Eagle's Medium (DMEM) - high glucose	D5796	Sigma-Aldrich
Dulbecco's Phosphate Buffered Saline (PBS)	D8537	Sigma-Aldrich
Fetal Bovine Serum Superior (FCS)	S0615	Biochrom
Heparin Sodium, 25'000 I.U.		ratiopharm
Insulin, 40 I.U./mL		Sanofi
Penicillin-Streptomycin	P4333	Sigma-Aldrich
Human recombinant S100A1		Self-produced, for detailed protocol see [64,165]
Thiopental Sodium, 0.5 g		Inresa Arzneimittel
Trypsin-EDTA (0.25%)	25200056	Thermo Fisher Scientific

5.1.3 Materials for Gene Knockdown by siRNA

Reagent	Catalog number	Manufacturer
Silencer® Select Negative Control No. 1 siRNA	4390843	Thermo Fisher Scientific
TLR4, siRNA ID: s131044	4390771	Thermo Fisher Scientific
Lipofectamine® RNAiMAX Transfection Reagent	13778075	Thermo Fisher Scientific

5.1.4 ELISA Kit

Kit	Catalog number	Manufacturer
Mouse/Rat CCL2/JE/MCP-1 Quantikine ELISA Kit	MJE00	R&D Systems

5.1.5 Materials for Protein and RNA Isolation and qPCR

Chemical/ reagent	Catalog number	Manufacturer
Bromophenol blue	108122	Merck Millipore
Chloroform	22711	VWR
Dodecyl sulfate sodium salt (SDS)	822050	Merck Millipore
Ethanol	32205	Sigma-Aldrich

Glycerol solution	49781	Sigma-Aldrich
iQ™ SYBR® Green Supermix	170-8884	Bio-Rad
iScript™ cDNA Synthesis Kit	1708891	Bio-Rad
Isopropanol	33539	Sigma-Aldrich
Polyacryl carrier	PC152	MRC
TRIS- HCl	T5941	Sigma-Aldrich
TRIzol® Reagent	15596-026	Thermo Fisher Scientific
Water for molecular biology, DEPC- treated and sterile filtered	95284	Sigma-Aldrich
2- Mercaptoethanol	805740	Merck Millipore

Gene symbol, primer assay name	Catalog number	Manufacturer
Ccl2, Rn_Ccl2_1_SG	QT00183253	Qiagen
Tlr4, Rn_Tlr4_1_SG	QT00387184	Qiagen

Gene symbol	Forward primer	Reverse primer
18s	GTAACCCGTTGAACCCCATT	GGCCTCACTAAACCATCCAA

5.1.6 Materials Used by Dr. Martin Busch

Chemical/ reagent	Catalog number	Manufacturer
Total RNA Purification Plus Micro Kit	48500	Norgen Biotek

Gene symbol	Forward primer	Reverse primer
HPRT1	CCAGCGTCGTGATTAGTGAT	AGAGGGCCACAATGTGAT
CCL2	GGTCTCTGTCACGCTTCTG	TTCTCCAGCCGACTCATTG

5.2 Methods

5.2.1 Isolation and Culturing of Adult Rat Cardiac Fibroblasts

5.2.1.1 Preparation of Isolation and Perfusion Buffers

All buffers for the isolation of adult rat cardiac cells were prepared in ion free water Chromasolv Plus (Sigma-Aldrich). pH values were adjusted with 1M NaOH.

Table 1: Composition of the cell isolation and perfusion buffer.

	M (mol/g)	C (mM)	g/L for 1L	
10x stock solution				
Sodium chloride (NaCl)	58.4	850	50	Adjusted to pH 7.3, sterile filtered, stored at 4°C
Potassium chloride (KCl)	74.6	54	4	
Magnesium Sulfate (MgSO4)	120.4	41.5	5	
Na Pyruvat	110.0	50	5.5	
Sodium bicarbonate (NaHCO3)	84.0	200	16.8	
D (+) Glucose	180.2	115	20.7	
HEPES	238.3	200	47.7	
Na-Glutamate	169.1	254	43.0	
Na-Acetate	82.0	48.8	4.0	
Phenol Red sodium salt	376.4	0.5	0.2	
1x isolation buffer (supplemented on the day of isolation)				
BDM	101.1	10	1	
Creatine	149.2	4.4	0.66	
Taurine	125.2	30	3.75	
Mercaptopropionylglycin	163.2	4.9	0.8	
Perfusion buffer (isolation buffer+ EDTA)				
EDTA tetrasodium salt dihydrate	416.2	0.09	0.04	

On the day of isolation, perfusion and cell isolation buffers were prepared. The pH for the final solutions was adjusted to 7.3.

5.2.1.2 Cell Culture Mediums

Adult rat cardiac fibroblasts were cultured in high glucose DMEM, supplemented with 10% FCS and 1% penicillin/ streptomycin (10% FCS DMEM). Before stimulation cells were starved in the DMEM, containing 1% penicillin/ streptomycin (P/S) and 0% or 0.5% FCS, depending on the subsequent experiments.

5.2.1.3 General Cell Culturing

Cells were cultured in a humidified, 37˚C, 5% CO_2 incubator. Cell culture work was performed under sterile conditions in a laminar flow hood.

5.2.1.4 Cardiac Cell Dissociation

Adult rat cardiac cells were isolated according to the protocol from Xu and Colecraft [166] with minor modifications. The rat heart was perfused with digestion buffer in the Langendorff technique, thus enabling dissociation of single cardiac cells (Figure 8).

Figure 8: Adult rat heart cell isolation by enzymatic digestion in the Langendorff technique.
(A) Adult rat heart was mounted on the cannula for the retrograde perfusion with digestion buffer through the coronary arteries.
(B) The cardiac tissues were digested in the closed circular system.
(C) Heart cells were dissociated from digested connective tissues yielding at least 60% viable, rod-shaped cardiomyocytes right after the isolation, thereby indicating sufficient enzymatic digestion.
(Scale bar represents 200 µm)

An adult male Wistar rat (250-350 g) was anesthetized with 1 mL Thiopental i.p. injection, 35 mg/mL, until loss of hind limb toe pinch reflex (surgical anesthesia). Incision areas on the abdomen and thorax were sterilized with 70% ethanol and opened with lateral cuts by scissors. The heart was exposed and cut out with a large portion of the aorta and quickly placed into a 10 cm Petri dish with 80 mL of room temperature perfusion buffer, supplemented with 8 I.U./mL heparin. The aorta was slid onto the cannula of the Langendorff apparatus, and fixed with a bulldog clamp. Perfusion was started immediately with a drip rate of ~100 drops/min. Filling of the coronary arteries was checked and evaluated in order to determine, if the heart was correctly positioned on the cannula. Then the clamp was replaced with a suture. In order to remove residual serum traces and free Ca^{2+}, the heart was washed with 70 mL of perfusion buffer, where the first 20 mL contained

8 I.U./mL heparin. During the wash step, the pulmonary vessels were tied, in order to increase the pressure within the coronary system.

When 26 mL of perfusion buffer were left in the system, collagenase II solution was added, thereby composing the digestion buffer for the heart cell dissociation. ~50 mg Collagenase II was dissolved in 14 mL of perfusion buffer and added to the residual buffer in the system, thus together making the concentration of Collagenase II ~1.25 mg/mL. The exact concentration of collagenase II was adjusted for each lot separately, varying from 1 to 1.5 mg/mL. Next the circulatory flow was established, and the heart was perfused with the drip rate of ~60 drops/min, 37˚C, for ~30 minutes. The perfusion was stopped, when the heart became flaccid and easily penetrable by fine tip forceps.

A small beaker was filled with 15mL of digestion buffer from the perfusion system for the first round of cell dissociation. Simultaneously, the ventricles were cut off and placed into the beaker. A 50 mL tube was filled with additional 15mL of digestion buffer (to be used later for the second round of cell dissociation). The ventricles were minced into approximately 10 pieces with scissors. For the first round of cell dissociation the suspension was incubated in the water bath (37°C) for ~3 minutes with gentle shaking. In order to facilitate the dissociation of the cells, the tissue pieces were gently triturated 5-7 times with the plastic Pasteur pipette with shortened tip (opening 3-4 mm Ø), followed by additional 3 minutes incubation in the water bath. The whole suspension was triturated 6-10 times before being filtered through a 440 µm cell strainer into a 50 mL tube. 15 mL of isolation buffer (perfusion buffer without EDTA) was added to the cell suspension, and the cell suspension was left at room temperature to settle. The rest of the tissues from the cell strainer was placed back into the beaker, and mixed with the previously collected additional 15 mL of digestion buffer for the second round of cell dissociation. The rest of the tissues were once again incubated twice in the water bath and filtered as described above. The resulting cell suspension from the second round of dissociation was similarly mixed with 15 mL of isolation buffer.

5.2.1.5 Separation of Cardiac Fibroblasts

For the isolation of cardiac fibroblasts, after the cell dissociation both portions of cell suspension were centrifuged for 1 minute at 50 g to pellet the cardiomyocytes. The supernatant was collected and centrifuged one more time for 5 minutes at 1000 g. The resulting pellets were pulled together by resuspending them in 20 mL 10% FCS DMEM, and transferred to T75 cell culture flask. After 2 hours, the attached cells were gently washed with PBS and fresh 10% FCS DMEM was added.

5.2.1.6 Culturing of Cardiac Fibroblasts

Four days after isolation, cardiac fibroblasts reached 100% confluence in the T75 cell culture flask. For the subculturing cells were washed twice with PBS, 3 mL of trypsin-EDTA 0.25% was added and fibroblasts were incubated for 3 minutes at 37˚C. Subsequently, 25 mL of 10% FCS DMEM was added to cells and the resulting fibroblast suspension was transferred into the T175 cell culture flask. After 2-3 days the cells were split again into 6-well plates with 100 000 cells per well. After 24-36 hours when the confluence was around 60-80%, the fibroblasts were washed twice with PBS and culturing medium was replaced by serum deprived medium. Cells were starved for 24 hours before further stimulation (for the differences in the siRNA transfection protocol see 5.2.2 siRNA Transfection). All experiments were performed on passage 2 (P2) (Figure 9).

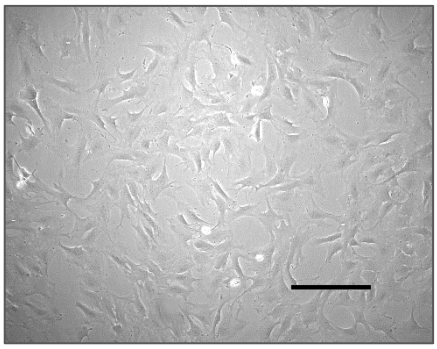

Figure 9: Density of cardiac fibroblasts at the beginning of stimulation.

At 60-80% confluence, fibroblasts were serum starved for 24 hours before further stimulation. (Scale bar represents 200 µm)

5.2.2 siRNA Transfection

For the TLR4 siRNA knockdown, adult rat cardiac fibroblasts were plated on 6-well plates, 100 000 cells per well. After 24-36 hours, when the confluence reached ~60% (Figure 10), the cells were washed 1x with PBS and 1.5 mL of 0% FCS DMEM per well was added.

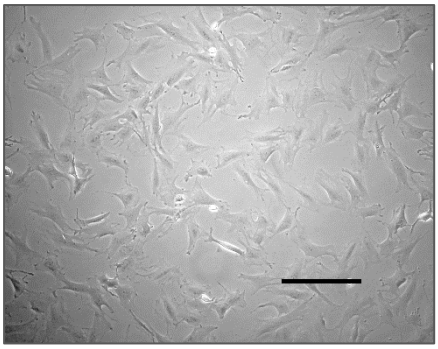

Figure 10: Density of adult rat cardiac fibroblasts before siRNA transfection.

For the optimal knockdown results, transfection with siRNA was performed at ~60% confluence. (ACF, scale bar represents 200 µm)

Transfection was performed with Lipofectamine RNA iMax Reagent according to the manufacturer's protocol. For one well 250 µL of DMEM without any supplementation was mixed with 5 µL of Lipofectamine and shortly vortexed. 10 µL of siRNA (stock solution of 10 µM, and final concentration of 50 nM per well) was added to 250 µL of DMEM without supplementation and shortly vortexed. 250 µL of transfection reagent mix was transferred to 250 µL of siRNA dilution, shortly vortexed and incubated at room temperature for 5 minutes. Finally 500 µL of the siRNA reagent complex was added to each well, and the cells were incubated for 48 hours before further stimulation. The efficiency of TLR4 siRNA knockdown was assessed against negative control siRNA (scramble) knockdown using qPCR. 48 h after transfection cardiac fibroblasts were stimulated with 1 µM of recombinant S100A1 for additional 24 h.

5.2.3 Enzyme Linked Immunosorbent Assay (ELISA)

For the detection of rat CCL2 in the supernatant, the commercially available sandwich-type ELISA kit was used according to the manufacturer's protocol. Blank controls, standards, control of the assay and samples were added in duplicates to the wells of microplates that were pre-coated with CCL2 capture antibody. After 2 hours of incubation at room temperature, the wells were thoroughly washed and antibody against CCL2 conjugated to horseradish peroxidase was pipetted into the each well. The plate was incubated once again for 2 hours at room temperature. Then the substrate solution was added. After 30 minutes of incubation at room temperature, protected from light, the stop solution was added, and the optical density was measured at the wavelength of 450 nm with correction wavelength set to 540 nm. The control value of the assay had to be in the range from 101 to 169 pg/mL. Detection range for the assay was 15.60- 1.000 pg/mL.

Correction optical density (540 nm) was subtracted from each data point. Subsequently, blank control (450 nm) was subtracted from each tested sample. For the calculation of the concentration of samples a 4-parameter logistic curve fit was created from OD and concentration values of standards with the web-based application elysaanalysis.com [167]. Resulting formula was used for the calculation of the concentration of the samples.

5.2.4 Isolation of RNA, Reverse Transcription, qPCR

5.2.4.1 Isolation of Total RNA

The total RNA from adult rat cardiac fibroblasts was isolated with TRIzol® Reagent according to the manufacturer's instructions with minor changes. In brief, the supernatant from 6-well plates was collected or discarded, 1 mL of TRIzol® was added in each well and incubated for 2 minutes at room temperature. Samples were collected, and then 200 µL of chloroform were added and mixed by vigorously shaking the tubes. For the phase separation, samples were centrifuged for 15 minutes at 18 000 g, 4˚C. From now on all steps were performed on ice. The upper aqueous phase that contains RNA was transferred to a new tube without disturbing the interphase or organic layer. In order to precipitate RNA, ice-cold 100% isopropanol and 1.5 µL of polyacryl carrier were added, then briefly mixed by inverting the tubes. After that, RNA was allowed to precipitate overnight at -20°C. To collect the RNA, the tubes were centrifuged for 15 min at 18 000 g, 4˚C. The pellet was washed twice with ice cold 75% ethanol and air dried for approximately 10 minutes and dissolved in 20 µL of DEPC-treated water. RNA quality and concentration were assessed with NanoDrop2000.

For the RNA isolation of Dr. Martin Busch's experiments Total RNA Purification Plus Micro Kit was used according to manufacturer's instructions.

5.2.4.2 Reverse Transcription

Reverse transcription of the RNA was performed with iScript cDNA synthesis kit following the manufacturer's protocol. 1 µg of RNA was mixed with 4 µL of iScript reaction mix and 1 µL of reverse transcriptase. The volume was scaled up to 20 µL with DEPC-treated water. The reaction was performed with the following protocol: annealing- 5 minutes at 25˚C, reverse transcription- 30 minutes at 42˚C, inactivation of the enzyme- 5 minutes at 85˚C. The produced cDNA was stored at -20˚C until further use.

5.2.4.3 Quantitative Real-Time PCR (qPCR)

For the qPCR reaction, iQ SYBR Green Supermix was used according to the user manual for the final volume of 15 µL per reaction. 7.5 µL of iQ SYBR Green Supermix was mixed

with 1 µL of the forward and reverse primer mix (final concentration 300 nM each, or according to the primer data sheet for commercially available ones). The cDNA was diluted 1:100 in DEPC-treated water. For one reaction 6.5 µL of diluted cDNA was used, resulting in 65 ng of cDNA per run. The qPCR was performed on Biorad MyIQ PCR cycler with the protocol, described in the Table 2.

Table 2: Protocol for qPCR.

Number of Cycles	Temperature	Dwell time	Step
1x	95°C	03:00	Denaturation
40x	95°C	00:10	Denaturation
	60°C	00:45	Annealing
	72°C	00:30	Elongation
1x	95°C	00:05	Termination
1x	55°C	01:00	Temperature gradient set point
80x	55→95°C, 0,5°C/increment	00:10	Melting curve
1x	4°C	∞	Hold

Dr. Martin Busch used iQ SYBR Green Supermix according to the user manual for the final volume of 20 µL per reaction. 10 µL of iQ SYBR Green Supermix was mixed with 1 µL of the forward and reverse primer mix (final concentration 250 nM each). 50 ng of cDNA was used per run, diluted in 2 µL of water. The total volume was scaled up to 20 µL with 7 µL of water. The qPCR was performed on CFX96 Touch™ Real-Time PCR detection system with the protocol, described in the Table 3.

Table 3: Protocol for qPCR, Dr. Martin Busch's experiments

Number of Cycles	Temperature	Dwell time	Step
1x	95°C	03:00	Denaturation
40x	95°C	00:15	Denaturation
	60°C	01:00	Annealing, elongation
1x	95°C	01:00	Termination
80x	55→95°C, 0,5°C/increment	00:05	Melting curve

18s was used as a reference gene (for the Dr. Martin Busch's experiments- HPRT1). Relative gene expression changes were calculated applying ΔΔCt method according to Livak and Schmittgen [168] with the following formula:

$$\text{fold change} = 2^{-\Delta\Delta C_t}$$

$$-\Delta\Delta C_t = -((C_t\text{GOI} - C_t 18s)_{\text{treatment}} - (C_t\text{GOI} - C_t 18s)_{\text{control}})$$

Ct- threshold cycle, GOI- gene of interest.

5.2.5 Transcriptome

In order to evaluate gene expression changes in cardiac fibroblasts in response to extracellular S100A1, serial transcriptome analysis was performed using microarray technology. Adult rat cardiac fibroblasts were starved for 24 hours in 0.5 % FCS DMEM (6-well plates, 2 mL of medium per well). For each time point a separate plate was prepared. Cells were stimulated with recombinant S100A1 for 1, 2, 4, 6, 8, 12, 18, 24 and 48 hours. Unstimulated control samples were collected before stimulation ("0 hours") and at each indicated time point. RNA was isolated with TRIzol® Reagent as described above. The total amount of 1 µg was submitted to the DKFZ Genomics and Proteomics Core Facility. RNA quality control was performed on an Agilent 2100 Bioanalyzer. Gene expression profiling was performed with Affymetrix GeneChip® Rat Gene 2.0 ST Array. The sample preparation for the hybridization on the arrays was carried out with the GeneChip® WT PLUS Reagent Kit (Affymetrix), according to the manufacturer's instructions. In brief, 200 ng of total RNA was used for the synthesis of the cDNA, which was further transcribed and amplified into cRNA. Next, single-stranded cDNA (ss-cDNA) was synthesized from cRNA, followed by fragmentation and biotinylation. Finally, 5.5 µg of fragmented and biotin-labeled ss-cDNA were hybridized for 17 h at 45°C on arrays with GeneChip® Hybridization, Wash and Stain Kit in automated system Fluidics Station 450 (both from Affymetrix). The scanning of gene microarray was done with a GeneChip® Scanner 3000 (Affymetrix).

The obtained data was processed in collaboration with Dr. Dr. Melanie Börries and Dr. Hauke Busch (Institute of Molecular Medicine and Cell Research, University of Freiburg). The functional enrichment analysis was performed with Gene Set Enrichment Analysis software [169,170].

5.2.6 Secretome

5.2.6.1 Sample Preparation and LC-MS/MS Data Acquisition

For the identification of secreted protein pattern by cardiac fibroblasts upon extracellular S100A1 stimulation secretome analysis was performed. Supernatant from stimulated and untreated cells was prepared as follows. Adult rat cardiac fibroblasts in 6-well plates were starved for 24 hours in 0% or 0.5% FCS DMEM, 2 mL per well. 1 mL of medium was aspirated from each well before stimulation with 1 µM recombinant S100A1. After 48 hours of incubation supernatant was collected. For the protein concentration an Amicon ultracentrifugation filter device (3 kDa pore size) was used according to the manufacturer's instructions. One mL of supernatant was added in the filter device and centrifuged for 110 minutes at 4000g, 8˚C using swinging bucket rotor. As a result one mL of supernatant was concentrated to 60 µL. In order to collect the concentrated supernatant in the collection tube, the reservoir of the filtrate was discarded, filtration device was inverted and centrifuged for 2 minutes at 1000g.

30 µL of concentrated supernatant was mixed with 3 µL of loading buffer (300 mM TRIS-HCl, 12% SDS, 0.3% Bromophenolblue, 60% glycerol, 12% β-mercaptoethanol). The further processing was done by the ZMBH Core Facility for Mass Spectrometry & Proteomics. After boiling for 3 minutes at 60˚C, samples were loaded into a 10% SDS acrylamide gel. The gel was run until the bromphenol blue front was about 2 cm into the well. Each lane was cut into four pieces according to their molecular size. Proteins in each piece were further digested with trypsin. The resulting peptides were labeled by reductive dimethylation, control samples being labeled as 'light' with mass increase of 28 kDa per primary amine and S100A1-treated samples as 'intermediate' with mass increase of 32 kDa per primary amine. Then control and S100A1-treated samples from the same molecular size range were mixed together and subjected to liquid chromatography-tandem mass spectrometry (LC-MS/MS) analysis with the Orbitrap Elite Hybrid Mass Spectrometer (Thermo Fisher Scientific).

5.2.6.2 Identification and Sorting of Valid Secreted Proteins

Protein identification performed Dr. Bernd Hessling with MaxQuant 1.5.2.8 software. Protein names and gene symbols were derived from the UniProt data base [171]. Data were sorted, marking common contaminants from sample preparation process (e.g. keratins, trypsin) and proteins of bovine origin, as well as false positive hits from decoy database.

The ratio of the treatment with S100A1 vs. control for each protein was calculated. In addition, the absolute amount of protein in the sample was determined with the absolute quantification (iBAQ) value. It represents the sum of intensities of detected peptides divided by the intensities of all theoretically obtainable peptides from the protein [172]. Ratios of the proteins were calculated from the intensities of peptides, which were detected both in control and S100A1 samples. iBAQ values were determined from the intensities of peptides, which were detected in the respective sample (Figure 11).

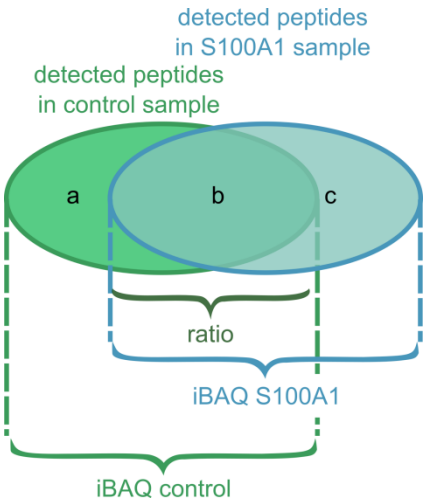

Figure 11: Data sets for the calculation of ratios and iBAQ values of proteins.

For the calculation of protein ratios from control vs. S100A1-treatment, only the intensities of peptides that were detected in both control and S100A1 stimulated samples were used (set b). The iBAQ value for each protein was determined from the intensities of all detected peptides for each samples: intensities from set b and c were used for the iBAQ value calculation of each protein from S100A1 sample, whereas intensities of set a and b were used for the iBAQ value calculation of each protein from control sample.
(iBAQ- intensity based absolute quantification)

Further data processing, annotation and statistical analysis was performed with Perseus 1.5.2.6 software (developed by group of Prof. Dr. Matthias Mann) with the assistance of Dr. Hessling. All values were logarithmically transformed and the median of triplicates was calculated, where appropriate. The data sets were reduced by excluding previously marked contaminants and false positive hits. To separate extracellular proteins from intracellular ones, filtering according to the UniProt identifier “gene ontology cellular compartment” (GOCC) was performed. Proteins annotated with one or more of the following GOCC names were included in downstream calculations: extracellular matrix, extracellular matrix part, extracellular membrane-bounded organelle, extracellular organelle, extracellular region, extracellular region part, extracellular space, and extracellular vesicular exosome.

5.2.6.3 Statistical Analysis and Biological Classification

The significance of the upregulation or downregulation of the proteins was calculated with one-sample t-test, as an input matrix using protein ratios. The relative changes were expressed as a median of protein ratios from triplicates.

Comparison and visualization of the protein composition from cell supernatants with or without FCS were performed with the web based application BioVenn [173]. In brief, the data sets of detected valid extracellular proteins from the 0% and 0.5% FCS groups were loaded into the software. The number of proteins was depicted as a Venn diagram that allows visualization of the groups of common proteins detected in both treatment conditions as well as proteins, detected only in one of the treatment condition.

For the correlation analysis Pearson correlation was employed. It measures the strength of increasing or decreasing linear association between two variables that are normally distributed [174].

Biological functions of the secretome were determined by grouping the proteins with one-dimensional (1D) annotation enrichment analysis and Fisher's exact test. Each protein was annotated according to its biological function, molecular function, cellular compartment and keywords from UniProt. Separate annotation category was created manually for distinct inflammatory proteins, and will be discussed in the Result section 6.2.4.

1D annotation enrichment analysis was performed as described by Cox and Mann [175]. Enrichment of proteins from one biological category was tested with the two-sample Wilcoxon-Mann-Whitney test. This tests estimates, whether the category of interest ranks statistically significantly higher or lower comparing with the distribution of the whole group. For the multiple hypotheses testing Benjamini-Hochberg false discovery rate (FDR) was set to 2%. The input data were ratios or iBAQ values of each protein from the secretome. The enrichment of the category was expressed by positioning it in the overall distribution of data points. It was depicted as a position score, calculated as follows:

$$s=\frac{2\times(R1-R2)}{n}$$

R1 was average rank of the input data from the group of interest, R2 was average rank of respective numerical items from the rest of the proteins and n was the total number of included proteins.

Biological function enrichment analysis for upregulated proteins was performed with Fisher's exact test. This test assesses, whether the non-random link between proteins

from predefined group exists. Within the computation proteins with ratios more than 4 were included. The Benjamini- Hochberg FDR was set to 2%. The enrichment of certain biological category was calculated with the following formula:

$$\text{enrichment factor} = \frac{\text{intersection size}}{\text{category size}} \times \frac{\text{total size}}{\text{selection size}}$$

Intersection size represented proteins with the ratio more than 4 that belonged to the certain category, category size was the number of all detected extracellular proteins from the category of interest, total size was the number of all detected extracellular proteins and the selection size was the number of proteins, which ratio was more than 4.

5.2.7 Statistics

For the cell culture experiments, data were plotted as mean ± SEM, unless indicated otherwise. For comparison of two groups unpaired two-tailed Student's test was used. For more than two groups one-way ANOVA was performed. Results were considered to be significant, if $p<0.05$.

6 Results

Myocardial infarction results in a massive release of DAMPs [176–178]. They contribute to the activation of a systemic immune response that is needed for the clearance of cellular debris [10,92]. It has been demonstrated that HMGB1 and IL1α influence cardiac fibroblasts by increasing pro-inflammatory gene expression and suppressing their transformation into myofibroblasts [131,132]. S100A1 is a cardiomyocyte-derived DAMP, which is internalized by cardiac fibroblasts [179]. Within this study, the response of cardiac fibroblasts to stimulation with S100A1 was investigated.

6.1 Gene Expression Profile of Cardiac Fibroblasts upon Stimulation with S100A1

In cardiac fibroblasts, extracellular S100A1 triggers upregulation of several inflammation related genes and proteins, such as intercellular adhesion molecule 1 or interleukin 10. At the same time it downregulates collagen 1α1 and α smooth muscle actin production [64]. In order to understand the complex transformation of the fibroblast phenotype upon stimulation with S100A1, a time-resolved transcriptome analysis was performed.

6.1.1 Principal Component Analysis of Time-Resolved Transcriptome

In order to investigate the transcriptomic changes of S100A1-treated cardiac fibroblasts over time, cells were stimulated with recombinant S100A1 for 1, 2, 4, 6, 8, 12, 18, 24, and 48 hours. After the acquisition of microarray data, intensities for each gene per time point were combined together for each experimental condition and principal component analysis was performed. All gene expressions per sample were reduced to two dimensions (principal components), which correspond to the greatest variances. With this approach it is possible to visualize the complete pattern of gene expression of a single sample as one point with two coordinates. The distance, which separates several probes from each other, is expressed in percentage and allows to assess the differences of transcriptome between several samples. Thereby, the impact of S100A1-treatment over time was evaluated by the calculation of principal components for each sample from control and stimulated groups.

As shown in Figure 12, treatment with S100A1 resulted in dynamic transcriptomic changes, which could be detected already at the early time points. At the 4 hour time point the gene expression pattern after the stimulation with S100A1 differed from the respective control sample by approximately 10% and 5% increase of principal component 2 (PC2) and principal component 1 (PC1), respectively. In the following time course, the S100A1-

treated fibroblasts deviated further from their corresponding controls. After 24 hours, the stimulated sample was separated from the respective control by approximately 20% and 5% increase of PC1 and PC2, respectively. At the final time point (48 hours) the S100A1-treated sample decreased by 5% on PC2, comparing to 24 hours. Thus, in the last time point the control and S100A1-stimulated sample differed by around 20% of PC1, whereas according to PC2 they located roughly at the same level. It is important to note that the incubation of control samples for 48 hours had only a minor effect on the gene expression profile. The data points between 0 and 48 hours differed for approximately 5% on principal component 2 without any notable perturbations during the whole period of incubation.

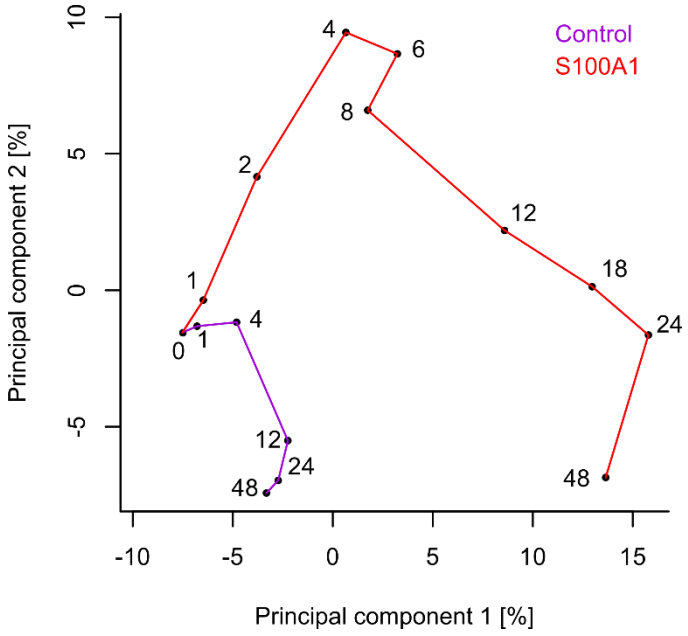

Figure 12: S100A1 elicits early gene expression profile changes in cardiac fibroblast with dynamic fluctuations over time.

Principal component analysis of the serial transcriptome. Cardiac fibroblasts were stimulated with the S100A1 for 0, 1, 2, 4, 6, 8, 12, 18, 24 and 48 hours. After the data acquisition from gene microarray, the intensities of each sample were grouped together and plotted with respect to other samples. The greatest variances were calculated in 2 dimensions (principal components). S100A1-treated fibroblasts showed early and dynamic fluctuations of the gene expression pattern over time. Starting from the 4 hours up to the final investigated time point the S100A1 stimulated samples strongly deviated from the gene expression profiles of earlier time points and respective controls. In contrast, the gene expression pattern of control samples had only minor changes over 48 hours of incubation. (ACF, n=1, S100A1 1µM, 0.5% FCS)

Cardiac fibroblast stimulation with S100A1 led to an early shift of the gene expression profile that dynamically fluctuated over time, strongly deviating from the unstimulated samples. In the next step gene expression pattern changes were analyzed further by linking them with possible subsequent biological events.

6.1.2 Transcriptome-Derived Biological Functions

The principal component analysis of the serial transcriptome revealed a prominent activation of cardiac fibroblasts with an alternating pattern of gene expression profile over time after the treatment with S100A1. For the evaluation of the biological events, which follow fibroblast stimulation, gene expression changes were sorted into categories of biological regulations and functions.

Transcriptomic changes of cardiac fibroblasts upon treatment with S100A1 were analyzed with a Gene Set Enrichment Analysis (GSEA) software, identifying biological categories that significantly differed between control and treated samples. Since the control samples were collected after 1, 4, 12, 24 and 48 hours, these time points were taken for the calculation of the enriched biological functions. The intensity of regulation for each category per time point was obtained as an adjusted significance level, where the p-value was calculated for the enrichment of category that was normalized to the gene set size. For the adjustment of the p-value the permutation based false discovery rate was applied. The adjusted significance represents the probability that the enrichment of a given category is a false positive hit [169,180]. Higher relative differences for genes from particular category yields lower adjusted p-value. Note that the adjusted p value 0.05 corresponds to 1.3 in $-\log_{10}$ scale.

In Figure 13 significantly upregulated biological functions and pathways are shown, indicating a strong link between the stimulation with S100A1 and positive activation of inflammatory processes in cardiac fibroblasts. The category with the lowest adjusted p-values was chemokine activity that was highly upregulated already at the one hour time point. The next most upregulated groups were categories of neutrophil chemotaxis and cellular response to tumor necrosis factor.

From the intracellular signaling pathways the TLR4, ERK1/2 and NFκB signaling cascades were detected to be activated, albeit with less pronounced upregulation comparing to the highest ranked categories of chemokine activity or cellular response to tumor necrosis factor. It is in agreement with previous studies, where TLR4 has been identified as a receptor for recombinant S100A1, further signaling components being ERK1/2 and NFκB [64,181].

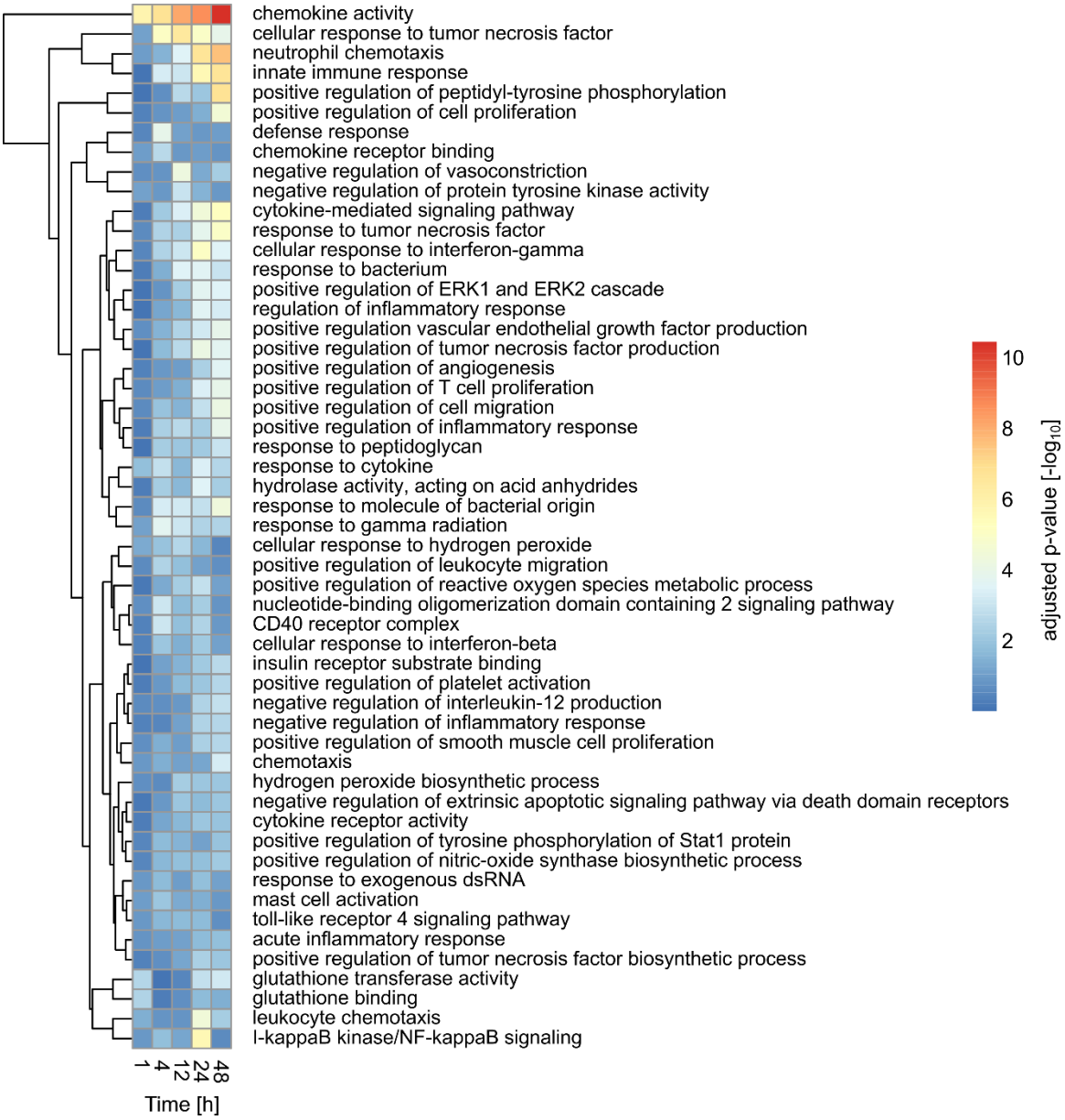

Figure 13: S100A1 triggers upregulation of inflammatory gene expression profile in cardiac fibroblasts.

Significantly upregulated biological functions of the transcriptome from ACF after 1, 4, 12, 24 and 48 hour stimulation with S100A1. Gene expression changes were clustered and annotated according to their biological functions with a gene set enrichment analysis (GSEA) software. The earliest and most prominently upregulated function were chemokine activity, cellular response to tumor necrosis factor and neutrophil chemotaxis.
(ACF, n=1, S100A1 1µM, 0.5 % FCS)

In the next step, calculation of the significantly downregulated categories was performed (Figure 14). Treatment of cardiac fibroblasts with S100A1 resulted in a decrease in the expression of genes, which are characteristics for the formation and function of myofibroblasts. Already at the 4 hour time point the category of extracellular matrix components was the most downregulated group. S100A1 stimulation also led to a

prominent suppression in the expression of genes, which are responsible for the stress fiber formation and cytoskeleton production, as well as for the collagen and collagen fibril organization. Besides the downregulation of various myofibroblast-related categories, according to the GSEA analysis S100A1 also suppressed mitosis related categories, for example, condensed chromosome kinetochore, chromosome segregation, and mitosis. However, the interpretation of the effect of S100A1 as an anti-mitotic and, therefore, anti-proliferative might be misleading, because the list of upregulated functions included also the category of positive regulation of proliferation, and previous studies have demonstrated no effect of S100A1 on the proliferation of cardiac fibroblasts [64,182].

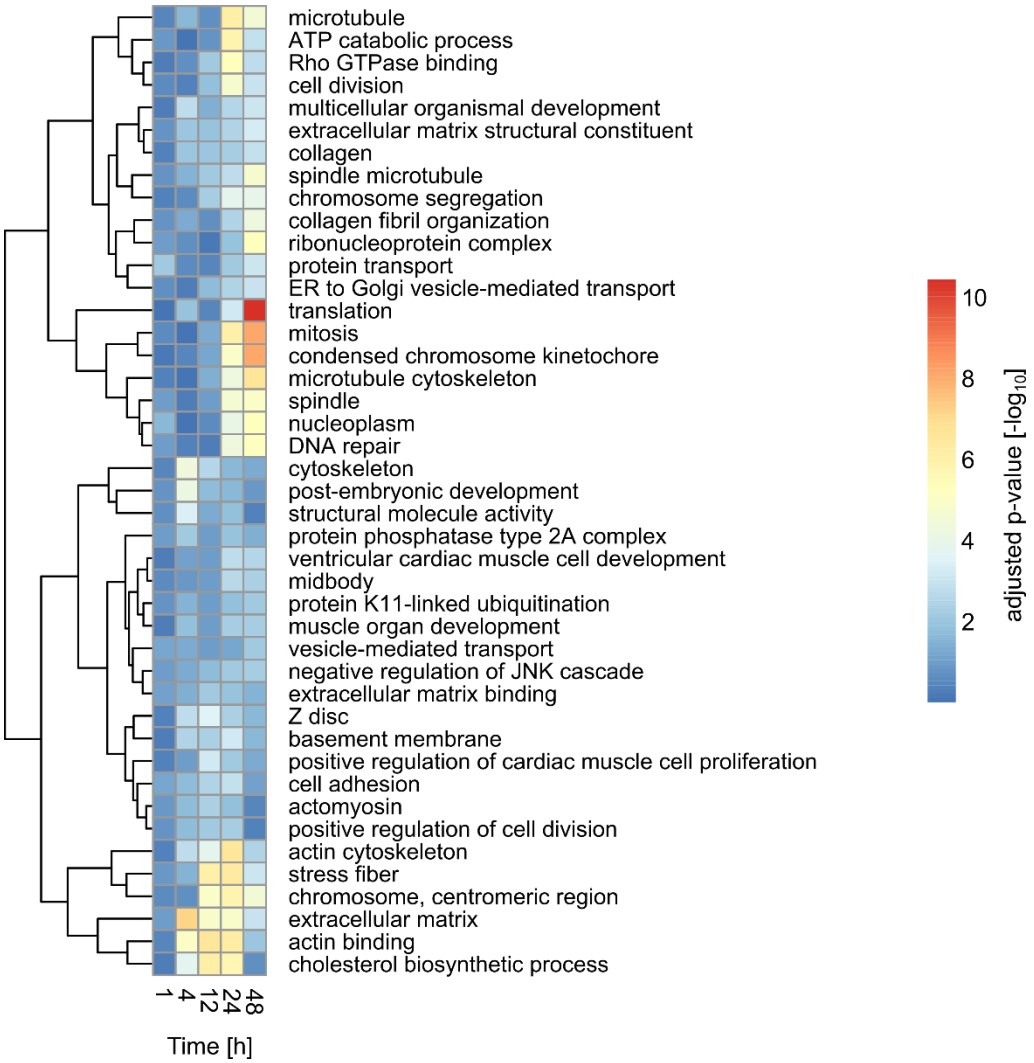

Figure 14: S100A1 stimulation leads to suppressed expression of extracellular matrix and cytoskeleton genes in cardiac fibroblasts.

Significantly downregulated biological functions of the transcriptome from ACF after 1, 4, 12, 24 and 48 hour stimulation with S100A1. Downregulated biological functions were calculated with GSEA. The earliest and most notably downregulated clusters of genes comprised categories of extracellular matrix and cytoskeleton.
(ACF, n=1, S100A1 1µM, 0.5 % FCS)

In summary, the analysis of transcriptome from S100A1-treated adult cardiac fibroblasts revealed an early and notable upregulation of the immune response gene expression, particularly, chemokine activity. It was accompanied by the downregulation of the functional categories, which are related to the formation of extracellular matrix. The activation of immune response and suppression of extracellular matrix formation suggest a phenotype of cardiac fibroblasts, which resembles the response to other cardiovascular DAMPs, interleukin 1 and HMGB1. Both of them are shown to induce the cytokine production in cardiac fibroblasts without increasing or even suppressing the classical myofibroblast-related markers, such as collagens or αSMA [106,127,128,132].

6.2 Characterization of S100A1-Evoked Pro-inflammatory Phenotype of Cardiac Fibroblasts on Protein Level

The biological functions of the cell are driven by proteins [183]. The rate of their production may differ from the respective gene expression [172]. Therefore, in the next step the expression levels of proteins were investigated in order to verify the transcriptome data and further analyze the phenotype of cardiac fibroblasts upon stimulation with S100A1. Liquid chromatography-tandem mass spectrometry (LC-MS/MS) technology was applied for protein detection. Since the most notable differences from the transcriptome analysis indicated changes in the production of secreted proteins, the secretome from cardiac fibroblasts was investigated further. The mass spectrometry-based analysis was performed on the supernatant from S100A1-treated and control fibroblasts.

Proteins were considered for the further analysis, if identified with at least 2 peptides, from which at least one was uniquely assigned to the particular protein. After filtering out the contaminants and false positive hits 606 proteins remained. From them 380 proteins were annotated to be extracellular (see section 5.2.6.2). 319 and 326 extracellular proteins overlapped in all 3 biological replicates from control and S100A1 samples, respectively. 316 extracellular proteins were detected in both control and S100A1-treated samples in all 3 biological replicates. Since mass spectrometry possesses high specificity, but relative low sensitivity [184–186], further analyses were performed with the set of all 380 proteins, thereby avoiding loss of proteins which might be missed in some experiments due to the limited power of detection.

6.2.1 Significantly Regulated Secreted Proteins

In order to visualize the effect of the stimulation with S100A1 on an individual secreted protein level, the relative fold change and significance for each protein were calculated by

one sample t-test. Proteins are depicted in a volcano plot (Figure 15), where red colored dots denote proteins with at least 2-fold (1 in $\log_2$ scale) upregulation and purple filled- at least 2-fold downregulation (-1 in $\log_2$ scale). For the separation between significantly and non-significantly regulated proteins, the threshold line for p value of 0.05 (1.3 in $-\log_{10}$ scale) is shown. All significantly up- or downregulated proteins are located above the line. The full list of differently changed proteins from the volcano plot and their p-values is included in the Supplementary table 1.

The volcano plot of single proteins revealed a marked effect of S100A1 on the relative increase of secreted proteins. Significantly downregulated proteins formed a numerously smaller group with less distinct fold changes between stimulated and unstimulated samples.

Ranked according to relative changes, the highest upregulated proteins from significantly increased ones were lipocalin 2 (Lcn2), chitinase-3-like protein 1 (Chi3l1), complement C3 and pentraxin 3 (Ptx3). In case of downregulated proteins, collagen 8a1 (Col8a1), C-type lectin domain family 3, member B (Clec3b), and osteoglycin (Ogn) had the lowest ratios from the significantly changed proteins.

The most prominently increased and significantly upregulated proteins possess various biological functions. Lipocalin 2 is reported to be involved in the attraction of neutrophils [187] and macrophage polarization into M1 phenotype [188]. In contrast, pentraxin 3 impedes recruitment of neutrophils and macrophages [189], but also protects cardiomyocytes from ischemia/reperfusion injury [190]. C3a, which is the subunit of C3, induces T helper 1 response and degranulation of peripheral blood mononuclear cells [191]. However, in the setting of ischemia/reperfusion injury C3a also confines neutrophils within the bone marrow [192]. Chitinase-3-like protein 1 is reported to protect macrophages against oxidant-induced cell death [193]. Altogether, all the highest rated upregulated proteins according to the volcano plot possessed diverse functions that do not complement each other.

The reported functions of the most downregulated from significantly regulated proteins correspond to the suppression of extracellular matrix formation. Collagen VIII is a structural component within the extracellular matrix [194] and osteoglycin takes part in its formation [195]. The functions of C-type lectin domain family 3, member B in the fields of cardiology or immunology are yet to be defined. This kind of functional suppression is consistent with the initially performed transcriptome analysis (see Section 6.1.2).

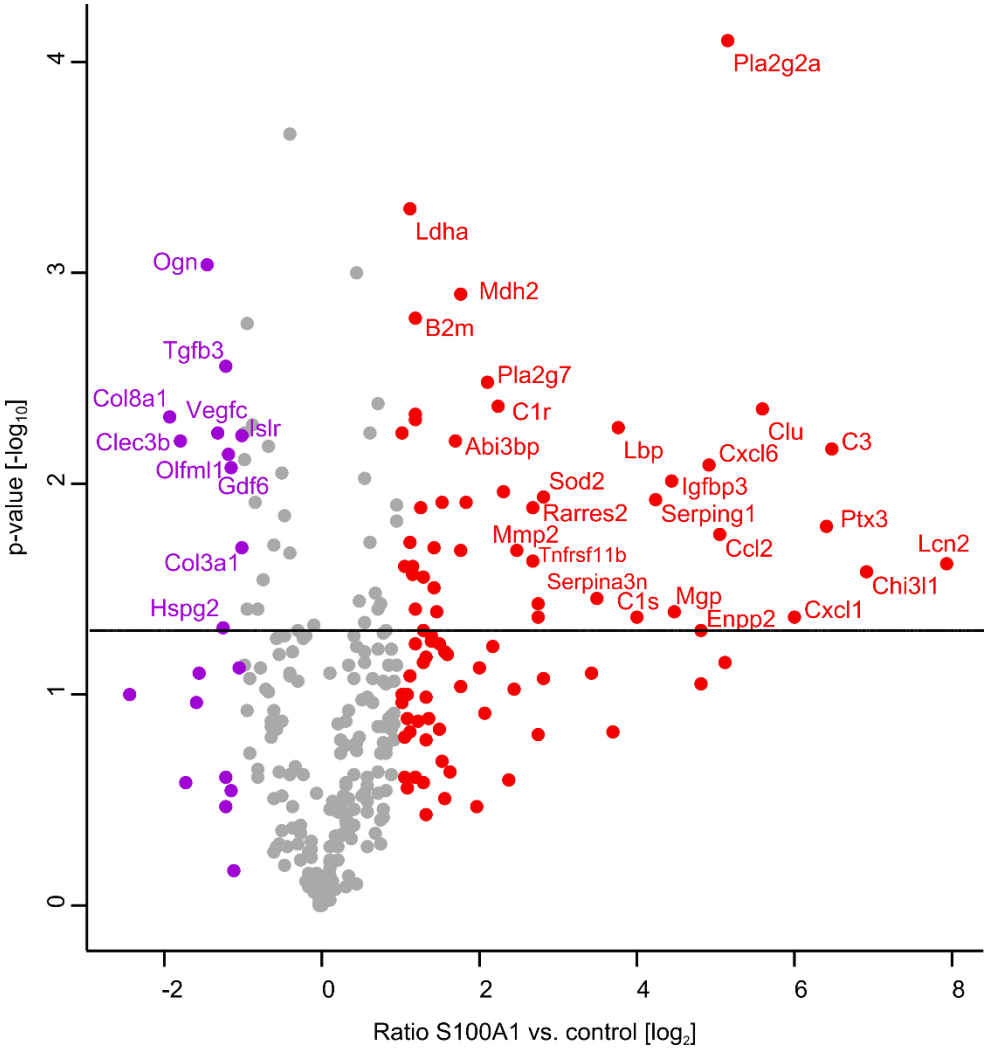

Figure 15: The profile of protein ratios indicates a prominent stimulatory and moderate suppressive effect of S100A1 on secreted proteins from cardiac fibroblasts.

Volcano plot of p-values against the ratios of secreted proteins upon the stimulation with S100A1. Purple filled circles- at least 2-fold downregulated proteins, red filled circles- at least 2-fold upregulated proteins. The majority of differentially regulated proteins is upregulated. Relative fold changes of the upregulated proteins reach higher values, as compared to the downregulated ones. The highest ranked upregulated proteins are Lcn2, Chi3l1, C3 and Ptx3, whereas the most dowregulated significantly regulated proteins are Col8a1, Clec3b and Ogn.
(ACF, n=3, S100A1 1µM, 48 h stimulation, 0% FCS, Lcn2- lipocalin 2, Chi3l1- chitinase-3-like protein 1, C3- complement C3, Ptx3- pentraxin 3, Col8a1- collagen 8 A1, Clec3b- C-type lectin domain family 3, member B, Ogn- osteoglycin)

The sorting of proteins according to their fold change versus control and significance allows to assess the effect of S100A1. It demonstrated a prominent stimulatory and moderate suppressive impact on the relative ratios of secreted proteins from cardiac fibroblasts. Moreover, the volcano plot enabled visualization of the proteins, which might be responsible for the biological effect of the secretome from S100A1 stimulated fibroblasts. However, the reported functions were not complementary for the proteins with highest significant relative changes. Therefore the biological activity of the secretome from

S100A1-treated cardiac fibroblasts was further analyzed by grouping proteins according to their biological functions.

6.2.2 Correlation between Transcriptome and Secretome

In order to analyze the link between gene expression changes and secreted proteins, relative fold changes from the transcriptome were correlated to the respective fold changes from the secretome. The differentially expressed mRNA translation into proteins may be delayed, the time lag between mRNA expression and protein production being 2-6 hours, when the correlation between gene expression and protein production are described to be the highest [196,197]. Since the protein secretion can potentially be even more delayed from the respective gene expression than protein production, the secretome analysis after 48 hours of stimulation was correlated with the previous available time point from the time-resolved transcriptome analysis, which was 24 hours.

As can be seen in Figure 16, the gene expression profile is highly correlated with the protein pattern from the secretome. The correlation is described by the Pearson correlation coefficient R=0.76. Among the secreted proteins, the most upregulated proteins were lipocalin 2 (Lcn2), chitinase-3-like protein 1 (Chi3l1), and complement C3 with higher fold changes on the protein level, as compared to the gene expression. On the transcriptome level, the highest relative increase was detected for Cxcl6, autotoxin (Enpp2) and phospholipase 2 group II a (Pla2g2a), all of which demonstrated more prominent relative ratios on the gene expression level as compared to the fold changes on the secretome level. Overall, higher fold changes of proteins are linked with lower fold changes of the respective gene expression, as can be seen from the equation of the trend line y=0.66x-0.23, where x and y denotes fold change from the secretome and fold change from the transcriptome, respectively.

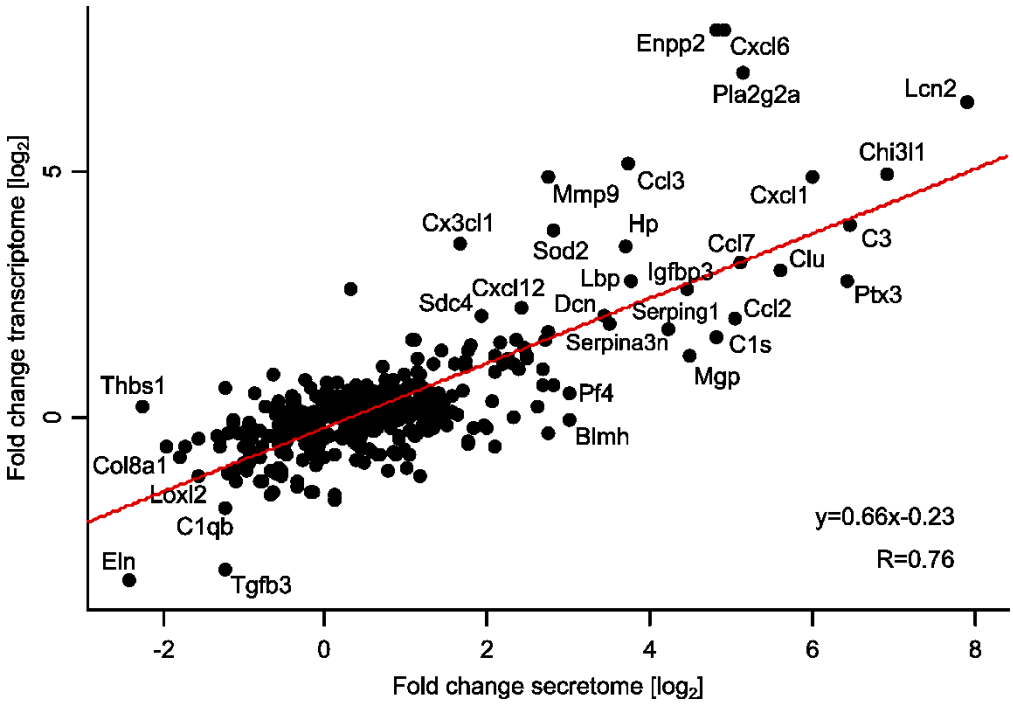

Figure 16: S100A1-triggered transcriptomic changes in cardiac fibroblasts are highly correlated with the relative changes of the protein secretion.

Relative gene expression changes after 24 hours are strongly correlated with the fold changes of the secreted proteins after 48 hours. The correlation is described by the Pearson correlation coefficient R=0.76. Higher fold changes of secretome are correlated with lower fold changes of transcriptome, as also seen in the equation of the trend line y=0.66x-0.23.
(ACF, S100A1 1µM, for the secretome- 0% FCS, n=3, 48 h stimulation, for the transcriptome- 0.5%FCS, n=1, 24 h stimulation, y denotes fold change secretome [log_2], x denotes fold change transcriptome [log_2])

The correlation of the serial transcriptome and secretome data demonstrates that according to the Pearson correlation the profile of secreted proteins after 48 hours is highly correlated with the respective gene expression pattern after 24 hours. It is consistent with the previously reported correlation analysis between the gene expression and protein production within the cell, where the profile of transcriptomic and proteomic fold changes are clearly interdependent [198]. However, the increase or decrease of the expression at the level of individual genes was not an indication that the secreted protein level will be changed to the same extent. Furthermore, it has been demonstrated that the amount of produced proteins mainly depends on the translational activity, and some gene increases might be silenced with a slowed or arrested further translation [172,199,200]. These results once again underline the importance of the verification of the transcriptome data on the level of proteins.

6.2.3 Biological Functions of Secretome

Analysis of the serial transcriptome from cardiac fibroblasts upon stimulation with S100A1 revealed a prominent upregulation of the inflammatory gene pattern with reduced stress fiber and extracellular matrix gene activity. In order to validate the transcriptional changes and define specific biological functions of the secreted protein profile, a functional enrichment analysis of the secretome was performed.

At first, all relative fold changes of the secreted proteins were sorted with 1D annotation enrichment. For the annotation, category identifiers of biological process, molecular function, and keywords from UniProt [171] were used. The enrichment was depicted as a position score, which shows the center of distribution for the values of the particular category in relation to the distribution of all values. Categories closer to -1 stand for the enrichment among proteins with low relative ratios, whereas shift towards 1 indicates the enrichment among proteins with high relative ratios (for the details see section 5.2.6.3 Statistical Analysis and Biological Classification).

In Figure 17 the 1D enrichment analysis of the most upregulated and downregulated protein categories is summarized. The upregulated protein categories comprised numerously more entities with higher position scores. Chemotaxis, chemokine receptor binding, and chemokine activity were the most prominently increased categories. At the same time the most downregulated categories were collagens and extracellular matrix part (the detailed analysis and list of proteins per category see Supplementary table 2, Supplementary table 3, Supplementary table 4). These data support results from transcriptome analysis, suggesting that S100A1 elicits distinct activation of cardiac fibroblasts from the well-known myofibroblast phenotype that is characterized by the increased extracellular matrix protein secretion [106,201].

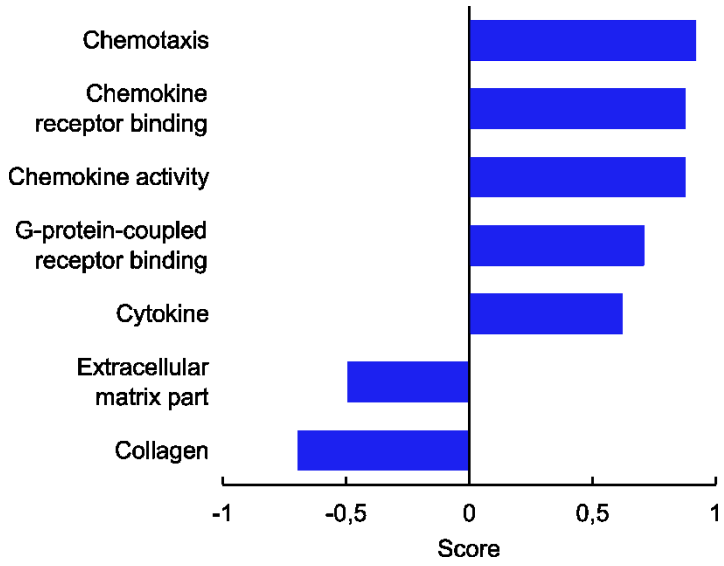

Figure 17: S100A1 evokes upregulation of inflammatory protein secretion and downregulation of extracellular matrix components in cardiac fibroblasts.

All secreted proteins were clustered together with a 1D annotation enrichment according to their relative ratios. The most downregulated categories are collagen and extracellular matrix part. The most upregulated functions are chemotaxis, chemokine receptor binding, and chemokine activity. Enrichment per category is indicated as a position score, where the center of values of particular category is depicted in relation to the center of values from the rest of members, which are included in the calculation.
(ACF, n=3, S100A1 1µM, 48 h stimulation, 0% FCS)

In order to cluster upregulated proteins into categories according to their biological function Fisher's exact test was applied. Similar to 1D annotation enrichment analysis, labels from UniProt, which comprised biological process, molecular function and keywords, were applied. In 1D annotation enrichment all ratios are taken into account, thus also a small increase in protein secretion contributes to the overall enrichment of the particular functional category. In contrast to 1D annotation enrichment, in the Fisher's exact test the threshold value for the upregulation of each protein must be introduced. Within this group no further ranking of the proteins according to their fold changes is applied. As a threshold level a 4-fold increase was used. Biological functions were ranked according to the enrichment factor, which indicates the number of proteins from the particular category with more than 4-fold upregulation versus the total number of detected proteins from the same category (for the formula of the calculation see section 5.2.6.3 Statistical Analysis and Biological Classification).

Results of the Fisher's exact test are shown in Figure 18. All the highest enriched functions were related to different aspects of inflammatory reaction. The three top-rated categories were chemokine-mediated signaling pathway, chemotaxis, and chemokine activity, which

indicates a strong induction of chemoattractant protein secretion. The full analysis of the Fisher's exact test is given in Supplementary table 5.

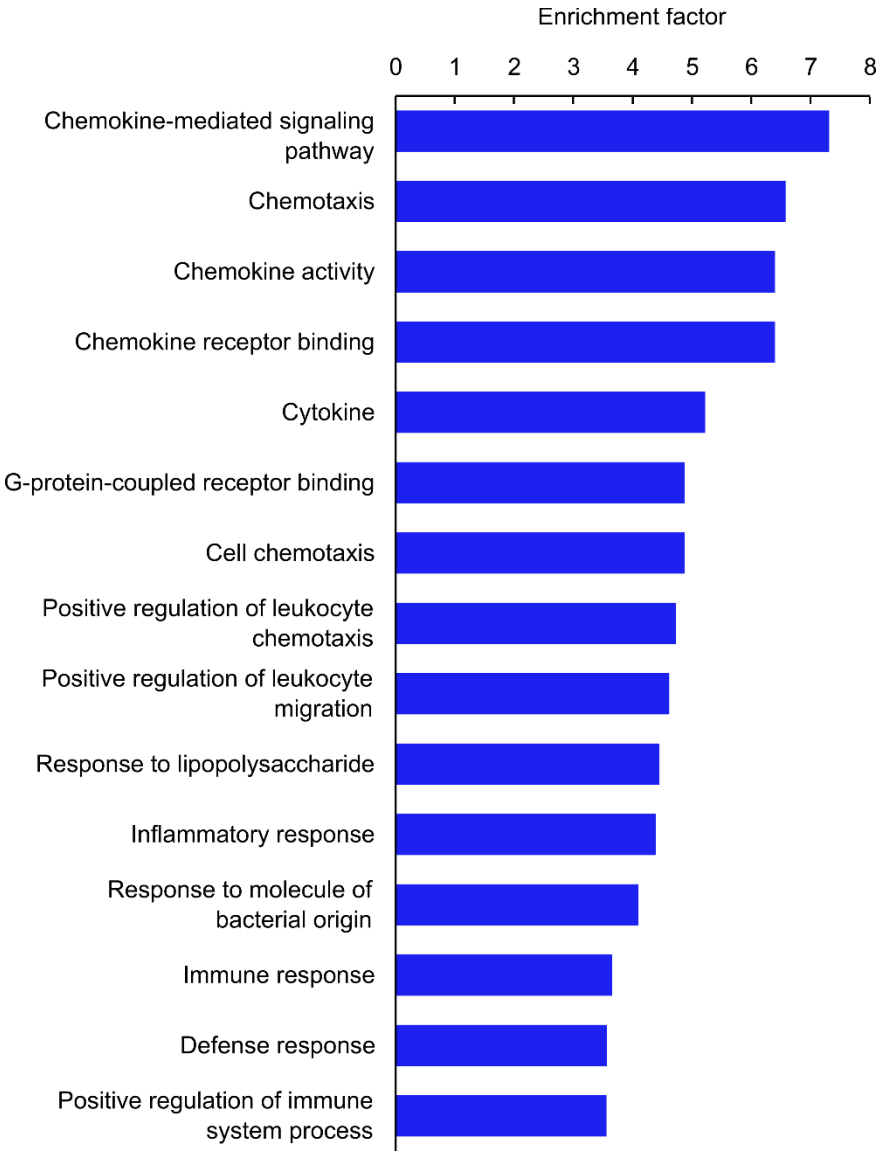

Figure 18: Functions that are responsible for chemoattraction are the most enriched categories among the upregulated proteins in the secretome from cardiac fibroblasts stimulated with S100A1.

Fisher's exact test of biological functions for more than 4-fold upregulated secreted proteins. The most enriched functions are chemokine-mediated signaling pathway, chemotaxis and chemokine receptor binding.
The value of enrichment factor indicates the size of the group of more than 4-fold upregulated proteins, which belong to the particular category, normalized with the number of all proteins from the same category.
(ACF, n=3, S100A1 1µM, 48 h stimulation, 0% FCS)

The highest stimulatory effect of S100A1 is exerted on the inflammatory response, as can be seen from the most upregulated biological functions (Figure 18). The proteins that define the first 15 most enriched categories from the Fisher's test are listed in Table 4.

Chemoattractants are highlighted in dark blue. They determined the first three most enriched functions from the Fisher's test. It is important to note that these proteins match also with the members of the first three most upregulated functions according to the 1D annotation enrichment analysis (see Supplementary table 3).

Table 4: Proteins that determine the enrichment of immune response functions according to Fisher's exact test in the secretome from S100A1 stimulated cardiac fibroblasts.

In dark blue highlighted proteins corresponds to the three most upregulated biological functions, which cover the chemoattraction functions.

Gene name	Protein name	Fold changes [log_2]	Gene name	Protein name	Fold changes [log_2]
Lcn2	Lipocalin-2	7.91	Pf4	Platelet factor 4	3.02
C3	Complement C3	6.46	Sod2	Manganese-superoxide dismutase	2.80
Ptx3	Pentraxin 3	6.41	Mmp9	Matrix metalloproteinase-9	2.74
Cxcl1	C-X-C motif chemokine 1	6.00	Cd44	Phagocytic glycoprotein-1	2.73
Ccl7	C-C motif chemokine 7	5.12	Tnfrsf11b	Osteoprotegerin	2.67
Ccl2	C-C motif chemokine 2	5.05	Rarres2	Chemerin	2.67
Cxcl6	C-X-C motif chemokine 6	4.91	Mmp2	Matrix metalloproteinase-2	2.49
C1s	Complement C1s subcomponent	4.81	Csf1	Macrophage colony-stimulating factor 1	2,45
Enpp2	Autotaxin	4.81	Cxcl12	Stromal cell-derived factor 1	2.41
Serping1	Plasma protease C1 inhibitor	4.22	Spp1	Osteopontin	2.35
Lbp	Lipopolysaccharide-binding protein	3.78	Mmp10	Stromelysin 2	2.33
Ccl3	C-C motif chemokine 3	3.73	C1r	Complement C1r subcomponent	2.25
Hp	Haptoglobin	3.71	Cxcl3	C-X-C motif chemokine 3	2.16
Serpina3n	Serine protease inhibitor A3N	3.49	Pla2g7	Phospholipase A2, group VII	2.09
Dcn	Decorin	3.43			

The functional enrichment analysis of the secretome indicated a prominent upregulation of immune response, in particular, chemoattractant function. It was accompanied by a moderately decreased secretion of extracellular matrix structural proteins, thereby confirming the results from the serial transcriptome analysis (see section 6.1.2). In the following analysis, the effect of stimulation with S100A1 on the absolute amounts of proteins was examined.

6.2.4 Effect of S100A1 on Absolute Protein Amounts

Previously described biological functions and significantly upregulated single proteins were calculated based on the relative changes of each protein in the supernatant from S100A1-stimulated fibroblasts. However, this approach neglects the total amounts of proteins. Hence, it is not possible to evaluate whether the S100A1-elicited changes of the protein profile and biological functions relevantly impacts the absolute profile of secreted proteins and prevailing functions of cardiac fibroblasts. To distinguish, whether the detected alterations are minor deviations or notable hallmarks of a new pattern of the secretome of cardiac fibroblasts, proteins were sorted and analyzed according to their absolute abundance, expressed as an iBAQ value (in $\log_{10}$). It represents the sum of the peak intensities of detected peptides from one protein divided by the number of theoretically obtainable peptides per respective protein (for detailed information see 5.2.6.2).

1D functional enrichment analysis was performed on the sets of iBAQ values obtained from control and S100A1-treated samples. S100A1-targeted proteins, which comprised the most upregulated biological functions according to relative ratios, were grouped into a separate category. According to Fisher's exact test the most upregulated biological functions were immune response categories (Figure 18). Thus, the respective S100A1-targeted proteins (highlighted in Table 4) were grouped in a separate category and termed "Immune response". It encompasses 29 proteins, such as lipocalin-2, complement C3 and pentraxin 3. From the upregulated immune response categories the top three most enriched ones were chemoattractant categories. The proteins, which defined this upregulation, were grouped in a separate category "Chemoattractant" (10 proteins, highlighted in dark blue, in Table 4). Majority of them were CC or CXC chemokines, such as CXCL1, CCL2 and CCL7.

In the control group (Figure 19A) the 1D enrichment analysis from iBAQ values revealed the significant enrichment of collagens, which was detected at the region of proteins with the highest absolute abundances (position score 0.57). It is in agreement with the basal function of cardiac fibroblasts as extracellular matrix maintaining cells [106]. After the stimulation with S100A1 the significantly enriched categories comprised S100A1-targeted immune response proteins and, particularly, chemoattractants (Figure 19B). Both of these categories were enriched among proteins with highest iBAQ values with a position score 0.65 for the group of S100A1-targeted chemoattractants and 0.53 for the category of S100A1-targeted immune response. Full 1D enrichment analysis is included the

Supplementary table 6. These data point towards a phenotypic shift of cardiac fibroblasts from collagen- to predominantly chemoattractant-secreting cells in response to S100A1.

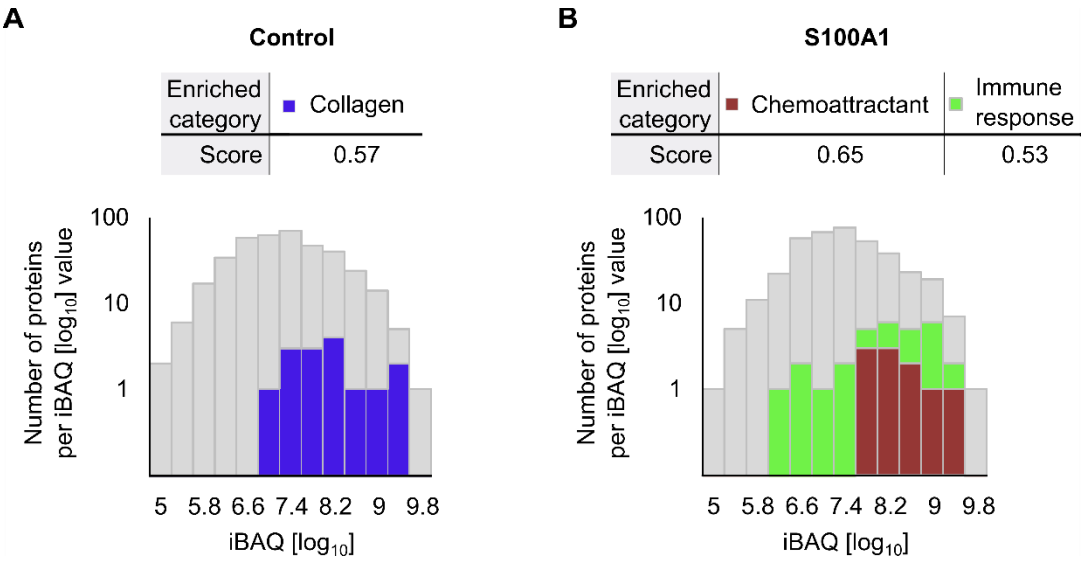

Figure 19: The most abundantly secreted proteins are changed from collagens in control to immune response factors and chemoattractants, in S100A1-treated fibroblasts.

The histogram of the distribution of absolute amounts of quantified proteins, expressed in iBAQ values (in units of $\log_{10}$), in (A) control and (B) S100A1-treated samples. The colored histograms depict proteins that were grouped in significantly enriched categories according to the 1D enrichment analysis from iBAQ values of all proteins. In control samples (A) the only significantly enriched functional category is collagen (blue histogram) with the position score of 0.57. In the S100A1-stimulated samples (B) the significantly enriched categories comprised S100A1-targeted chemoattractants (dark red histogram) and S100A1-targeted immune response proteins (green histogram) with a position score of 0.65 and 0.53, respectively.

Position score indicates the center of iBAQ distribution of the particular category relative to the distribution of all iBAQ values. Values closer to 1 indicates enrichment of the category among the proteins with the highest iBAQ values, whereas values towards -1 stands for the enrichment closer to the lowest iBAQ values.

(ACF, n=3, S100A1 1µM, 48 h stimulation, 0% FCS)

Next, the composition of the supernatant from S100A1 stimulated fibroblasts was evaluated. The absolute abundances of secreted proteins from the stimulated sample were plotted as the function of their fold changes (Figure 20). Green filled circles depict S100A1-targeted proteins that determine the most upregulated concordant biological functions according to Fisher's exact test, namely, immune response functions. Illustrated in dark red are proteins that define the three most upregulated categories, which are chemokine-mediated signaling pathway, chemotaxis, and chemokine activity according to Fisher's exact test. From the proteins with common biological functions the most abundant and the highest upregulated ones are CCL2, CCL7, CXCL1, pentraxin 3 (Ptx3), and lipocalin 2 (Lcn2). Additionally, the first three of them are members of the most enriched category upon S100A1 stimulation, "chemoattraction". Moreover, lipocalin 2 is also

reported to be a potent chemoattractant [187], thereby supporting the assumption that chemotaxis stimulation is the main biological function of the secretome from cardiac fibroblasts upon exposure to S100A1.

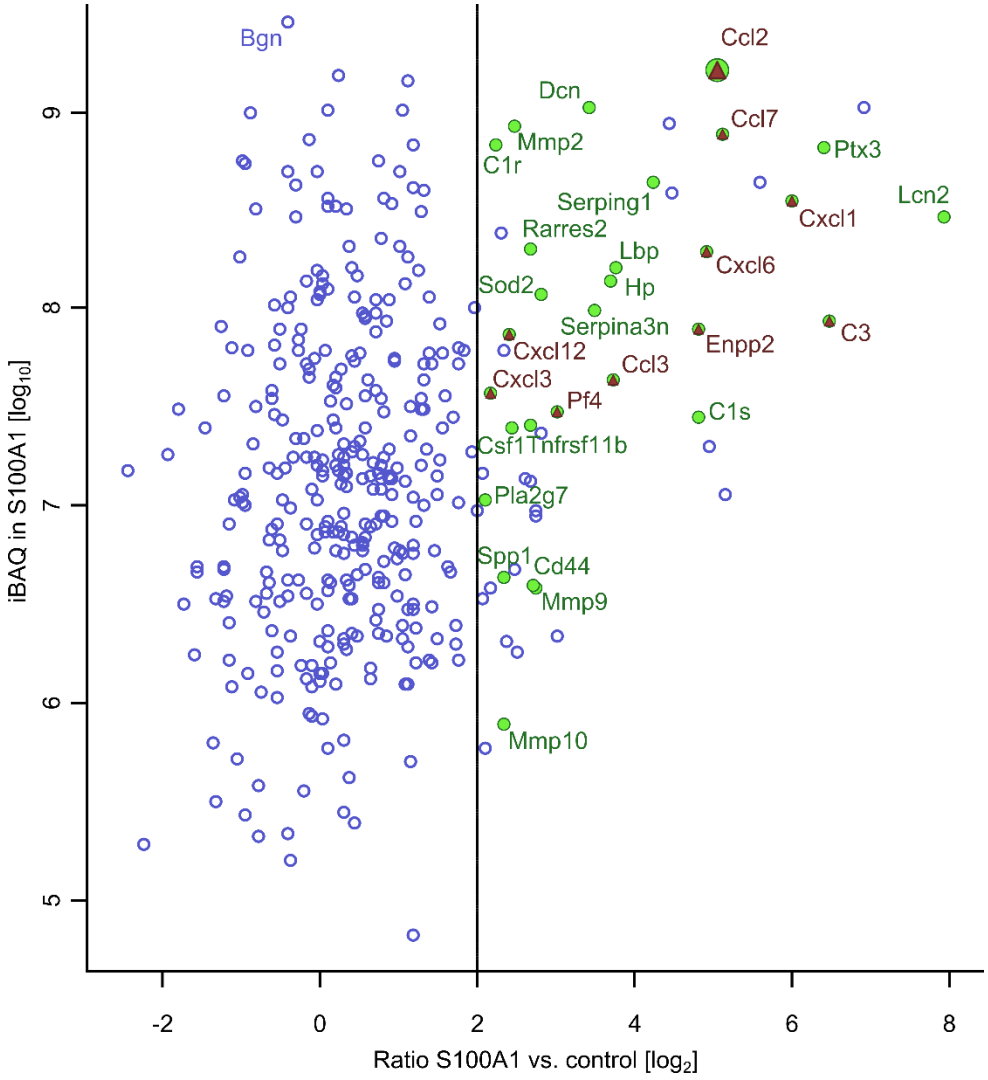

Figure 20: CCL2 is the most abundantly secreted upregulated protein in S100A1-stimulated cardiac fibroblasts.

Absolute amounts (iBAQ [log_{10}]) of each protein in S100A1-stimulated samples against respective ratios from the treatment with S100A1 versus controls (in units of log_2). CCL2 possesses the highest absolute amount from the detected S100A1-targeted immune response proteins.
Vertical line separates more than 4-fold upregulated proteins. Solid circles represent proteins, which define the upregulation of immune response function, as determined by the Fisher's exact test. Dark red triangles depict proteins, which determine the enrichment of predominantly upregulated chemoattraction function.
(ACF, n=3, S100A1 1µM, 48 h stimulation, 0% FCS)

Of all S100A1-targeted immune response proteins, CCL2 was determined to be the most abundant one. Evaluation of the iBAQ values for all detected proteins indicated that CCL2 was among the most secreted proteins from the whole secretome. The only protein that

had a higher iBAQ value than CCL2 was biglycane (Bgn), which was slightly downregulated upon the stimulation with S100A1.

The analysis of the absolute abundances of the proteins in the supernatant revealed that the secretome of the cardiac fibroblasts upon S100A1 stimulation was shifted towards an inflammation governing pattern. Detailed examination of the upregulated proteins indicated chemoattractant CCL2 [202] as the most abundantly secreted protein.

6.2.5 Comparison of Serum Starvation Conditions for Secretome Analysis

For the transcriptome experiment, cardiac fibroblasts were starved and stimulated in DMEM containing 0.5% FCS. For the mass spectrometry analysis, the external protein content in the supernatant had to be reduced to a minimum. Therefore, samples for the mass spectrometry based analysis were prepared in DMEM containing no FCS. To examine the effect of FCS on the secreted protein profile, the detectable protein composition was tested in the cell supernatant from DMEM with 0% or 0.5% FCS supplementation with or without additional exposure to S100A1.

The pattern of proteins after gel electrophoresis from the 0.5% FCS group showed a clear accumulation of the serum at the region of 60 kDa, indicating a strong contamination with serum albumin (Figure 21A). In the 0.5% FCS group the accumulated serum proteins would mask the proteins produced by cardiac fibroblasts, therefore this part of the gel was excluded from further mass spectrometry analysis. The protein lane from 0% FCS group, on the contrary, was subjected to the LC MS/MS in full length.

In the next step, the number of detectable extracellular proteins was compared between 0% and 0.5% FCS groups (Figure 21B). As expected, the 0% FCS treated sample contained more proteins than the 0.5% group. 363 and 292 proteins were identified in the 0% and 0.5% FCS group, respectively. 251 of them were detected in both groups.

In order to evaluate a possible impact of serum starvation conditions on the protein production and secretion, the absolute amounts of each protein from both groups were correlated using Pearson correlation coefficient. The absolute protein amounts were calculated as an iBAQ (intensity based absolute quantification) value. As shown in the Figure 21C, iBAQ values for proteins from 0% and 0.5% FCS group are strongly correlated, as described by a Pearson correlation coefficient of R=0.72.

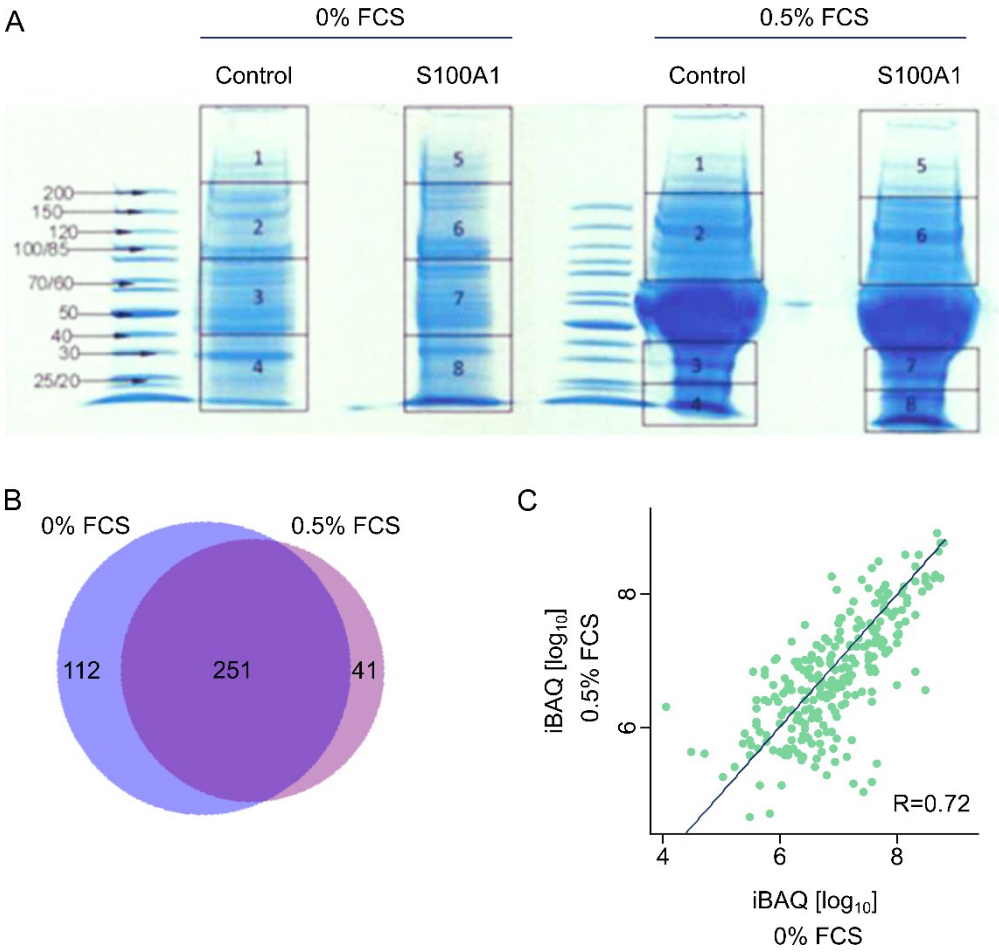

Figure 21: Cardiac fibroblast treatment with 0.5% FCS in comparison with 0% FCS leads to less proteins detected in the supernatant by mass spectrometry without affecting their absolute amount.

(A) Proteins were separated with a gel electrophoresis and stained with Coomassie blue. Samples with 0.5% FCS treatment showed accumulation of calf serum proteins with the maximum at around 60 kDa. For the 0.5% FCS group this part of the gel was excluded from the further analysis.
(B) Proteins were detected by LC MS/MS. The count of proteins in 0% FCS and 0.5% FCS treated samples were compared with a BioVenn, a web application for the comparison and visualization of biological lists. More proteins was detected in the 0% FCS treated sample.
(C) Absolute amount of each protein was expressed as iBAQ. The iBAQ values were correlated between the 0% and 0.5% FCS treated groups. 0% versus 0.5% FCS treatment had no substantial effect on the secreted protein amount, since iBAQ values from both groups were strongly lineary correlated (Pearson correlation coefficient R=0.72).
(ACF, n=1, S100A1 1µM, 48 h stimulation)

In conclusion, the presence or absence of serum during the stimulation period had no major effect on the amounts of detectable secreted proteins; however, due to the serum protein accumulation at the region of around 60 kDa this part of the gel could not be used for the secreted protein detection with mass spectrometry, resulting in lower number of identified proteins.

6.3 CCL2 Expression and Secretion by Cardiac Fibroblasts upon Stimulation with S100A1

According to the transcriptome and secretome data, the most upregulated biological function in response to S100A1 was chemokine activity. Analysis of single proteins from the secretome revealed that CCL2 is the most abundantly secreted chemokine. Therefore, the molecular mechanisms underlying increased CCL2 expression and secretion in S100A1-stimulated cardiac fibroblasts were further investigated.

6.3.1 Verification of S100A1-Triggered Upregulation of CCL2

Since the gene microarray-based approach possesses a high background noise, the investigation of single gene expression pattern requires qPCR [170,203]. Due to the limited sensitivity of the unlabeled mass spectrometry-based data acquisition [186], for the examination of time-dependent secretion pattern of individual proteins an ELISA assay is required. Therefore, CCL2 gene expression and protein secretion were verified and investigated by qPCR and ELISA, respectively.

In order to validate CCL2 gene expression with qPCR, cardiac fibroblasts were stimulated with S100A1 for 24 hours. CCL2 gene expression was significantly upregulated, showing a 10 fold increase over control (Figure 22A). The secreted protein was verified by treating cardiac fibroblasts with S100A1 for 48 hours. Subsequently the conditioned medium was subjected to ELISA analysis (Figure 22B). The treatment with S100A1 led to a substantial increase of CCL2 amount. In the control samples approximately 1.5 ng/mL of CCL2 was detected, whereas in the supernatant from stimulated cardiac fibroblasts the amount of CCL2 was increased to 27 ng/mL.

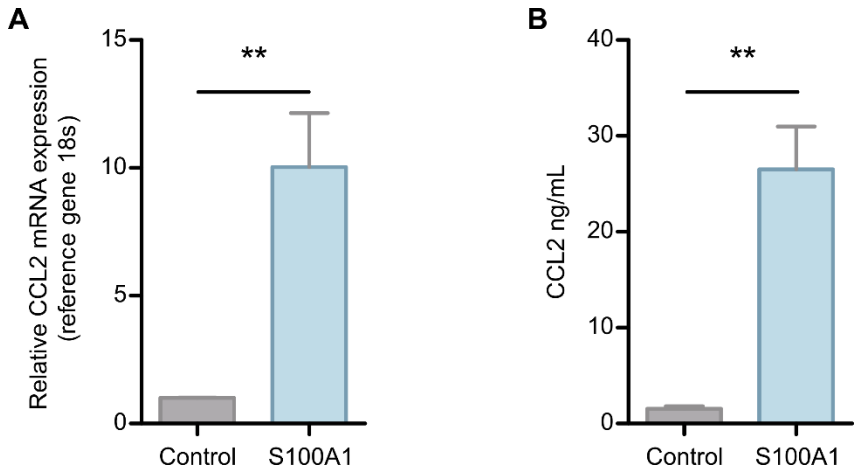

Figure 22: S100A1 stimulation of cardiac fibroblasts induces a robust upregulation of CCL2 gene expression and protein secretion.

(A) The verification of CCL2 gene expression increase with qPCR. CCL2 expression shows a prominent relative upregulation after 24 h treatment with S100A1. (n=5)
(B) ELISA verification of the upregulated CCL2 protein secretion upon treatment with S100A1 for 48 h. Stimulated samples contained high absolute amount of CCL2 protein, resulting in a prominent increase over control. (n=4)
(ACF, S100A1 1µM, 0% FCS **p<0.01 vs. control)

To examine the expression time course of CCL2, cardiac fibroblasts were stimulated with S100A1 for 4, 8, 12, 24 and 48 hours. In the data, kindly provided by Dr. Martin Busch, the expression increase of CCL2 mRNA started already at 4 hours (Figure 23).

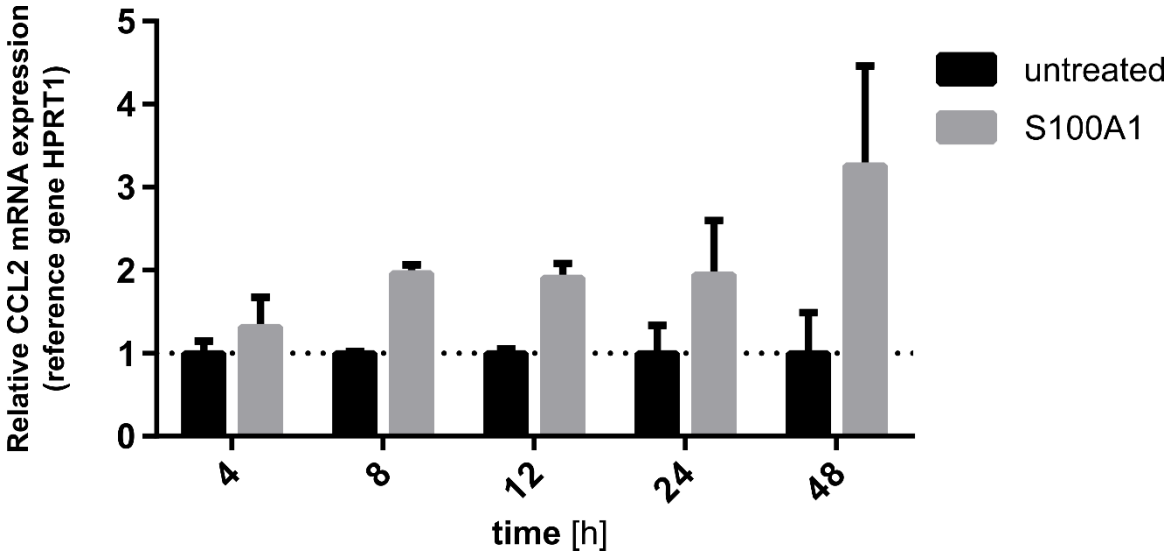

Figure 23: S100A1 induces an early upregulation of CCL2 gene expression.

Cardiac fibroblasts were incubated with S100A1 for 4, 8, 12, 24 and 48 hours. qPCR measurement indicated an increase of CCL2 mRNA already after 4 hours of stimulation.
(ACF, n=2, S100A1 1µM, 0% FCS)
Data and figure courtesy of Dr. Martin Busch.

The ELISA-based protein measurement indicated a very early upregulation of CCL2 at the secreted protein level (Figure 24A). The supernatant from S100A1-stimulated cardiac fibroblasts already after 4 hours contained 1.9 ng/mL of CCL2. After 48 hours the amount increased to 26 ng/mL. For comparison, control samples at 4 hour time point contained only 0.07 ng/mL CCL2, which increased to 2.3 ng/mL at 48 hours. Measuring CCL2 mRNA expression in the corresponding experiment, CCL2 was increased over control 23-fold and 21-fold at the 4 hour and 48 hour time points, respectively (Figure 24B).

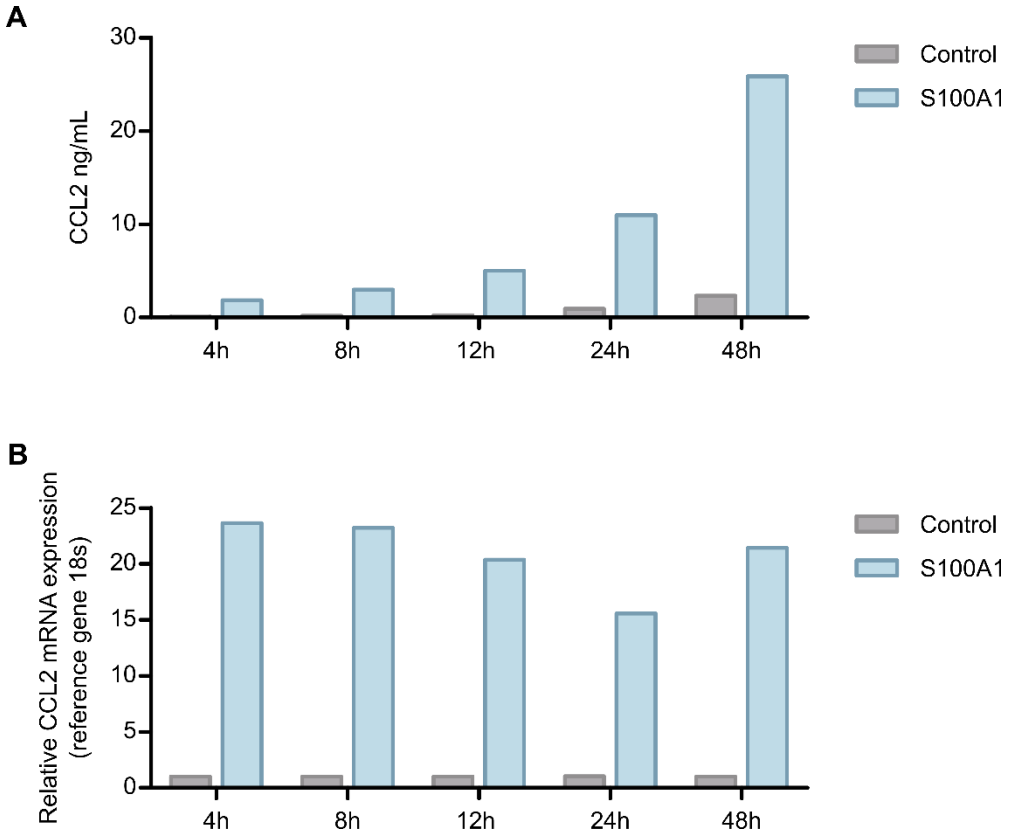

Figure 24: S100A1 evokes an early and stable upregulation of CCL2 protein secretion and mRNA expression.

Cardiac fibroblasts were stimulated with S100A1 for 4, 8, 12, 24, and 48 hours.
(A) ELISA of secreted CCL2. The increase of CCL2 protein in the supernatant was detectable already after 4 hours and notably accumulated over 48 hours.
(B) qPCR of CCL2 mRNA expression from the corresponding ELISA experiment. CCL2 was robustly increased at all measured time points.
(ACF, n=1, S100A1 1µM, 0% FCS)

The ELISA and qPCR experiments indicated a strong and early upregulation of CCL2 protein secretion and gene expression in cardiac fibroblasts upon stimulation with S100A1. The examination of mRNA expression and protein secretion time course showed a

prominent induction of CCL2 production already after 4 hours. Further incubation resulted in a substantial accumulation of CCL2 in the supernatant at all subsequent time points.

6.3.2 TLR4-Mediated Increase of CCL2 Expression

After internalization by cardiac fibroblasts, S100A1 binds to TLR4 [64]. TLR4 is crucially involved in the eliciting of inflammatory response after the myocardial infarction [204,205]. Activation of TLR4 has been shown to trigger CCL2 production [206]. Therefore, the involvement of TLR4 in S100A1-induced increase of CCL2 expression was investigated.

At first, TLR4 was chemically inhibited by using CLI095, which is also known as a resatorvid. It binds specifically to the intracellular domain of TLR4 and interferes with the subsequent interaction with TLR4 adaptor proteins that are needed for downstream signal transduction [207]. Results of chemical inhibition are shown in Figure 25. 30 minutes pre-incubation of cardiac fibroblasts with CLI095 completely abolished the S100A1-triggered CCL2 upregulation.

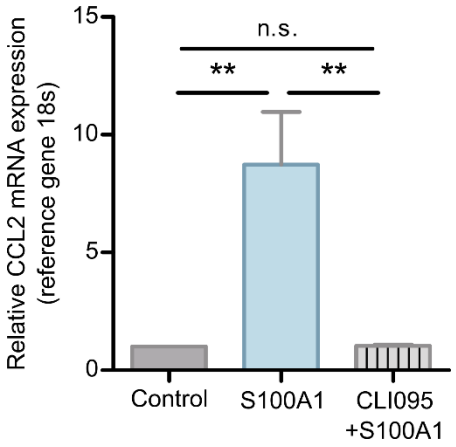

Figure 25: Chemical inhibition of TLR4 abolishes S100A1-induced CCL2 upregulation in cardiac fibroblasts.

Cardiac fibroblasts were treated with S100A1 for 24 hours with or without a 30 minute pre-incubation with TLR4 chemical inhibitor CLI095. The blockage of TLR4 resulted in a completely abrogated CCL2 mRNA increase upon the stimulation with S100A1, measured with qPCR.
(ACF, n=3, S100A1 1µM, CLI095 3 µM, 0% FCS **p<0.01)

In order to verify the TLR4 pathway-dependent suppression of CCL2 expression, a knockdown of TLR4 was established. 48 hours after transfection with TLR4 and scramble siRNA, qPCR analysis indicated knockdown to 10% TLR4 expression in comparison to scramble controls (Figure 26A). Consequently, cardiac fibroblast stimulation with S100A1 for 24 hours was performed 48 hours after transfection. After the stimulation with S100A1, CCL2 was significantly upregulated in cardiac fibroblasts, which were transfected with the scramble siRNA. The stimulation resulted in a 21-fold increase of CCL2 over the untreated

scramble control (Figure 26B). TLR4 knockdown suppressed the S100A1-mediated upregulation of CCL2.

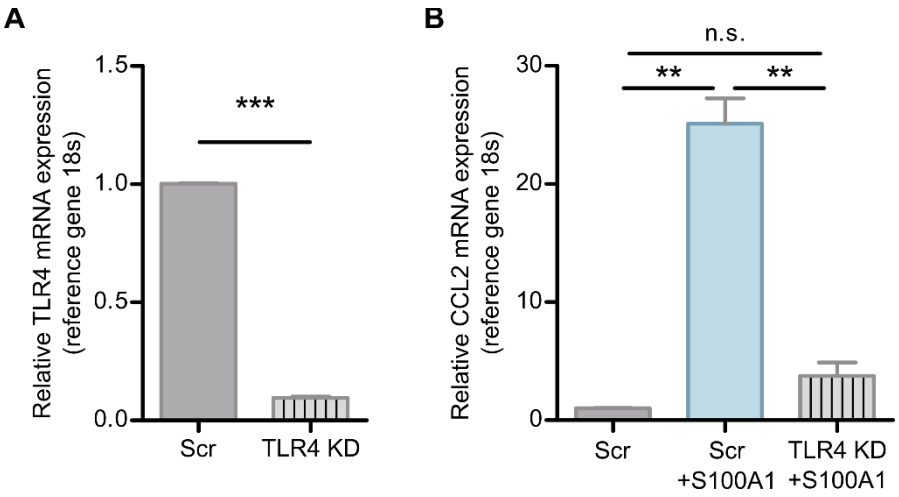

Figure 26: TLR4 knockdown blocks the increase of CCL2 in S100A1-stimulated cardiac fibroblasts.

(A) Cardiac fibroblasts were transfected with scramble (Scr) and TLR4 siRNA. After 48 h the efficiency of knockdown was verified with the qPCR, which showed a 10% rest expression of TLR4.
(B) 48 h after the transfection cells were stimulated with S100A1 for 24 hours. TLR4 knockdown suppressed the upregulation of secreted CCL2 from S100A1-stimulated cardiac fibroblasts.
(ACF, n=3, S100A1 1µM, Scr and TLR4 siRNA 50 nM, 0% FCS **p<0.01 ***p<0.001)

Taken together, the data from chemical inhibition and knockdown of TLR4 provide evidence for a direct involvement of TLR4 activation in S100A1-triggered increase of CCL2 expression in cardiac fibroblasts.

7 Discussion

Upon myocardial infarction, S100A1 is released from damaged cardiomyocytes and rapidly endocytosed by neighboring cardiac fibroblasts *in vivo* [64,158,159]. S100A1 internalization subsequently triggers activation of ERK1/2 and NFκB signaling pathways in cardiac fibroblasts, resulting in fundamental gene expression changes of inflammatory and fibrotic genes. The aim of this study was to provide a detailed characterization of the S100A1-mediated cardiac fibroblast phenotype in order to define its possible biological function *in vivo*. For this purpose time-resolved whole transcriptome and comprehensive secretome analyses were performed on S100A1-treated adult rat cardiac fibroblasts *in vitro*. Within the first hours of S100A1 stimulation, cardiac fibroblasts acquired a marked chemoattractant phenotype. The most abundantly secreted chemokine was CCL2, a cytokine that is reported to be critically involved in the healing cascade after myocardial infarction [208]. The initial cellular source of CCL2 after myocardial infarction *in vivo* is so far poorly understood [209]. This study provides first evidence for a rapidly evolving chemoattractant phenotype of cardiac fibroblasts upon exposure to extracellular S100A1. This indicates that cardiac fibroblasts might actively participate in the initiation of the inflammatory response to ischemia/reperfusion injury *in vivo*.

7.1 Time-Resolved Transcriptomic Analysis of Cardiac Fibroblast Phenotype upon Stimulation with S100A1

Previous studies on both adult and neonatal cardiac fibroblast cell cultures showed an anti-fibrotic and both pro- and anti-inflammatory response upon the stimulation with S100A1 [64,210]. Effect on the inflammatory response was demonstrated by the increase of pro-inflammatory ICAM1 and anti-inflammatory IL10 expression. Anti-fibrotic effect was detected by a prominent downregulation of collagen 1 and αSMA [64,210]. Since the downregulation of pro-fibrotic genes contradicts the classical fibroblast activation and transformation into myofibroblasts [211], a time-resolved transcriptome analysis was performed in order to elucidate the whole gene expression profile of cardiac fibroblasts upon their exposure to extracellular S100A1. This approach was chosen because it offers a comprehensive and unbiased estimation of all gene expression driven events, discriminated by an early or late manifestation. For the evaluation of the complete transcriptomic profile over time a principal component analysis was performed. It reduces multiple gene expressions of samples to only two dimensions, which represents the greatest variances of gene expressions between different samples. Thereby, principal component analysis allows the evaluation of the degree by which samples differ from each other.

S100A1 elicited an early and marked cardiac fibroblast activation. Notably, already after 2 to 4 hours of stimulation with S100A1, the gene expression profile strongly deviated away from the control fibroblasts. The gene expression pattern upon treatment with S100A1 dynamically changed until the last measured time point at 48 hours. The effect of cell culturing conditions on the gene expression changes were measured by the principal component analysis of unstimulated samples, which showed only modest changes.

In order to understand the biological role of the gene expression changes upon S100A1 stimulation a gene set enrichment analysis (GSEA) was performed. GSEA is a computational tool that allows to build a hypothesis about possible biological functions. It is based on the clustering of gene expression ratios according to their involvement in different biological pathways [169,170]. This approach provides several advantages over the conventional focus on the individual most up- or downregulated genes, especially in the evaluation of differentially regulated cellular processes. First, the biological function may be driven by the majority of regulated genes, which individually do not possess high relative changes. Second, the group of the most upregulated genes may include members without a concordant biological function. Finally, it may be hard to reproduce the results of relative changes of individual genes, since the gene microarrays possess a high background noise. GSEA overcomes these limitations by an unbiased functional classification that is based on the analysis of all gene expression changes [169,170,203].

GSEA of S100A1 stimulated cardiac fibroblasts revealed an early and strong upregulation of inflammatory biological functions. Already after 1 hour, the chemokine activity was the most upregulated function, remaining the most notably increased biological activity at all subsequent time points. It is in line with the transcriptome analysis of cardiac fibroblasts upon the treatment with S100A8/9, which is another DAMP that is involved in cardiovascular pathologies [98]. There the most upregulated function has been reported to be chemokine activity [134]. Also other highly upregulated functions upon stimulation with S100A1 covered different aspects of inflammatory activity, such as response to tumor necrosis factor or neutrophil chemotaxis.

Besides biological functions, GSEA categories include intracellular signaling pathways, which are predicted according to gene expression changes that are reported to be driven by the activation of particular signaling cascades. Stimulation with S100A1 led to enrichment of categories ERK1/2, NFκB and TLR4 signaling pathway. To TLR4 signaling pathway annotated genes with the highest relative expression changes after 24 hours were Tnip3, Lbp and Nfkbia. For I-kappaB kinase/NF-kappa B signaling the top three genes were ILβ, ILα and Tnfaip3, and for ERK1 and ERK2 cascade- Pla2g2a, CCL3 and

Chi3l1 [212]. Activation of these pathways agrees well with previous results about the signaling cascades, which are activated by the extracellular S100A1 [64,157,181].

The downregulated GSEA categories comprised of genes that are responsible for cytoskeleton and stress fibers, as well as extracellular matrix formation. This finding emphasizes a new type of fibroblast activation that differs from the formation of myofibroblasts, which are characterized by an increased αSMA content and extensive collagen production [63,64,201]. This observation resembles the response to IL1α and cytokine ILβ, which have been reported to also decrease αSMA and collagen production [131,213]. In addition, the downregulated categories included also cholesterol biosynthetic activity and various mitosis related categories, such as spindle microtubule, condensed chromosome kinetochore and chromosome segregation. The suppression of mitotic components and cholesterol synthesis, which is a structural cell membrane component [214], might indicate an inhibited proliferative activity. At the same time the category positive cell proliferation was listed among the upregulated functions. In addition, previous studies have demonstrated no impact of extracellular S100A1 on the proliferation rate of cardiac fibroblasts [64,179,182].

7.2 Changes of Cardiac Fibroblast Secretome upon Stimulation with S100A1

The amount of proteins, which are determinants of the biological phenotype, mainly depends on the efficiency of translation, therefore the cellular response on mRNA level requires confirmation on protein level [215]. Since the most prominently changed biological categories from the transcriptome analysis implied production of secreted proteins, such as cytokines and collagens, extracellular proteins were of particular interest for this study. In order to further investigate the phenotype of S100A1-treated adult cardiac fibroblasts, their secretome was analyzed with mass spectrometry.

Mass spectrometry allows a large-scale investigation of extracellular matrix protein secretion upon different stimuli, as well as evaluation of the composition and secretion rate of signaling molecules, that ensure the subsequent intercellular communication [216,217]. To date, this study provides the first analysis of the complete secretome of cardiac fibroblasts upon their exposure to a cardiovascular DAMP.

7.2.1 Relative Changes in Amounts of Secreted Proteins

The effect of S100A1 on cardiac fibroblasts was analyzed by calculating relative changes of individual proteins and grouping their ratios into clusters according to their biological

functions. Relative changes of individual secreted proteins were evaluated by visualizing the p-value against relative ratio in a volcano plot.

The visualization of the relative changes of individual secreted proteins upon the treatment with S100A1 in the volcano plot revealed a strong stimulatory and low suppressive effect. The majority of secreted proteins belonged to the upregulated proteins that possessed also the most notable relative changes.

Conventionally, the volcano plot is also used to define the proteins, which are the most probable candidates for the cause of the biological effect of stimulation under investigation [218,219]. However, the determination of the biological effect via the investigation of functions of individual, highest ranked proteins faces several problems. For example, highest ranked proteins may have contradictive functions, small relative changes collectively may notably impact the biological function, and a small number of experiments is linked to reduced power of significance due to biological variance.

To overcome the limitations of individual protein analysis, biological functions of the secretome from S100A1-treated fibroblasts were evaluated by grouping proteins into functional categories. Enrichment and significance of each category were calculated with 1D annotation enrichment and Fisher's exact test. 1D annotation enrichment employs all relative changes, independent of their numerical value. Fisher's exact test uses relative changes above or below a certain threshold, thereby only assessing biological functions from the most notably changed proteins.

1D annotation enrichment analysis revealed a strong activation of proteins with a chemokine activity, which was also reflected in the results from transcriptome analysis. The most downregulated categories were collagens and extracellular matrix part, however, with a mediocre median ratio of downregulation. Since upregulated proteins formed the major part of population, Fishers exact test was applied to the group of proteins with at least 4-fold increase. The first 15 most upregulated functions comprised various inflammatory related categories, from which the most upregulated ones again were chemokines and chemotaxis. These findings indicate that the stimulation of cardiac fibroblasts with S100A1 induces the chemoattractant function, while simultaneously suppressing myofibroblast-related activation.

7.2.2 Absolute Changes in Amounts of Secreted Proteins

While the investigation of relative protein changes is useful for the characterization of the secretome's biological function, the relative ratios cannot predict the impact of the global

secreted protein profile. If, for example, the protein content in the control sample is close to zero, a prominent relative ratio can potentially be derived from a small absolute amount of protein in the stimulated sample.

In order to investigate the impact of S100A1-elicited changes on the cardiac fibroblast secretome, proteins were evaluated according to their absolute amounts applying protein functional clustering by 1D annotation enrichment analysis. In the control samples, the most significantly enriched category was collagen. Upon stimulation with S100A1, the most significantly enriched category was chemoattractants, representing the category with the highest average absolute amount. In other words, S100A1-treated cardiac fibroblasts predominantly secrete chemoattractants, whereas the secretome from control cells is dominated by collagens, as assessed by absolute abundances of secreted proteins. This suggests that cardiac fibroblasts could execute the surveilling and alarming function in the initial inflammatory phase of myocardial infarction by sensing DAMPs and subsequently acquiring a pronounced chemoattractant phenotype.

Since cardiac fibroblasts also produce collagenases MMP2 and MMP9 upon treatment with S100A1, it is not possible to specifically attribute the reduced amount of collagens to downregulated production or to increased degradation. For the detection with mass spectrometry, proteins are cleaved into peptides with trypsin. Identification of detected peptides using sequence databases is therefore performed based on a C-terminal tryptic cleavage at lysine and arginine residues [220]. If the protein is already extensively digested by another enzymes, mass spectrometry analysis might be misleading, because the cleavage products are not recognized by the database and, consequently, the level of detected collagens is artificially lower. Yet, the downregulation of collagen gene expression was also demonstrated on transcriptome level. Together these results indicate that reduced synthesis of collagens plays an important role in the decreased amount of collagens in the secretome from S100A1-treated cardiac fibroblasts.

S100A1 triggers the conversion of cardiac fibroblasts into cells that secrete chemoattractants in high abundances. In order to extract the proteins, which determine the chemoattractant phenotype, they were ranked according to their absolute abundance and relative ratios in S100A1-stimulated sample. The highest ranked chemoattractants were CCL2, CXCL1 and CCL7, with CCL2 being the most prominently produced one. Moreover, in the complete secretome only biglycane was secreted more than CCL2. Hence, upon exposure to the S100A1, cardiac fibroblasts extensively secrete the highly potent chemoattractant CCL2 [221], which has previously been reported to be involved in

the healing cascade after myocardial infarction by attracting inflammatory cells [222] and protecting cardiomyocytes from hypoxia-induced injury [223].

7.2.3 Limitations of Secretome Analysis

Secretome analysis enabled the elucidation of S100A1-targeted biological functions and highlighted specific proteins that define this phenotype. However, the detected protein profile represented accumulated proteins over 48 hours of treatment. Therefore, the detected biological functions and the underlying protein profile illustrated the sum of all secretory events during a 48 hour time frame, regardless of early or late manifestation.

Since the secreted proteins are highly diluted in the cell culture supernatant, their successful detection by mass spectrometry requires the concentration of the media [224]. For this study, a centrifuge filtration device with a pore size of 3 kDa was used, which might have led to the loss of small proteins and bioactive peptides. Yet, chemokines, which are small cytokines with a molecular size of 8 to 10 kDa [202,221], were detected and calculated to be the most abundantly secreted portion of the secretome.

7.3 Serum Impact on Secretome from Cardiac Fibroblasts

Since the secretome analysis by mass spectrometry was performed without labeling during cell culturing, 0% FCS starvation was chosen in order to reduce the interference of serum proteins with the detection of secreted proteins [224]. However, alteration of the serum amount may affect the abundance of secreted proteins [186], therefore, secretomes from 0% and 0.5% FCS starved cardiac fibroblasts were compared. The highly abundant bovine serum albumin in the 0.5% FCS treated samples masked extracellular proteins of a comparable molecular weight, therefore this region was excluded from the further analysis of the 0.5% FCS group. Consequently, in samples with 0.5% FCS, the number of detected proteins was notably smaller, as compared to control samples. Yet, the absolute amount of each protein that was detected under both treatment conditions strongly correlated between the 0% and 0.5% FCS treated samples. Hence, no relevant impact of serum on the abundance of extracellular proteins was observed.

In this study, transcriptome analysis was performed in the presence of 0.5% FCS, but secretome analysis with 0% FCS. Despite the differences in cell treatment, the correlation between the transcriptome and secretome was consistent with the previously described association between gene expression and protein production. The amount of produced protein depends on the efficiency of translation, where one mRNA can be translated into up to 1300 proteins per hour [172,215]. Still, the fold changes on transcriptome level are

clearly associated with the fold changes on protein level [196,198]. The transcription profile changes of S100A1-treated fibroblasts were highly correlated with secretion, however the extent of secretion changes was more prominent.

7.4 Upregulation of CCL2 in Cardiac Fibroblasts upon Treatment with S100A1

In the setting of myocardial infarction, the absence of CCL2 results in delayed infiltration of macrophages, defective efferocytosis of injured cardiomyocytes and reduced density of myofibroblasts, highlighting the importance of CCL2 in the resolution of tissue injury [208]. However, the initial cellular source of CCL2 and the triggering factors of its production after myocardial infarction are so far poorly understood. S100A1 is rapidly released from damaged cardiomyocytes and immediately internalized by the neighboring cardiac fibroblasts [64,105], thus signaling cardiac injury. In this study, a mass spectrometry-based investigation of the secretome from S100A1-stimulated cardiac fibroblasts revealed CCL2 as the most abundantly produced upregulated protein. A prominent increase of CCL2 in cardiac fibroblasts was also confirmed with qPCR on gene expression level and with ELISA on protein level.

Previous studies have demonstrated that internalized S100A1 binds to TLR4 in cardiac fibroblasts [64]. TLR4 activation has been reported to be linked to increased CCL2 production [206,225]. Therefore, the cascade of TLR4 signaling was investigated as a potential mechanism of S100A1-triggered upregulation of CCL2 in S100A1-treated cardiac fibroblasts. Both chemical inhibition and siRNA mediated knockdown of TLR4 in cardiac fibroblasts resulted in a complete abolishment of S100A1-mediated increase of CCL2 expression. The downstream activation from TLR4 can be driven by two distinct adaptor proteins, MyD88 and TRIF [75]. Additional investigations are required in order to elucidate which of these signaling pathways are involved in the increased CCL2 production by cardiac fibroblasts upon stimulation with S100A1.

The secretome analysis in this work has highlighted cardiac fibroblasts as a prominent source of CCL2 in response to S100A1, which is a cardiomyocyte derived DAMP, released upon myocardial infarction. For the investigation of the time frame, which is needed for the initiation of CCL2 secretion, ELISA technique was used. ELISA is less specific than mass spectrometry, but more sensitive [184,185]. Examination of gene expression and secreted protein amount revealed an early and prominent increase of CCL2 already after 4 hours with steady relative increase on gene expression levels and prominent accumulation in the supernatant on protein level over 48 hours of stimulation. Since the experiment was

performed in one biological replicate, further experiments are required for the statistical confirmation of the findings.

Altogether, these results show that CCL2 is rapidly produced by cardiac fibroblast and secreted in high amounts upon S100A1 stimulation. Further studies are needed to clarify, whether this effect is restricted only to the exposure to S100A1 or if other DAMPs, which are released from cardiomyocytes after infarction, can trigger a similar early induction of CCL2 production in cardiac fibroblasts.

7.5 S100A1-Targeted Upregulated Proteins in the Healing of Myocardial Infarction

As has been shown in a previous study, the blockage of extracellular S100A1 after ischemia/reperfusion injury results in an increased infarct size and a reduced left ventricular ejection fraction [64]. It was hypothesized that the beneficial effect of extracellular S100A1 on healing cascade after cardiac injury might be conveyed through activated cardiac fibroblasts [64].

During the current study cardiac fibroblasts have been identified as a potent source of chemoattractants upon stimulation with S100A1. The secreted protein profile suggests effect on various inflammatory cells. For example, CXCL1 and CXCL6 are classical neutrophil chemoattractants [226–228]. Additionally, CXCL1 participates also in the recruitment of monocytes by potentiating their arrest [229]. CXCL12 is a potent chemoattractant for lymphocytes and monocytes [230]. CCL2 and CCL7 are strong monocyte chemoattractants, which participate also in the recruitment of T lymphocytes [221,222,231,232]. Further studies should reveal how the influx of inflammatory cells is governed by S100A1-stimulated cardiac fibroblasts over the course of myocardial healing *in vivo*.

Interestingly, these classical chemoattractants are reported to indirectly and directly potentiate angiogenesis. During wound healing angiogenesis require controlled extracellular matrix proteolysis that activates angiogenic growth factors and facilitates endothelial cell migration [233]. Chemoattractant-mediated influx of neutrophils, which further secrete proteolytic enzymes, enables initiation of neoangiogenesis [234]. Additionally, CXCL1 and CXCL6 induces endothelial cell chemotaxis *in vitro* and neovascularization of rat cornea *in vivo* [235]. CXCL12 chemoattracts hematopoietic stem cells [236]. CCL2 induces migration of endothelial cells and CCL7 stimulates chemotaxis of circulating angiogenic cells and angiogenesis in Matrigel plugs, implanted in mice

[237,238]. These findings suggest facilitation of restorative angiogenesis by S100A1-induced proteins through promoting inflammatory and endothelial cell migration.

Several upregulated proteins upon stimulation with S100A1 have been reported to be involved in the cardiomyocyte survival after ischemic injury. For example, pentraxin 3, CXCL12 and CCL2 have been shown to protect cardiomyocytes from ischemic injury [190,223,239], whereas Pla2g2a is known to mark ischemically damaged cardiomyocytes by binding to the flip-flopped components of the cell membrane and thereby facilitating their clearance [240]. These findings point out a potential indirect S100A1 involvement in the preservation of viable cardiomyocytes during the ischemia/reperfusion stress.

To sum up, S100A1 mediates an intense activation of cardiac fibroblasts, triggering massive production and secretion of chemoattractants, which are reported to recruit various inflammatory and endothelial cells. This activation might accelerate resolution of the infarction by timely clearance of cellular debris and promoted angiogenesis. In addition, S100A1-stimulated cardiac fibroblasts secrete also cardiomyocyte-protecting proteins together with marker for terminally injured cells. Such composition might selectively preserve viable cardiomyocytes, while simultaneously potentiating clearance of lethally damaged cells. Further investigation should clarify whether these effects are responsible for the protective activity of extracellular S100A1 on the size of infarction and heart function after the ischemia/reperfusion injury *in vivo*.

8 Conclusion and Outlook

Myocardial infarction elicits a strong inflammatory response that ensures the resolution of injured tissues and initiates subsequent replacement of the lost area with a durable scar. DAMPs are the principal signaling molecules, which evoke the inflammatory cascade, however, the underlying cellular mechanism of how inflammatory cells are alarmed and guided to the injury is largely unknown. This study elucidated the detailed effect of S100A1, which is a cardiomyocyte derived DAMP, on cardiac fibroblast secretory profile. A potential initial signaling mechanism for the attraction of inflammatory cells upon myocardial injury was discovered.

Upon exposure to S100A1 cardiac fibroblasts acquire a pronounced inflammatory phenotype, characterized by expressed gene and secreted protein profile. Unlike the transformation into myofibroblasts, this type of fibroblast activation is a rapid process, which take effect already in the first hours of stimulation. Besides increased inflammatory protein secretion it is also characterized by decreased extracellular matrix production. Such activation pattern suggests the importance of fibroblasts not only in the phase of scar formation but also in the initiation of the inflammatory stage after the myocardial infarction. In the presence of extracellular S100A1 the most abundantly secreted upregulated proteins in cardiac fibroblasts are chemoattractants, and among them- CCL2, which is a crucial chemokine for the inflammatory monocyte recruitment.

The findings from this work have raised several questions, which should be addressed in further studies:

1) Do other cardiovascular DAMPs, which are released along with S100A1, elicit similar activation of an early inflammatory protein profile in cardiac fibroblasts?
2) Is the inflammatory phenotype of cardiac fibroblasts reversible after the withdrawal of stimuli?
3) Is the inflammatory phenotype the predominant early activation form of cardiac fibroblasts in the *in vivo* setting of myocardial infarction?
4) What is the contribution of cardiac fibroblasts to the initiation of inflammatory response upon myocardial infarction *in vivo*?

Currently, scar formation is the best described function of cardiac fibroblast upon myocardial infarction, where fibroblasts transform into secretory active myofibroblasts. This study demonstrates an early and strong transformation of cardiac fibroblasts into chemoattractant phenotype upon exposure to S100A1, which is released from injured cardiomyocytes. Accordingly, it provides the first evidence that the initial function of cardiac

fibroblasts upon myocardial infarction might be sensing the tissue injury and triggering the influx of debris-resolving inflammatory cells.

9 References

[1] Thygesen K, Alpert JS, Jaffe AS, Simoons ML, Chaitman BR, White HD, et al. Third universal definition of myocardial infarction. Eur Heart J 2012;33:2551–67.

[2] Steg PG, James SK, Atar D, Badano LP, Lundqvist CB, Borger MA, et al. ESC Guidelines for the management of acute myocardial infarction in patients presenting with ST-segment elevation. Eur Heart J 2012;33:2569–619.

[3] Roffi M, Patrono C, Collet J-P, Mueller C, Valgimigli M, Andreotti F, et al. 2015 ESC Guidelines for the management of acute coronary syndromes in patients presenting without persistent ST-segment elevation. Eur Heart J 2016;37:267–315.

[4] Montecucco F, Carbone F, Schindler TH. Pathophysiology of ST-segment elevation myocardial infarction: novel mechanisms and treatments. Eur Heart J 2016;37:1268–83.

[5] Giannitsis E, Katus HA. Cardiac troponin level elevations not related to acute coronary syndromes. Nat Rev Cardiol 2013;10:1–12.

[6] Javed U, Aftab W, Ambrose JA, Wessel RJ, Mouanoutoua M, Huang G, et al. Frequency of Elevated Troponin I and Diagnosis of Acute Myocardial Infarction. Am J Cardiol 2009;104:9–13.

[7] Mendis S, Puska P, Norrving B editors. Global atlas on cardiovascular disease prevention and control. World Health Organisation, Geneva; 2011.

[8] Mozaffarian D, Benjamin EJ, Go AS, Arnett DK, Blaha MJ, Cushman M, et al. Heart Disease and Stroke Statistics—2016 Update: A Report From the American Heart Association. Circulation 2016;133:38–360.

[9] Kober L. Heart failure in 2015: Better results from prevention than from additional treatment. Nat Rev Cardiol 2016;13:75–7.

[10] Frangogiannis NG. The inflammatory response in myocardial injury, repair, and remodelling. Nat Rev Cardiol 2014;11:255–65.

[11] Larsen AI, Galbraith PD, Ghali WA, Norris CM, Graham MM, Knudtson ML. Characteristics and outcomes of patients with acute myocardial infarction and angiographically normal coronary arteries. Am J Cardiol 2005;95:261–3.

References

[12] Braunwald E. Shattuck lecture–cardiovascular medicine at the turn of the millennium: triumphs, concerns, and opportunities. N Engl J Med 1997;337:1360–1369.

[13] Go AS, Mozaffarian D, Roger VL, Benjamin EJ, Berry JD, Blaha MJ, et al. Heart Disease and Stroke Statistics - 2014 Update: A report from the American Heart Association. Circulation 2014;129:28–292.

[14] Hellermann JP, Goraya TY, Jacobsen SJ, Weston SA, Reeder GS, Gersh BJ, et al. Incidence of heart failure after myocardial infarction: Is it changing over time? Am J Epidemiol 2003;157:1101–7.

[15] Garcia-Dorado D, Rodríguez-Sinovas A, Ruiz-Meana M, Inserte J. Protection against myocardial ischemia-reperfusion injury in clinical practice. Rev Esp Cardiol (Engl Ed) 2014;67:394–404.

[16] Liehn EA, Postea O, Curaj A, Marx N. Repair after myocardial infarction, between fantasy and reality: The role of chemokines. J Am Coll Cardiol 2011;58:2357–62.

[17] Blankesteijn WM, Creemers E, Lutgens E, Cleutjens JPM, Daemen MJAP, Smits JFM. Dynamics of cardiac wound healing following myocardial infarction: Observations in genetically altered mice. Acta Physiol Scand 2001;173:75–82.

[18] Xin M, Olson EN, Bassel-Duby R. Mending broken hearts: cardiac development as a basis for adult heart regeneration and repair. Nat Rev Mol Cell Biol 2013;14:529–41.

[19] Reimer K a, Lowe JE, Rasmussen MM, Jennings RB. The wavefront phenomenon of ischemic cell death. 1. Myocardial infarct size vs duration of coronary occlusion in dogs. Circulation 1977;56:786–94.

[20] Ghigo A, Franco I, Morello F, Hirsch E. Myocyte signalling in leucocyte recruitment to the heart. Cardiovasc Res 2014;102:270–80.

[21] Hu J, Van den Steen PE, Sang Q-X a, Opdenakker G. Matrix metalloproteinase inhibitors as therapy for inflammatory and vascular diseases. Nat Rev Drug Discov 2007;6:480–98.

[22] Forbes SJ, Rosenthal N. Preparing the ground for tissue regeneration: from mechanism to therapy. Nat Med 2014;20:857–69.

[23] Vandervelde S, Van Amerongen MJ, Tio RA, Petersen AH, Van Luyn MJA, Harmsen MC. Increased inflammatory response and neovascularization in reperfused vs. nonreperfused murine myocardial infarction. Cardiovasc Pathol 2006;15:83–90.

[24] Knorr M, Münzel T, Wenzel P. Interplay of NK cells and monocytes in vascular inflammation and myocardial infarction. Front Physiol 2014;5:295.

[25] Dutta P, Nahrendorf M. Monocytes in myocardial infarction. Arterioscler Thromb Vasc Biol 2015;35:1066–70.

[26] Nahrendorf M, Swirski FK. Monocyte and macrophage heterogeneity in the heart. Circ Res 2013;112:1624–33.

[27] Jung K, Kim P, Leuschner F, Gorbatov R, Kim JK, Ueno T, et al. Endoscopic time-lapse imaging of immune cells in infarcted mouse hearts. Circ Res 2013;112:891–9.

[28] Nahrendorf M, Swirski FK, Aikawa E, Stangenberg L, Wurdinger T, Figueiredo J-L, et al. The healing myocardium sequentially mobilizes two monocyte subsets with divergent and complementary functions. J Exp Med 2007;204:3037–47.

[29] Ma Y, Yabluchanskiy A, Lindsey ML. Neutrophil roles in left ventricular remodeling following myocardial infarction. Fibrogenesis Tissue Repair 2013;6:11.

[30] Zhao W, Zhao T, Chen Y, Ahokas RA, Sun Y. Reactive oxygen species promote angiogenesis in the infarcted rat heart. Int J Exp Pathol 2009;90:621–9.

[31] Liu XH, Pan LL, Deng HY, Xiong QH, Wu D, Huang GY, et al. Leonurine (SCM-198) attenuates myocardial fibrotic response via inhibition of NADPH oxidase 4. Free Radic Biol Med 2013;54:93–104.

[32] Territo MC, Ganz T, Selsted ME, Lehrer R. Monocyte-chemotactic activity of defensins from human neutrophils. J Clin Invest 1989;84:2017–20.

[33] Zizzo G, Hilliard BA, Monestier M, Cohen PL. Efficient clearance of early apoptotic cells by human macrophages requires M2c polarization and MerTK induction. J Immunol 2012;189:3508–20.

[34] Horckmans M, Ring L, Duchene J, Santovito D, Schloss MJ, Drechsler M, et al. Neutrophils orchestrate post-myocardial infarction healing by polarizing macrophages towards a reparative phenotype. Eur Heart J 2016:ehw002.

References

[35] Rydell-Törmänen K, Uller L, Erjefält JS. Neutrophil cannibalism--a back up when the macrophage clearance system is insufficient. Respir Res 2006;7:143.

[36] Nathan C. Points of control in inflammation. Nature 2002;420:846–52.

[37] Frangogiannis NG. Regulation of the inflammatory response in cardiac repair. Circ Res 2012;110:159–73.

[38] Lech M, Anders HJ. Macrophages and fibrosis: How resident and infiltrating mononuclear phagocytes orchestrate all phases of tissue injury and repair. Biochim Biophys Acta 2013;1832:989–97.

[39] Libby P, Maroko PR, Bloor CM, Sobel BE, Braunwald E. Reduction of Experimental Myocardial Infarct Size by Corticosteroid Administration. J Clin Invest 1973;52:599–607.

[40] Hammerman H, Kloner R a., Hale S, Schoen FJ, Braunwald E. Dose-dependent effects of short-term methylprednisolone on myocardial infarct extent, scar formation, and ventricular function. Circulation 1983;68:446–52.

[41] Seropian IM, Toldo S, Van Tassell BW, Abbate A. Anti-inflammatory strategies for ventricular remodeling following St-segment elevation acute myocardial infarction. J Am Coll Cardiol 2014;63:1593–603.

[42] Giugliano GR, Giugliano RP, Gibson CM, Kuntz RE. Meta-analysis of corticosteroid treatment in acute myocardial infarction. Am J Cardiol 2003;91:1055–9.

[43] Jugdutt BI, Hutchins GM, Bulkley BH, Becker LC. Salvage of Ischemic Myocardium by Ibuprofen Durin Infarction in the Conscious Dog. Am J Cardiol 1980;46:74–82.

[44] Brown EJ, Kloner RA, Schoen FJ, Hammerman H, Hale S, Braunwald E. Scar thinning due to ibuprofen administration after experimental myocardial infarction. Am J Cardiol 1983;51:877–83.

[45] Pfeffer MA, Braunwald E. Ventricular Remodeling After Myocardial Infarction Experimental Observations and Clinical Implications. Circulation 1989;81:1161–72.

[46] Silverman HS, Pfeifer MP. Relation between use of antiinflammatory agents and left ventricular free wall rupture during acute myocardial infarction. Am J Cardiol 1987;59:363–4.

[47] Dobaczewski M, Bujak M, Zymek P, Ren G, Entman ML, Frangogiannis NG. Extracellular matrix remodeling in canine and mouse myocardial infarcts. Cell Tissue Res 2006;324:475–88.

[48] Tomasek JJ, Gabbiani G, Hinz B, Chaponnier C, Brown R a. Myofibroblasts and mechano-regulation of connective tissue remodelling. Nat Rev Mol Cell Biol 2002;3:349–63.

[49] Czubryt MP. Common threads in cardiac fibrosis, infarct scar formation, and wound healing. Fibrogenes Tissue Repair 2012;5:19.

[50] Dobaczewski M, Gonzalez-Quesada C, Frangogiannis NG. The extracellular matrix as a modulator of the inflammatory and reparative response following myocardial infarction. J Mol Cell Cardiol 2010;48:504–11.

[51] Bogatyryov Y, Kelly M, Christensen LP, Tomanek RJ, Dedkov EI. Structural Composition of Myocardial Infarction Scar Does Not Differ Between Male and Female Middle-Aged Rats. FASEB J 2012;26.

[52] Szaraz P, Lucato A, Li SH, Wu J, Gauthier-Fisher A, Li R-K, et al. Local Injection of First Trimester Human Umbilical Cord Perivascular Cells (FTM-HUCPVCs) After Myocardial Infarction Increases Extracellular Matrix Processing Activity, Vascular Density and Blood Vessel Size Within the Infarct Scar. Circulation 2015;132:A19359.

[53] Ma Y, Yabluchanskiy A, Iyer RP, Cannon PL, Flynn ER, Jung M, et al. Temporal neutrophil polarization following myocardial infarction. Cardiovasc Res 2016;110:51–61.

[54] Weber KT, Sun Y, Bhattacharya SK, Ahokas R a, Gerling IC. Myofibroblast-mediated mechanisms of pathological remodelling of the heart. Nat Rev Cardiol 2013;10:15–26.

[55] Saxena A, Russo I, Frangogiannis NG. Inflammation as a therapeutic target in myocardial infarction: Learning from past failures to meet future challenges. Transl Res 2016;167:152–66.

[56] Mallory GK, White PD, Salcedo-Salgar J. The Speed of Healing of Myocardial Infarcts. A study of the pathologic anatomy in seventy-two cases. Am Heart J 1936;18:647–671.

References

[57] Matzinger P. Tolerance, danger, and the extended family. Annu Rev Immunol 1994;12:991–1045.

[58] Matzinger P. The danger model: a renewed sense of self. Science 2002;296:301–5.

[59] Seong S-Y, Matzinger P. Hydrophobicity: an ancient damage-associated molecular pattern that initiates innate immune responses. Nat Rev Immunol 2004;4:469–78.

[60] Oppenheim JJ, Yang D. Alarmins: Chemotactic activators of immune responses. Curr Opin Immunol 2005;17:359–65.

[61] Bianchi ME. DAMPs, PAMPs and alarmins: all we need to know about danger. J Leukoc Biol 2007;81:1–5.

[62] Kaczmarek A, Vandenabeele P, Krysko D V. Necroptosis: The Release of Damage-Associated Molecular Patterns and Its Physiological Relevance. Immunity 2013;38:209–23.

[63] Zhang W, Lavine KJ, Epelman S, Evans SA, Weinheimer CJ, Barger PM, et al. Necrotic myocardial cells release damage-associated molecular patterns that provoke fibroblast activation in vitro and trigger myocardial inflammation and fibrosis in vivo. J Am Heart Assoc 2015;4:e001993.

[64] Rohde D, Schön C, Boerries M, Didrihsone I, Ritterhoff J, Kubatzky KF, et al. S100A1 is released from ischemic cardiomyocytes and signals myocardial damage via Toll-like receptor 4. EMBO Mol Med 2014;6:778–94.

[65] Vogl T, Eisenblatter M, Voller T, Zenker S, Hermann S, van Lent P, et al. Alarmin S100A8/S100A9 as a biomarker for molecular imaging of local inflammatory activity. Nat Commun 2014;5:4593.

[66] Santoni G, Cardinali C, Morelli MB, Santoni M, Nabissi M, Amantini C. Danger- and pathogen-associated molecular patterns recognition by pattern-recognition receptors and ion channels of the transient receptor potential family triggers the inflammasome activation in immune cells and sensory neurons. J Neuroinflammation 2015;12:21.

[67] Takeuchi O, Akira S. Pattern Recognition Receptors and Inflammation. Cell 2010;140:805–20.

[68] Christ A, Temmerman L, Legein B, Daemen MJAP, Biessen EAL. Dendritic cells in cardiovascular diseases epiphenomenon, contributor, or therapeutic opportunity. Circulation 2013;128:2603–13.

[69] Marchant DJ, Boyd JH, Lin DC, Granville DJ, Garmaroudi FS, McManus BM. Inflammation in myocardial diseases. Circ Res 2012;110:126–44.

[70] Michelsen KS, Doherty TM, Shah PK, Arditi M. TLR signaling: an emerging bridge from innate immunity to atherogenesis. J Immunol 2004;173:5901–7.

[71] Mann DL. Innate immunity and the failing heart: The cytokine hypothesis revisited. Circ Res 2015;116:1254–68.

[72] Ishimura MN, Aito SN, Nishimura M, Naito S. Tissue-specific mRNA expression profiles of human toll-like receptors and related genes. Biol Pharm Bull 2005;28:886–92.

[73] Murphy JE, Padilla BE, Hasdemir B, Cottrell GS, Bunnett NW. Endosomes: a legitimate platform for the signaling train. Proc Natl Acad Sci U S A 2009;106:17615–22.

[74] Kumagai Y, Akira S. Identification and functions of pattern-recognition receptors. J Allergy Clin Immunol 2010;125:985–92.

[75] Chao W. Toll-like receptor signaling: a critical modulator of cell survival and ischemic injury in the heart. Am J Physiol Heart Circ Physiol 2009;296:H1–12.

[76] Kawai T, Akira S. The role of pattern-recognition receptors in innate immunity: update on Toll-like receptors. Nat Immunol 2010;11:373–84.

[77] Kagan JC, Su T, Horng T, Chow A, Akira S, Medzhitov R. TRAM couples endocytosis of Toll-like receptor 4 to the induction of interferon-beta. Nat Immunol 2008;9:361–8.

[78] Gangloff M. Different dimerisation mode for TLR4 upon endosomal acidification? Trends Biochem Sci 2012;37:92–8.

[79] Bhattacharyya S, Kelley K, Melichian DS, Tamaki Z, Fang F, Su Y, et al. Toll-like receptor 4 signaling augments transforming growth factor-β responses: a novel mechanism for maintaining and amplifying fibrosis in scleroderma. Am J Pathol 2013;182:192–205.

References

[80] Seki E, De Minicis S, Osterreicher CH, Kluwe J, Osawa Y, Brenner D a, et al. TLR4 enhances TGF-beta signaling and hepatic fibrosis. Nat Med 2007;13:1324–32.

[81] Zacharowski K, Otto M, Hafner G, Chatterjee PK, Thiemermann C. Endotoxin Induces a Second Window of Protection in the Rat Heart as Determined by Using p-Nitro-Blue Tetrazolium Staining, Cardiac Troponin T Release, and Histology. Arterioscler Thromb Vasc Biol 1999;19:2276–80.

[82] Meng X, Ao L, Brown JM, Meldrum DR, Sheridan BC, Cain BS, et al. LPS induces late cardiac functional protection against ischemia independent of cardiac and circulating TNF-alpha. Am J Physiol 1997;273:H1894-902.

[83] Timmers L, Sluijter JPG, Van Keulen JK, Hoefer IE, Nederhoff MGJ, Goumans MJ, et al. Toll-like receptor 4 mediates maladaptive left ventricular remodeling and impairs cardiac function after myocardial infarction. Circ Res 2008;102:257–64.

[84] Chong AJ, Shimamoto A, Hampton CR, Takayama H, Spring DJ, Rothnie CL, et al. Toll-like receptor 4 mediates ischemia/reperfusion injury of the heart. J Thorac Cardiovasc Surg 2004;128:170–9.

[85] Kim S-C, Ghanem A, Stapel H, Tiemann K, Knuefermann P, Hoeft A, et al. Toll-like receptor 4 deficiency: Smaller infarcts, but nogain in function. BMC Physiol 2007;7:5.

[86] Burns K, Janssens S, Brissoni B, Olivos N, Beyaert R, Tschopp J. Inhibition of interleukin 1 receptor/Toll-like receptor signaling through the alternatively spliced, short form of MyD88 is due to its failure to recruit IRAK-4. J Exp Med 2003;197:263–8.

[87] O'Neill L a J, Golenbock D, Bowie AG. The history of Toll-like receptors - redefining innate immunity. Nat Rev Immunol 2013;13:453–60.

[88] Warner N, Nunez G. MyD88: A Critical Adaptor Protein in Innate Immunity Signal Transduction. J Immunol 2013;190:3–4.

[89] Feng Y, Zhao H, Xu X, Buys ES, Raher MJ, Bopassa JC, et al. Innate immune adaptor MyD88 mediates neutrophil recruitment and myocardial injury after ischemia-reperfusion in mice. Am J Physiol Heart Circ Physiol 2008;295:H1311–8.

[90] Feng Y, Zou L, Si R, Nagasaka Y, Chao W. Bone marrow MyD88 signaling modulates neutrophil function and ischemic myocardial injury. Am J Physiol Cell Physiol 2010;299:C760-9.

[91] Frangogiannis NG. Pathophysiology of myocardial infarction. Compr Physiol 2015;5:1841–75.

[92] De Haan JJ, Smeets MB, Pasterkamp G, Arslan F. Danger signals in the initiation of the inflammatory response after myocardial infarction. Mediators Inflamm 2013;2013:206039.

[93] Su Z, Zhang P, Yu Y, Lu H, Liu Y, Ni P, et al. HMGB1 Facilitated Macrophage Reprogramming towards a Proinflammatory M1-like Phenotype in Experimental Autoimmune Myocarditis Development. Sci Rep 2016;6:21884.

[94] Park JS, Gamboni-Robertson F, He Q, Svetkauskaite D, Kim J, Strassheim D, et al. High mobility group box 1 protein interacts with multiple Toll-like receptors. Am J Physiol Cell Physiol 2006;290:917–24.

[95] Hirata Y, Kurobe H, Higashida M, Fukuda D, Shimabukuro M, Tanaka K, et al. HMGB1 plays a critical role in vascular inflammation and lesion formation via toll-like receptor 9. Atherosclerosis 2013;231:227–33.

[96] Andrassy M, Volz HC, Igwe JC, Funke B, Eichberger SN, Kaya Z, et al. High-mobility group box-1 in ischemia-reperfusion injury of the heart. Circulation 2008;117:3216–26.

[97] Vogl T, Tenbrock K, Ludwig S, Leukert N, Ehrhardt C, van Zoelen M a D, et al. Mrp8 and Mrp14 are endogenous activators of Toll-like receptor 4, promoting lethal, endotoxin-induced shock. Nat Med 2007;13:1042–9.

[98] Averill MM, Kerkhoff C, Bornfeldt KE. S100A8 and S100A9 in cardiovascular biology and disease. Arterioscler Thromb Vasc Biol 2012;32:223–9.

[99] Liu L, Yang M, Kang R, Dai Y, Yu Y, Gao F, et al. HMGB1-DNA complex-induced autophagy limits AIM2 inflammasome activation through RAGE. Biochem Biophys Res Commun 2014;450:851–6.

[100] Scaffidi P, Misteli T, Bianchi ME. Release of chromatin protein HMGB1 by necrotic cells triggers inflammation. Nature 2002;418:191–5.

References

[101] Wang H, Bloom O, Zhang M, Vishnubhakat JM, Ombrellino M, Che J, et al. HMG-1 as a late mediator of endotoxin lethality in mice. Science 1999;285:248–51.

[102] Gardella S, Andrei C, Ferrera D, Lotti L V., Torrisi MR, Bianchi ME, et al. The nuclear protein HMGB1 is secreted by monocytes via a non-classical, vesicle-mediated secretory pathway. EMBO Rep 2002;3:995–1001.

[103] Yang H, Lundback P. Redox modification of cysteine residues regulates the cytokine activity of high mobility group box-1 (HMGB1). Mol Med 2012;18:1.

[104] Kitahara T, Takeishi Y, Harada M, Niizeki T, Suzuki S, Sasaki T, et al. High-mobility group box 1 restores cardiac function after myocardial infarction in transgenic mice. Cardiovasc Res 2008;80:40–6.

[105] Bi H, Yang Y, Huang J, Li Y, Ma C, Cong B. Immunohistochemical detection of S100A1 in the postmortem diagnosis of acute myocardial infarction. Diagn Pathol 2013;8:84.

[106] Dostal D, Glaser S, Baudino TA. Cardiac fibroblast physiology and pathology. Compr Physiol 2015;5:887–909.

[107] Camelliti P, Borg TK, Kohl P. Structural and functional characterisation of cardiac fibroblasts. Cardiovasc Res 2005;65:40–51.

[108] Chang HY, Chi J-TJ, Dudoit S, Bondre C, van de Rijn M, Botstein D, et al. Diversity, topographic differentiation, and positional memory in human fibroblasts. Proc Natl Acad Sci U S A 2002;99:12877–82.

[109] Souders CA, Bowers SLK, Baudino TA. Cardiac fibroblast: the renaissance cell. Circ Res 2009;105:1164–76.

[110] Chen W, Frangogiannis NG. Fibroblasts in post-infarction inflammation and cardiac repair. Biochim Biophys Acta 2013;1833:945–53.

[111] Pinto AR, Ilinykh A, Ivey MJ, Kuwabara JT, D'Antoni M, Debuque RJ, et al. Revisiting Cardiac Cellular Composition. Circ Res 2016;118:400–9.

[112] Banerjee I, Fuseler JW, Price RL, Borg TK, Baudino TA. Determination of cell types and numbers during cardiac development in the neonatal and adult rat and mouse. Am J Physiol Heart Circ Physiol 2007;293:1883–91.

[113] LeGrice IJ, Smaill BH, Chai LZ, Edgar SG, Gavin JB, Hunter PJ. Laminar structure of the heart: ventricular myocyte arrangement and connective tissue architecture in the dog. Am J Physiol 1995;269:H571-82.

[114] Camelliti P, Green CR, LeGrice I, Kohl P. Fibroblast Network in Rabbit Sinoatrial Node: Structural and Functional Identification of Homogeneous and Heterogeneous Cell Coupling. Circ Res 2004;94:828–35.

[115] Rog-Zielinska EA, Norris RA, Kohl P, Markwald R. The living scar – cardiac fibroblasts and the injured heart. Trends Mol Med 2016;22:99–114.

[116] Kohl P, Gourdie RG. Fibroblast-myocyte electrotonic coupling: Does it occur in native cardiac tissue? J Mol Cell Cardiol 2014;70:37–46.

[117] Baum J, Duffy HS. Fibroblasts and myofibroblasts: what are we talking about? J Cardiovasc Pharmacol 2011;57:376–9.

[118] Zhang X, Azhar G, Nagano K, Wei JY. Differential vulnerability to oxidative stress in rat cardiac myocytes versus fibroblasts. J Am Coll Cardiol 2001;38:2055–62.

[119] Ma Y, De Castro Brás LE, Toba H, Iyer RP, Hall ME, Winniford MD, et al. Myofibroblasts and the extracellular matrix network in post-myocardial infarction cardiac remodeling. Pflugers Arch Eur J Physiol 2014;466:1113–27.

[120] van den Borne SWM, Diez J, Blankesteijn WM, Verjans J, Hofstra L, Narula J. Myocardial remodeling after infarction: the role of myofibroblasts. Nat Rev Cardiol 2010;7:30–7.

[121] Swaney JS, Roth DM, Olson ER, Naugle JE, Meszaros JG, Insel PA. Inhibition of cardiac myofibroblast formation and collagen synthesis by activation and overexpression of adenylyl cyclase. Proc Natl Acad Sci U S A 2005;102:437–42.

[122] Driesen RB, Nagaraju CK, Abi-Char J, Coenen T, Lijnen PJ, Fagard RH, et al. Reversible and irreversible differentiation of cardiac fibroblasts. Cardiovasc Res 2014;101:411–22.

[123] Weber KT. Fibrosis and hypertensive heart disease. Curr Opin Cardiol 2000;15:264–72.

[124] Petrov V V, Fagard RH, Lijnen PJ. Stimulation of collagen production by transforming growth factor-beta1 during differentiation of cardiac fibroblasts to myofibroblasts. Hypertension 2002;39:258–63.

References

[125] Shephard P, Martin G, Smola-Hess S, Brunner G, Krieg T, Smola H. Myofibroblast differentiation is induced in keratinocyte-fibroblast co-cultures and is antagonistically regulated by endogenous transforming growth factor-beta and interleukin-1. Am J Pathol 2004;164:2055–66.

[126] Frangogiannis NG. Interleukin-1 in cardiac injury, repair, and remodeling: pathophysiologic and translational concepts. Discov 2015;3:1–14.

[127] Brønnum H, Eskildsen T, Andersen DC, Schneider M, Sheikh SP. IL-1β suppresses TGF-β-mediated myofibroblast differentiation in cardiac fibroblasts. Growth Factors 2013;31:81–9.

[128] Saxena A, Chen W, Su Y, Rai V, Uche OU, Li N, et al. IL-1 induces proinflammatory leukocyte infiltration and regulates fibroblast phenotype in the infarcted myocardium. J Immunol 2013;191:4838–48.

[129] Prabhu SD, Frangogiannis NG. The Biological Basis for Cardiac Repair After Myocardial Infarction. Circ Res 2016;119:91–112.

[130] Turner NA, Das A, O'Regan DJ, Ball SG, Porter KE. Human cardiac fibroblasts express ICAM-1, E-selectin and CXC chemokines in response to proinflammatory cytokine stimulation. Int J Biochem Cell Biol 2011;43:1450–8.

[131] van Nieuwenhoven FA, Hemmings KE, Porter KE, Turner NA. Combined effects of interleukin-1α and transforming growth factor-β1 on modulation of human cardiac fibroblast function. Matrix Biol 2013;32:399–406.

[132] Rossini A, Zacheo A, Mocini D, Totta P, Facchiano A, Castoldi R, et al. HMGB1-stimulated human primary cardiac fibroblasts exert a paracrine action on human and murine cardiac stem cells. J Mol Cell Cardiol 2008;44:683–93.

[133] Schiopu A, Cotoi OS. S100A8 and S100A9: DAMPs at the crossroads between innate immunity, traditional risk factors, and cardiovascular disease. Mediators Inflamm 2013;2013:828354.

[134] Wu Y, Li Y, Zhang C, Xi A, Wang Y, Cui W, et al. S100a8/a9 released by CD11b+Gr1+ neutrophils activates cardiac fibroblasts to initiate angiotensin II-induced cardiac inflammation and injury. Hypertension 2014;63:1241–50.

[135] Donato R. Intracellular and extracellular roles of S100 proteins. Microsc Res Tech 2003;60:540–51.

[136] Zimmer DB, Wright Sadosky P, Weber DJ. Molecular mechanisms of S100-target protein interactions. Microsc Res Tech 2003;60:552–9.

[137] Marenholz I, Heizmann CW, Fritz G. S100 proteins in mouse and man: From evolution to function and pathology (including an update of the nomenclature). Biochem Biophys Res Commun 2004;322:1111–22.

[138] Bresnick AR, Weber DJ, Zimmer DB. S100 proteins in cancer. Nat Rev Cancer 2015;15:96–109.

[139] Goch G, Vdovenko S, Kozłsowska H, Bierzyñski A. Affinity of S100A1 protein for calcium increases dramatically upon glutathionylation. FEBS J 2005;272:2557–65.

[140] Cannon BR, Zimmer DB, Weber DJ. S100A1 (S100 calcium binding protein A1). Atlas Genet Cytogenet Oncol Haematol 2011;15:873–6.

[141] Kato K, Kimura S. S100ao (alpha alpha) protein is mainly located in the heart and striated muscles. Biochim Biophys Acta 1985;842:146–50.

[142] Rohde D, Ritterhoff J, Voelkers M, Katus H a, Parker TG, Most P. S100A1: a multifaceted therapeutic target in cardiovascular disease. J Cardiovasc Transl Res 2010;3:525–37.

[143] Ehlermann P, Remppis a, Guddat O, Weimann J, Schnabel P a, Motsch J, et al. Right ventricular upregulation of the Ca(2+) binding protein S100A1 in chronic pulmonary hypertension. Biochim Biophys Acta 2000;1500:249–55.

[144] Ritterhoff J, Most P. Targeting S100A1 in heart failure. Gene Ther 2012;19:613–21.

[145] Most P, Bernotat J, Ehlermann P, Pleger ST, Reppel M, Börries M, et al. S100A1: a regulator of myocardial contractility. Proc Natl Acad Sci U S A 2001;98:13889–94.

[146] Völkers M, Loughrey CM, MacQuaide N, Remppis A, DeGeorge BR, Wegner F v., et al. S100A1 decreases calcium spark frequency and alters their spatial characteristics in permeabilized adult ventricular cardiomyocytes. Cell Calcium 2007;41:135–43.

[147] Ritterhoff J, Völkers M, Seitz A, Spaich K, Gao E, Peppel K, et al. S100A1 DNA-based Inotropic Therapy Protects Against Proarrhythmogenic Ryanodine Receptor 2 Dysfunction. Mol Ther 2015;23:1320–30.

References

[148] Boerries M, Most P, Gledhill JR, Walker JE, Katus H a, Koch WJ, et al. Ca2+ -dependent interaction of S100A1 with F1-ATPase leads to an increased ATP content in cardiomyocytes. Mol Cell Biol 2007;27:4365–73.

[149] Fukushima H, Chung CS, Granzier H. Titin-isoform dependence of titin-actin interaction and its regulation by S100A1/ Ca2+ in skinned myocardium. J Biomed Biotechnol 2010;2010:727239.

[150] Wright NT, Cannon BR, Zimmer DB, Weber DJ. S100A1: Structure, Function and Therapeutical Potential. Curr Chem Biol 2009;3:138–45.

[151] Teichert-Kuliszewska K, Tsoporis JN, Desjardins JF, Yin J, Wang L, Kuebler WM, et al. Absence of the calcium-binding protein, S100A1, confers pulmonary hypertension in mice associated with endothelial dysfunction and apoptosis. Cardiovasc Res 2015;105:8–19.

[152] Rohde D, Busch M, Volkert A, Ritterhoff J, Katus HA. Cardiomyocytes , endothelial cells and cardiac fibroblasts : S100A1's triple action in cardiovascular pathophysiology. Future Cardiol 2015;11:309–21.

[153] O'Dowd BS, Zhao WQ, Ng KT, Robinson SR. Chicks injected with antisera to either S-100 alpha or S-100 beta protein develop amnesia for a passive avoidance task. Neurobiol Learn Mem 1997;67:197–206.

[154] Huttunen HJ, Kuja-Panula J, Sorci G, Agneletti AL, Donato R, Rauvala H. Coregulation of neurite outgrowth and cell survival by amphoterin and S100 proteins through receptor for advanced glycation end products (RAGE) activation. J Biol Chem 2000;275:40096–105.

[155] Mariggió MA, Fulle S, Calissano P, Nicoletti I, Fanó G. The brain protein S-100ab induces apoptosis in PC12 cells. Neuroscience 1994;60:29–35.

[156] Fulle S, Mariggió MA, Belia S, Petrelli C, Ballarini P, Guarnieri S, et al. Rapid desensitization of PC12 cells stimulated with high concentrations of extracellular S100. Neuroscience 1999;89:991–7.

[157] Most P, Boerries M, Eicher C, Schweda C, Ehlermann P, Pleger ST, et al. Extracellular S100A1 Protein Inhibits Apoptosis in Ventricular Cardiomyocytes via Activation of the Extracellular Signal-regulated Protein Kinase 1/2 (ERK1/2). J Biol Chem 2003;278:48404–12.

[158] Usui A, Kato K, Sasa H, Minaguchi K, Abe T, Murase M, et al. S-100ao protein in serum during acute myocardial infarction. Clin Chem 1990;36:639–41.

[159] Kiewitz R, Acklin C, Minder E, Huber PR, Schafer BW, Heizmann CW. S100A1, a new marker for acute myocardial ischemia. Biochem Biophys Res Commun 2000;274:865–71.

[160] Murray PJ. The primary mechanism of the IL-10-regulated antiinflammatory response is to selectively inhibit transcription. Proc Natl Acad Sci U S A 2005;102:8686–91.

[161] Daniel C, Vogelbacher R, Stief A, Grigo C, Hugo C. Long-term gene therapy with thrombospondin 2 inhibits TGF-beta activation, inflammation and angiogenesis in chronic allograft nephropathy. PLoS One 2013;8:e83846.

[162] Zinovkin RA, Romaschenko VP, Galkin II, Zakharova V V., Pletjushkina OY, Chernyak B V., et al. Role of mitochondrial reactive oxygen species in age-related inflammatory activation of endothelium. Aging (Albany NY) 2014;6:661–74.

[163] Teicher BA, Fricker SP. CXCL12 (SDF-1)/CXCR4 pathway in cancer. Clin Cancer Res 2010;16:2927–31.

[164] Bradley JR. TNF-mediated inflammatory disease. J Pathol 2008;214:149–60.

[165] Ehlermann P, Remppis A, Most P, Bernotat J, Heizmann CW, Katus HA. Purification of the Ca2+-binding protein S100A1 from myocardium and recombinant Escherichia coli. J Chromatogr B 2000;737:39–45.

[166] Xu X, Colecraft HM. Primary culture of adult rat heart myocytes. J Vis Exp 2009;June 16.

[167] http://www.elisaanalysis.com/app.

[168] Schmittgen TD, Livak KJ. Analyzing real-time PCR data by the comparative CT method. Nat Protoc 2008;3:1101–8.

[169] Mootha VK, Lindgren CM, Eriksson K-F, Subramanian A, Sihag S, Lehar J, et al. PGC-1alpha-responsive genes involved in oxidative phosphorylation are coordinately downregulated in human diabetes. Nat Genet 2003;34:267–73.

References

[170] Subramanian A, Tamayo P, Mootha VK, Mukherjee S, Ebert BL, Gillette M a, et al. Gene set enrichment analysis: a knowledge-based approach for interpreting genome-wide expression profiles. Proc Natl Acad Sci U S A 2005;102:15545–50.

[171] http://www.uniprot.org/.

[172] Schwanhäusser B, Busse D, Li N, Dittmar G, Schuchhardt J, Wolf J, et al. Global quantification of mammalian gene expression control. Nature 2011;473:337–42.

[173] Hulsen T, de Vlieg J, Alkema W. BioVenn - a web application for the comparison and visualization of biological lists using area-proportional Venn diagrams. BMC Genomics 2008;9:488.

[174] Altman N, Krzywinski M. Points of Significance: Association, correlation and causation. Nat Methods 2015;12:899–900.

[175] Cox J, Mann M. 1D and 2D annotation enrichment: a statistical method integrating quantitative proteomics with complementary high-throughput data. BMC Bioinformatics 2012;13:S12.

[176] Jacquet S, Yin X, Sicard P, Clark J, Kanaganayagam GS, Mayr M, et al. Identification of cardiac myosin-binding protein C as a candidate biomarker of myocardial infarction by proteomics analysis. Mol Cell Proteomics 2009;8:2687–99.

[177] Cordwell SJ, Edwards AVG, Liddy KA, Moshkanbaryans L, Solis N, Parker BL, et al. Release of tissue-specific proteins into coronary perfusate as a model for biomarker discovery in myocardial ischemia/reperfusion injury. J Proteome Res 2012;11:2114–26.

[178] Thorp EB. Contrasting inflammation resolution during atherosclerosis and post myocardial infarction at the level of monocyte/macrophage phagocytic clearance. Front Immunol 2012;3:1–8.

[179] Rohde D. Extrazelluläres S100A1 : ein neuer Regulator der Funktion kardialer Fibroblasten nach Myokardinfarkt. MD thesis, Heidelberg University, Germany, 2011.

[180] http://software.broadinstitute.org/gsea/doc/GSEAUserGuideTEXT.htm.

[181] Yu J, Lu Y, Li Y, Xiao L, Xing Y, Li Y, et al. Role of S100A1 in hypoxia-induced inflammatory response in cardiomyocytes via TLR4/ROS/NF-κB pathway. J Pharm Pharmacol 2015:1240–50.

[182] Börries M. Extrazelluläre Effekte des Ca^{2+}-bindenden Proteins S100A1: Grundlegende Experimente zur Morphologie und Funktion neonataler Kardiomyozyten in Abhängigkeit der Kulturbedingungen. MD thesis, University of Lübeck, Germany, 2003.

[183] O'Connor C, Adams JU. Proteins Are Responsible for a Diverse Range of Structural and Catalytic Functions in Cells. Essentials Cell Biol., Cambridge, MA: NPG Education; 2010.

[184] Brown KJ, Formolo C a, Seol H, Marathi RL, An E, Pillai D, et al. Advances in the proteomic investigation of the cell secretome. Expert Rev Proteomics 2012;9:337–45.

[185] Pan S, Aebersold R, Chen R. Mass spectrometry based targeted protein quantification: methods and applications. J Proteome Researh 2008;8:787–97.

[186] Eichelbaum K, Winter M, Diaz MB, Herzig S, Krijgsveld J. Selective enrichment of newly synthesized proteins for quantitative secretome analysis. Nat Biotechnol 2012;30:984–90.

[187] Schroll A, Eller K, Feistritzer C, Nairz M, Sonnweber T, Moser PA, et al. Lipocalin-2 ameliorates granulocyte functionality. Eur J Immunol 2012;42:3346–57.

[188] Cheng L, Xing H, Mao X, Li L, Li X, Li Q. Lipocalin-2 promotes M1 macrophages polarization in a mouse cardiac ischaemia-reperfusion injury model. Scand J Immunol 2015;81:31–8.

[189] Zhu H, Cui D, Liu K, Wang L, Huang L, Li J. Long pentraxin PTX3 attenuates ischemia reperfusion injury in a cardiac transplantation model. Transpl Int 2014;27:87–95.

[190] Danieli P, Copes F, Dekker L, Malpasso G, Roccio M, Bassani R, et al. Pentraxin-3 and galectin-1 are key mediators of the cardioprotective paracrine effects exerted by fetal mesenchymal stem cells isolated from human placenta. Eur Heart J 2013;34:P3271.

[191] Coulthard LG, Woodruff TM. Is the Complement Activation Product C3a a Proinflammatory Molecule? Re-evaluating the Evidence and the Myth. J Immunol 2015;194:3542–8.

References

[192] Wu MCL, Brennan FH, Lynch JPL, Mantovani S, Phipps S, Wetsel RA, et al. The receptor for complement component C3a mediates protection from intestinal ischemia-reperfusion injuries by inhibiting neutrophil mobilization. Proc Natl Acad Sci U S A 2013;110:9439–44.

[193] He C, Lee C, DelaCruz CS, Lee CM, Zhou Y, Ahangari F, et al. Chitinase 3-like 1 regulates cellular and tissue responses via IL-13 receptor α2. Cell Rep 2013;4:830–41.

[194] Skrbic B, Engebretsen KVT, Strand ME, Lunde IG, Herum KM, Marstein HS, et al. Lack of collagen VIII reduces fibrosis and promotes early mortality and cardiac dilatation in pressure overload in mice. Cardiovasc Res 2015;106:32–42.

[195] Van Aelst LNL, Voss S, Carai P, Van Leeuwen R, Vanhoutte D, Sanders-Van Wijk S, et al. Osteoglycin prevents cardiac dilatation and dysfunction after myocardial infarction through infarct collagen strengthening. Circ Res 2015;116:425–36.

[196] Fournier ML, Paulson A, Pavelka N, Mosley AL, Gaudenz K, Bradford WD, et al. Delayed correlation of mRNA and protein expression in rapamycin-treated cells and a role for Ggc1 in cellular sensitivity to rapamycin. Mol Cell Proteomics 2010;9:271–84.

[197] Robles MS, Cox J, Mann M. In-Vivo Quantitative Proteomics Reveals a Key Contribution of Post-Transcriptional Mechanisms to the Circadian Regulation of Liver Metabolism. PLoS Genet 2014;10:e1004047.

[198] Lundberg E, Fagerberg L, Klevebring D, Matic I, Geiger T, Cox J, et al. Defining the transcriptome and proteome in three functionally different human cell lines. Mol Syst Biol 2010;6:1–10.

[199] Vogel C, Marcotte EM. Insights into the regulation of protein abundance from proteomic and transcriptomic analyses. Nat Rev Genet 2012;13:227–32.

[200] Greenbaum D, Colangelo C, Gernstein M, Williams K. Comparing protein abundance and mRNA expression levels on a genomic scale. Genome Biol 2003;4:117.

[201] Van Linthout S, Miteva K, Tschöpe C. Crosstalk between fibroblasts and inflammatory cells. Cardiovasc Res 2014;102:258–69.

[202] Deshmane SL, Kremlev S, Amini S, Sawaya BE. Monocyte Chemoattractant Protein-1 (MCP-1): An Overview. J Interf Cytokine Res 2009;29:313–26.

[203] Li Y-H, Chen H, Li Y, Wu S-Y, Wangta-Liu, Lin G, et al. Progranulin regulates zebrafish muscle growth and regeneration through maintaining the pool of myogenic progenitor cells. Sci Rep 2013;3:1176.

[204] Fallach R, Shainberg A, Avlas O, Fainblut M, Chepurko Y, Porat E, et al. Cardiomyocyte Toll-like receptor 4 is involved in heart dysfunction following septic shock or myocardial ischemia. J Mol Cell Cardiol 2010;48:1236–44.

[205] Vilahur G, Badimon L. Ischemia/reperfusion activates myocardial innate immune response: The key role of the toll-like receptor. Front Physiol 2014;5:496–501.

[206] Guijarro-Muñoz I, Compte M, Álvarez-Cienfuegos A, Álvarez-Vallina L, Sanz L. Lipopolysaccharide activates toll-like receptor 4 (TLR4)-mediated NF-κB signaling pathway and proinflammatory response in human pericytes. J Biol Chem 2014;289:2457–68.

[207] Matsunaga N, Tsuchimori N, Matsumoto T, Ii M. TAK-242 (resatorvid), a small-molecule inhibitor of Toll-like receptor (TLR) 4 signaling, binds selectively to TLR4 and interferes with interactions between TLR4 and its adaptor molecules. Mol Pharmacol 2011;79:34–41.

[208] Dewald O, Zymek P, Winkelmann K, Koerting A, Ren G, Abou-Khamis T, et al. CCL2/monocyte chemoattractant protein-1 regulates inflammatory responses critical to healing myocardial infarcts. Circ Res 2005;96:881–9.

[209] Dutta P, Sager HB, Stengel KR, Naxerova K, Courties G, Saez B, et al. Myocardial Infarction Activates CCR2(+) Hematopoietic Stem and Progenitor Cells. Cell Stem Cell 2015;16:477–87.

[210] Schön C. S100A1: Ein neues kardiales Damage-Associated Molecular Pattern. MD thesis, Heidelberg University, Germany, 2015.

[211] Kendall RT, Feghali-Bostwick CA. Fibroblasts in fibrosis: Novel roles and mediators. Front Pharmacol 2014;5 MAY:1–13.

[212] http://amigo.geneontology.org/amigo.

References

[213] Siwik D a, Chang DL, Colucci WS. Interleukin-1beta and tumor necrosis factor-alpha decrease collagen synthesis and increase matrix metalloproteinase activity in cardiac fibroblasts in vitro. Circ Res 2000;86:1259–65.

[214] Ikonen E. Cellular cholesterol trafficking and compartmentalization. Nat Rev Mol Cell Biol 2008;9:125–38.

[215] Fu Y, Dominissini D, Rechavi G, He C. Gene expression regulation mediated through reversible m^6A RNA methylation. Nat Rev Genet 2014;15:293–306.

[216] Schäfer M, Oeing CU, Rohm M, Baysal-Temel E, Lehmann LH, Bauer R, et al. Ataxin-10 is part of a cachexokine cocktail triggering cardiac metabolic dysfunction in cancer cachexia. Mol Metab 2016;5:67–78.

[217] Abonnenc M, Nabeebaccus AA, Mayr U, Barallobre-Barreiro J, Dong X, Cuello F, et al. Extracellular matrix secretion by cardiac fibroblasts: Role of MicroRNA-29b and MicroRNA-30c. Circ Res 2013;113:1138–47.

[218] Oberg AL, Mahoney DW. Statistical methods for quantitative mass spectrometry proteomic experiments with labeling. BMC Bioinformatics 2012;13:S7.

[219] Zhang W, Wei Y, Ignatchenko V, Li L, Sakashita S, Pham NA, et al. Proteomic profiles of human lung adeno and squamous cell carcinoma using super-SILAC and label-free quantification approaches. Proteomics 2014;14:795–803.

[220] Olsen J V, Ong S-E, Mann M. Trypsin Cleaves Exclusively C-terminal to Arginine and Lysine Residues. Mol Cell Proteomics 2004;3:608–14.

[221] Rollins BJ. Chemokines. Blood 1997;90:909–28.

[222] Bardina S V, Michlmayr D, Hoffman KW, Obara CJ, Sum J, Charo IF, et al. Differential Roles of Chemokines CCL2 and CCL7 in Monocytosis and Leukocyte Migration during West Nile Virus Infection. J Immunol 2015;195:4306–18.

[223] Tarzami ST, Calderon TM, Deguzman A, Lopez L, Kitsis RN, Berman JW. MCP-1/CCL2 protects cardiac myocytes from hypoxia-induced apoptosis by a Gai-independent pathway. Biochem Biophys Res Commun 2005;335:1008–16.

[224] Stastna M, Van Eyk JE. Investigating the secretome lessons about the cells that comprise the heart. Circ Cardiovasc Genet 2012;5:8–19.

[225] Arnott C, Punnia-Moorthy G, Tan J, Sadeghipour S, Bursill C, Patel S. The Vascular Endothelial Growth Factor Inhibitors Ranibizumab and Aflibercept Markedly Increase Expression of Atherosclerosis-Associated Inflammatory Mediators on Vascular Endothelial Cells. PLoS One 2016;11:e0150688.

[226] Bigorgne AE, John B, Ebrahimkhani MR, Shimizu-Albergine M, Campbell JS, Crispe IN. TLR4-dependent secretion by hepatic stellate cells of the neutrophil-chemoattractant CXCL1 mediates liver response to gut microbiota. PLoS One 2016;11:1–13.

[227] Van Damme J, Wuyts a, Froyen G, Van Coillie E, Struyf S, Billiau a, et al. Granulocyte chemotactic protein-2 and related CXC chemokines: from gene regulation to receptor usage. J Leukoc Biol 1997;62:563–9.

[228] Fox SE, Lu W, Maheshwari A, Christensen RD, Calhoun DA. The effects and comparative differences of neutrophil specific chemokines on neutrophil chemotaxis of the neonate. Cytokine 2005;29:135–40.

[229] Smith DF, Galkina E, Ley K, Huo Y. GRO family chemokines are specialized for monocyte arrest from flow. Am J Physiol Heart Circ Physiol 2005;289:H1976-84.

[230] Bleul CC, Fuhlbrigge RC, Casasnovas JM, Aiuti a, Springer T a. A highly efficacious lymphocyte chemoattractant, stromal cell-derived factor 1 (SDF-1). J Exp Med 1996;184:1101–9.

[231] Carr MW, Roth SJ, Luther E, Rose SS, Springer T a. Monocyte chemoattractant protein 1 acts as a T-lymphocyte chemoattractant. Proc Natl Acad Sci U S A 1994;91:3652–6.

[232] Roth SJ, Carr MW, Springer TA. C-C chemokines, but not the C-X-C chemokines Il-8 and IP-10, stimulate transendothelial chemotaxis of T lymphocytes. Eur J Immunol 1995;25:3482–8.

[233] Van Hinsbergh VWM, Engelse MA, Quax PHA. Pericellular proteases in angiogenesis and vasculogenesis. Arterioscler Thromb Vasc Biol 2006;26:716–28.

[234] Tazzyman S, Lewis CE, Murdoch C. Neutrophils: Key mediators of tumour angiogenesis. Int J Exp Pathol 2009;90:222–31.

References

[235] Strieter RM, Polverini PJ, Kunkel SL, Arenberg DA, Burdick MD, Kasper J, et al. The functional role of the ELR motif in CXC chemokine-mediated angiogenesis. J Biol Chem 1995;270:27348–57.

[236] Lapidot T, Dar A, Kollet O. How do stem cells nd their way home? Blood 2005;106:1901–10.

[237] Stamatovic SM, Keep RF, Mostarica-Stojkovic M, Andjelkovic A V. CCL2 regulates angiogenesis via activation of Ets-1 transcription factor. J Immunol 2006;177:2651–61.

[238] Bousquenaud M, Schwartz C, Léonard F, Rolland-Turner M, Wagner D, Devaux Y. Monocyte chemotactic protein 3 is a homing factor for circulating angiogenic cells. Cardiovasc Res 2012;94:519–25.

[239] Hu X, Dai S, Wu W-J, Tan W, Zhu X, Mu J, et al. Stromal Cell Derived Factor-1 Confers Protection Against Myocardial Ischemia/Reperfusion Injury: Role of the Cardiac Stromal Cell Derived Factor-1 CXCR4 Axis. Circulation 2007;116:654–63.

[240] Nijmeijer R, Willemsen MJ, Meijer CJ, Visser CA, Verheijen RH, Gottlieb RA, et al. Type II secretory phospholipase A2 binds to ischemic flip-flopped cardiomyocytes and subsequently induces cell death. AmJ Physiol Hear CircPhysiol 2003;285:H2218–24.

10 Appendix

Supplementary table 1: Up- and downregulated proteins from the volcano plot of the secretome from the Figure 15.

In the table are listed proteins with at least 2-fold up- or downregulation.

No.	Gene symbol	Protein name	Fold change [log_2]	p-value [$-log_{10}$]	iBAQ in control [log_{10}]	iBAQ in S100A1 [log_{10}]
1	Lcn2	Lipocalin 2	7.91	1.63	6.66	8.47
2	Chi3l1	Chitinase-3-like protein 1	6.91	1.58	7.35	9.02
3	C3	Complement C3	6.46	2.16	6.58	7.94
4	Ptx3	Pentraxin 3	6.41	1.79	7.42	8.82
5	Cxcl1	C-X-C motif chemokine 1	6.00	1.37	6.41	8.55
6	Clu	Clusterin	5.60	2.35	6.96	8.64
7	Pla2g2a	Phospholipase A2, membrane associated	5.14	4.09	4.89	7.05
8	Ccl7	C-C motif chemokine 7	5.12	1.15	7.62	8.88
9	Ccl2	C-C motif chemokine 2	5.05	1.76	8.12	9.21
10	Cxcl6	C-X-C motif chemokine 6	4.91	2.09	6.48	8.29
11	C1s	Complement C1s	4.81	1.06	6.29	7.45
12	Enpp2	Autotaxin	4.81	1.30	7.09	7.90
13	Mgp	Matrix Gla protein	4.48	1.39	7.28	8.59
14	Igfbp3	Insulin-like growth factor-binding protein 3	4.45	2.01	7.96	8.94
15	Serping1	Plasma protease C1 inhibitor	4.22	1.92	7.97	8.64
16	C1s	Complement C1s subcomponent	3.99	1.37	8.49	8.93
17	Lbp	Lipopolysaccharide-binding protein	3.78	2.26	7.45	8.21
18	Hp	Haptoglobin	3.71	0.82	6.50	8.14
19	Serpina3n	Serine protease inhibitor A3N	3.49	1.45	7.17	7.99
20	Dcn	Decorin	3.43	1.10	8.01	9.01
21	Mmp14	Matrix metalloproteinase-14	2.82	1.08	6.55	7.37
22	Sod2	Manganese-superoxide dismutase	2.80	1.94	7.43	8.08
23	Fst	Follistatin	2.76	0.81	6.31	6.97
24	Atp5b	ATP synthase, subunit beta	2.76	1.43	6.25	6.95
25	Mmp9	Matrix metalloproteinase-9	2.74	1.37	5.30	6.58
26	Tnfrsf11b	Osteoprotegerin	2.67	1.63	6.79	7.40
27	Rarres2	Chemerin	2.67	1.89	7.37	8.30
28	Mmp2	Matrix metalloproteinase-2	2.49	1.68	8.42	8.92
29	Csf1	Macrophage colony-stimulating factor 1	2.45	1.03	6.77	7.40

30	Ltbp1	Latent-transforming growth factor beta-binding protein 1	2.38	0.60	5.57	6.32
31	Lgals3bp	Galectin-3-binding protein	2.31	1.96	7.97	8.39
32	C1r	Complement C1r subcomponent	2.25	2.37	8.57	8.83
33	Cp	Ceruloplasmin	2.18	1.22	6.07	6.58
34	Pla2g7	Phospholipase A2, group VII	2.09	2.48	6.50	7.03
35	Aprt	Adenine phosphoribosyltransferase	2.07	0.92	5.91	6.52
36	Pgk1	Phosphoglycerate kinase 1	2.00	1.13	6.49	6.98
37	Hist1h2bl	Histone H2B	1.97	0.48	7.69	8.00
38	Cfl1	Cofilin-1	1.82	1.91	7.46	7.79
39	Thbs2	Thrombospondin-2	1.78	1.69	7.36	7.72
40	Gda	Guanine deaminase	1.76	1.04	6.50	7.01
41	Mdh2	Malate dehydrogenase	1.76	2.89	7.30	7.80
42	Abi3bp	Protein Abi3bp	1.70	2.20	6.92	7.45
43	Ran	GTP-binding nuclear protein Ran	1.62	0.64	6.27	6.68
44	Mmp11	Stromelysin-3	1.59	1.20	7.24	7.55
45	Sod1	Superoxide dismutase [Cu-Zn]	1.57	1.20	7.38	7.77
46	Epdr1	Mammalian ependymin-related protein 1	1.55	0.51	7.44	7.39
47	Akr1b1	Aldose reductase	1.52	0.68	7.01	7.23
48	Eef1a1	Elongation factor 1-alpha 1	1.52	1.91	7.61	7.92
49	Pdia6	Protein disulfide-isomerase A6	1.49	1.25	6.82	7.15
50	C4	Complement C4	1.48	0.83	6.83	7.06
51	Capg	Macrophage-capping protein	1.47	1.39	6.41	6.77
52	Gstm2	Glutathione S-transferase Mu 2	1.43	1.70	6.17	6.48
53	Ctsh	Pro-cathepsin H	1.43	1.50	7.43	7.73
54	Pdia3	Protein disulfide-isomerase A3	1.40	1.26	7.49	7.77
55	Eno1	Alpha-enolase	1.39	1.28	7.71	8.05
56	Rpl12	60S ribosomal protein L12	1.37	0.89	7.01	7.28
57	H3f3c	Histone H3	1.33	0.43	7.27	7.50
58	Calu	Calumenin	1.33	0.79	7.48	7.64
59	Sdf4	45 kDa calcium-binding protein	1.33	0.99	6.58	7.01
60	Timp1	Metalloproteinase inhibitor 1	1.32	1.18	8.26	8.59
61	Ppib	Peptidyl-prolyl cis-trans isomerase B	1.30	1.15	8.32	8.49
62	Prdx2	Peroxiredoxin-2	1.30	1.56	7.20	7.49
63	Hspa5	78 kDa glucose-regulated protein	1.29	1.30	7.23	7.54
64	Fabp5	Fatty acid-binding protein, epidermal	1.28	0.58	7.06	7.21

65	Ppia	Peptidyl-prolyl cis-trans isomerase A	1.26	1.89	7.94	8.20
66	Cap1	Adenylyl cyclase-associated protein 1	1.21	0.88	6.04	6.38
67	Prelp	Prolargin	1.20	0.61	6.70	6.79
68	Serpinb6	Protein Serpinb6	1.20	2.30	6.44	6.76
69	B2m	Beta-2-microglobulin	1.18	2.78	8.65	8.83
70	Ctsb	Cathepsin B	1.18	2.33	8.39	8.62
71	Gaa	Lysosomal alpha-glucosidase	1.18	1.40	6.31	6.49
72	Eef2	Elongation factor 2	1.17	1.24	6.83	7.04
73	Gdi2	Rab GDP dissociation inhibitor beta	1.15	1.61	7.13	7.36
74	Sdcbp	Syntenin-1	1.14	1.57	7.22	7.50
75	Hsp90aa1	Heat shock protein HSP 90-alpha	1.14	1.09	6.48	6.47
76	Postn	Periostin	1.12	1.73	8.96	9.16
77	Ldha	L-lactate dehydrogenase	1.11	3.30	8.06	8.26
78	Kpnb1	Importin subunit beta-1	1.11	0.82	5.78	6.09
79	Emilin1	Elastin microfibril interfacer 1	1.10	0.89	6.74	7.13
80	Aldoa	Fructose-bisphosphate aldolase A	1.08	1.00	7.79	8.12
81	Got1	Aspartate aminotransferase, cytoplasmic	1.08	0.56	6.35	6.65
82	Btd	Biotinidase	1.06	0.79	6.16	6.32
83	Dpysl2	Dihydropyrimidinase-related protein 2	1.05	1.01	6.11	6.39
84	Actg1	Actin, cytoplasmic 2	1.05	1.60	8.83	9.00
85	Wdr1	WD repeat-containing protein 1	1.04	0.61	6.66	6.76
86	Nme2	Nucleoside diphosphate kinase B	1.02	0.96	8.15	8.32
87	Csrp1	Cysteine and glycine-rich protein 1	1.01	1.00	6.50	6.77
88	Sod3	Extracellular superoxide dismutase [Cu-Zn]	1.01	2.24	8.51	8.70
89	Col3a1	Collagen, type III, alpha 1	-1.01	1.70	8.75	8.27
90	Islr	Immunoglobulin superfamily containing leucine-rich repeat protein	-1.02	2.23	7.57	7.04
91	Loxl3	Lysyl oxidase-like 3	-1.04	1.13	6.18	5.71
92	LOC680322	Histone H2A	-1.12	0.17	7.54	7.80
93	Qsox1	Sulfhydryl oxidase 1	-1.14	0.55	7.21	6.90
94	Gdf6	Growth/differentiation factor 6	-1.15	2.08	6.91	6.40
95	Olfml1	Olfactomedin-like protein 1	-1.19	2.14	7.13	6.54
96	Tgfb3	Transforming growth factor beta-3	-1.22	2.55	7.14	6.69

97	C1qb	Complement C1q subcomponent subunit B	-1.22	0.61	6.98	6.67
98	Tpp1	Tripeptidyl-peptidase 1	-1.23	0.47	7.80	7.56
99	Hspg2	Protein Hspg2	-1.23	1.32	8.36	7.91
100	Vegfc	Vascular endothelial growth factor C	-1.30	2.23	7.02	6.52
101	Ogn	Osteoglycin	-1.45	3.03	8.08	7.39
102	Loxl2	Lysyl oxidase homolog 2	-1.56	1.11	7.33	6.70
103	Gpc6	Protein Gpc6	-1.59	0.96	6.88	6.24
104	Fstl3	Follistatin-related protein 3	-1.72	0.59	7.12	6.50
105	Clec3b	C-type lectin domain family 3, member B	-1.80	2.20	8.22	7.49
106	Col8a1	Collagen, type VIII, alpha 1	-1.94	2.32	7.79	7.26
107	Eln	Elastin	-2.42	1.00	8.29	7.18

Supplementary table 2: 1D annotation enrichment analysis of the ratios of proteins [log_2] from the secretome (see section 6.2.3 Biological Functions of Secretome).

Size- the number of proteins, forming the particular category; position score- the center of iBAQ value distribution of the particular category relative to the distribution of all iBAQ values; adjusted p-value- p-value for the enrichment of category with Benjamini-Hochberg FDR 2%; mean- mean of the fold-changes of proteins from the particular category; median- median of the fold-changes of proteins from the particular category.

Category	Size	Score	Adjusted p-value	Mean	Median
Collagen	15	-0.70	4.65E-06	-0.59	-0.49
Extracellular matrix part	52	-0.49	4.97E-06	-0.17	-0.32
Cytokine	14	0.62	0.00296	2.77	2.56
G-protein-coupled receptor binding	11	0.71	0.00652	3.32	3.02
Chemokine activity	8	0.88	0.01437	3.62	3.37
Chemokine receptor binding	8	0.88	0.00718	3.62	3.37
Chemotaxis	10	0.92	4.70E-05	4.29	4.86

Supplementary table 3: Proteins from the upregulated categories according to the 1D annotation enrichment analysis of median ratios of proteins [log_2] from secretome.

Gene symbol	Fold change [log_2]	Category				
		Chemotaxis	Chemokine receptor binding	Chemokine activity	G-protein-coupled receptor binding	Cytokine
C3	6.46	x			x	
Calm1	0.57				x	
Ccl2	5.05	x	x	x	x	x
Ccl3	3.73	x	x	x	x	x
Ccl7	5.12	x				x
Csf1	2.45					x
Cx3cl1	1.67	x	x	x	x	x
Cxcl1	6.00	x	x	x	x	x
Cxcl12	2.41		x	x	x	
Cxcl3	2.16	x	x	x	x	x
Cxcl6	4.91	x	x	x	x	x
Enpp2	4.81	x				
Flna	0.56				x	
Gdf6	-1.15					x
Gpi	0.78					x
Grn	0.01					x
Pf4	3.02	x	x	x	x	x
Spp1	2.35					x
Tnfrsf11b	2.67					x

Supplementary table 4: Proteins from downregulated categories according to the 1D annotation enrichment analysis of median ratios of proteins [log_2] from secretome.

Gene symbol	Fold change [log_2]	Category	
		Collagen	Extracellular matrix part
Col11a1	-0.68	x	x
Col12a1	-0.17	x	
Col14a1	-0.09	x	
Col15a1	-0.54	x	x
Col1a1	-0.93	x	x
Col1a2	-0.98	x	x
Col3a1	-1.01	x	x
Col4a1	-0.24	x	x
Col4a2	-0.35	x	x
Col5a1	-0.83	x	x
Col5a2	-0.49	x	x
Col6a1	-0.08	x	
Col6a2	-0.13	x	x
Col6a3	-0.36	x	
Col8a1	-1.94	x	x
Agrn	0.11		x
Ang	0.34		x
Anxa2	0.07		x
Bmp1	-0.73		x
C1qa	-1.10		x
C1qb	-1.22		x
C1qc	-0.54		x
C1qtnf5	-0.26		x
Ccdc80	0.03		x

Cst3	0.10	x
Dag1	-0.54	x
Dcn	3.43	x
Eln	-2.42	x
Emilin1	1.10	x
Fbln1	0.39	x
Fbln5	-0.58	x
Fbn1	-0.42	x
Fn1	-0.02	x
Hspg2	-1.23	x
Itgb1	0.05	x
Lama2	-0.39	x
Lama4	0.10	x
Lama5	-0.71	x
Lamb1	0.04	x
Lamb2	0.11	x
Lamc1	-0.02	x
Lox	0.74	x
Loxl1	-0.47	x
Loxl2	-1.56	x
Ltbp1	2.38	x
Lum	0.72	x
Mfap5	-0.42	x
Nid1	-0.29	x
Nid2	0.31	x
Plod1	0.24	x
Serpinf1	-0.39	x
Sparc	-0.88	x
Tgfb2	-0.66	x
Thbs2	1.78	x
Timp1	1.32	x
Timp2	-0.02	x

Supplementary table 5: Top 15 of the most enriched categories according to the Fisher's exact test of proteins with more than 4-fold upregulation from secretome.

Total size- the number of all proteins; selection size- the number of proteins with at least 4-fold upregulation; category size- the number of all proteins, which form the particular category; intersection size- the number of proteins with at least 4-fold upregulation from the particular category; enrichment factor- the size of the group of at least 4-fold upregulated proteins from the particular category, normalized with the count of all proteins from the same category; adjusted p-value- p-value for the enrichment of category with Benjamini-Hochberg FDR 2%.

Category	Total size	Selection size	Category size	Intersection size	Enrichment factor	Adjusted p-value
Chemokine-mediated signaling pathway	380	52	6	6	7.31	0.00061
Chemotaxis	380	52	10	9	6.58	4.39E-05
Chemokine activity	380	52	8	7	6.39	0.00198
Chemokine receptor binding	380	52	8	7	6.39	0.00149
Cytokine	380	52	14	10	5.22	8.87E-05
G-protein-coupled receptor binding	380	52	12	8	4.87	0.00609
Cell chemotaxis	380	52	15	10	4.87	0.00038
Positive regulation of leukocyte chemotaxis	380	52	17	11	4.73	0.00024
Positive regulation of leukocyte migration	380	52	19	12	4.62	0.00012
Response to lipopolysaccharide	380	52	23	14	4.45	3.27E-05
Inflammatory response	380	52	25	15	4.38	2.08E-05
Response to molecule of bacterial origin	380	52	25	14	4.09	8.89E-05
Immune response	380	52	32	16	3.65	8.92E-05
Defense response	380	52	41	20	3.56	1.68E-05
Positive regulation of immune system process	380	52	37	18	3.56	3.51E-05

Supplementary table 6: 1D annotation enrichment analysis, calculated from absolute amounts of proteins, expressed in iBAQ values [log_{10}], in secretome of control and S100A1-treated samples.

Size- the number of proteins, which form the particular category; position score- the center of iBAQ value distribution of the particular category relative to the distribution of all iBAQ values; adjusted p-value- p-value for the enrichment of category with Benjamini-Hochberg FDR 2%; mean- the mean of the iBAQ values of proteins from the particular category; median- the median of the iBAQ values of proteins from the particular category.

Control

Category	Size	Score	Adjusted p-value	Mean	Median
Collagen	15	0.57	0.00019	7.94	7.99

S100A1

Category	Size	Score	Adjusted p-value	Mean	Median
Immune response	30	0.53	1.77E-06	7.95	8.03
Chemoattractant	10	0.65	0.00047	8.13	7.92

Supplementary table 7: 2-fold up- or downregulated genes upon stimulation with S100A1 from the transcriptome analysis after 48 hours.

Gene symbol	Fold change [log_2]	Gene symbol	Fold change [log_2]	Gene symbol	Fold change [log_2]
Cxcl6	8.15	Serping1	2.58	Flrt2	2.03
Enpp2	7.71	Duox1	2.58	Ecscr	2.03
Pla2g2a	6.94	Chrm2	2.57	Pdgfra	2.03
Lcn2	6.79	Ccl7	2.55	Slc43a3	2.02
Chi3l1	5.82	Enpep	2.54	Plek	2.02
Cfb	5.71	Cxcl2	2.54	Rnd1	2.02
Sfrp2	5.33	Thbs2	2.53	Cyp7b1	2.00
Slpi	4.92	LOC685067	2.52	C1s	1.99
C3	4.90	Irg1	2.50	Il1rn	1.99
Mmp9	4.83	Bst1	2.49	Il2rg	1.99
Cxcl1	4.77	Isyna1	2.48	Dcn	1.98
Vcam1	4.39	Tnip3	2.47	Mgst2	1.98
Naaa	4.31	C4b	2.46	Ccl9	1.98
Ccl3	4.23	Ch25h	2.46	Cldn15	1.97
Hp	4.18	Cxadr	2.45	Cx3cl1	1.97
Clu	4.13	Parm1	2.43	Socs3	1.97
Sod2	4.06	Trem1	2.41	Slamf6	1.97
Nos2	3.71	Tnip1	2.38	Cd302	1.96
Lrrn4	3.67	Acvr1b	2.36	Adora2a	1.96
Il1b	3.52	Galnt14	2.35	Htr2a	1.95
Selp	3.48	Tlr2	2.35	Lcp1	1.95
Ccl12	3.42	RGD1560281	2.35	Slc6a12	1.94
Emr1	3.38	Serpina3n	2.35	Aldh1a2	1.94
Igfbp3	3.36	Ugcg	2.35	Kif26b	1.93
Opn3	3.26	Grem2	2.34	Csf2rb	1.93
Rac2	3.22	Steap4	2.34	Tnfaip3	1.93
Lbp	3.22	Fgl2	2.34	Ncf1	1.92
Siglec5	3.16	Ntn1	2.32	Usp53	1.92
Ptx3	3.15	Slamf9	2.31	Irak3	1.92
Tlr1	3.13	Tmem176a	2.30	Slc39a14	1.92
Arpc1b	3.07	Fcgr1a	2.29	Gpr88	1.91
Mt1m	3.04	Jak2	2.29	Lrba	1.91
Cxcl12	3.03	Adamts9	2.26	Sulf1	1.90
Il1a	2.99	Usp18	2.24	Duoxa1	1.90
Spp1	2.98	Birc3	2.24	Slc1a3	1.90
Tmem178a	2.96	Agtr1a	2.21	Siglec8	1.90
Lgals9	2.90	Ptpn6	2.20	LOC103693629	1.89
Mme	2.88	Fyb	2.20	Tgfbr3	1.88
Ccl20	2.88	Rgs16	2.19	Slc13a3	1.88
Itgal	2.87	Cilp	2.16	Tmem176b	1.88
Ccl4	2.85	C6	2.15	Fcgr2b	1.87
Prkcb	2.85	C5ar1	2.14	LOC24906	1.87
LOC500066	2.85	Cd180	2.13	Sdc4	1.86
Fmod	2.82	Pstpip2	2.11	Msln	1.86
Il6	2.82	Upp1	2.10	Hsd11b1	1.85
Pik3cg	2.79	Cpxm1	2.09	Adm	1.85
Slc11a1	2.78	Ebi3	2.09	Gsap	1.84
Evi2b	2.78	Sema6d	2.08	Grem1	1.83
Lifr	2.76	Serpinb2	2.08	Abcb1b	1.83
Rasl12	2.75	Ntm	2.07	Srgn	1.83
Pla2g7	2.69	Steap2	2.07	Nfkbia	1.82
Itgb2	2.63	Efna5	2.06	St3gal6	1.81
Rasgef1b	2.62	Nfkbiz	2.04	Pik3r5	1.81
St6galnac2	2.60	Plbd1	2.04	RGD1561730	1.81

Appendix

Ctsh	1.81	Ppap2a	1.52	Selplg	1.34
Cxcl16	1.80	Dpep1	1.52	Plscr1	1.34
Angptl4	1.80	Mmd	1.51	Evi2a	1.33
Cd200	1.79	Mycbp2	1.51	Stard10	1.33
Apoe	1.77	Lrrc25	1.50	Serpinb9	1.33
Hs6st1	1.77	Steap1	1.50	Lpar1	1.33
Cdon	1.77	Cdhr4	1.49	Sox4	1.33
Il18	1.76	Bcl3	1.49	Cdc42ep5	1.33
Enpp3	1.76	Gas1	1.48	Star	1.33
Arhgdib	1.75	LOC681325	1.48	Mmp11	1.32
Glul	1.75	Slfn2	1.46	Tnfrsf14	1.32
Ncf4	1.74	Pim1	1.46	Nr1h4	1.32
Npr3	1.74	Pla2g5	1.46	Il33	1.31
Slco4a1	1.71	Cebpd	1.45	LOC100362819	1.31
Fam169b	1.70	Elf5	1.45	Ank3	1.31
Hpx	1.70	Gda	1.45	Ptk2b	1.31
LOC681383	1.70	Spn	1.45	Aqp1	1.31
Nrp2	1.70	NEWGENE_1565505	1.45	Ampd3	1.30
Coro1a	1.69	Optc	1.44	Osmr	1.30
Sh2b2	1.69	C1r	1.43	Sema5a	1.30
Ginm1	1.68	Fbxl5	1.43	Rasgrp3	1.30
Pik3ap1	1.68	Cacna2d3	1.43	Rasgrp1	1.29
Angpt1	1.68	Niacr1	1.43	Tnfrsf1b	1.29
Ccl2	1.68	Pde7b	1.42	MGC112715	1.29
Kcnj8	1.67	Phyhipl	1.42	Tshz2	1.28
Tpbg	1.67	Nabp1	1.42	Itgam	1.28
Serinc2	1.66	Icam1	1.42	Fbxo32	1.28
Chml	1.66	Mzt2b	1.41	C2	1.28
Ltbp1	1.65	Hcls1	1.41	Fmo1	1.27
Xdh	1.65	Pkhd1l1	1.40	Plscr2	1.26
Slc16a2	1.65	Fcer1g	1.40	Scimp	1.26
Gxylt2	1.64	Tfpi2	1.40	LOC678893	1.26
Epas1	1.64	Sorcs1	1.40	Tank	1.26
Zfand5	1.63	Gpr126	1.39	Adamts7	1.26
Aldoc	1.63	Ddhd2	1.39	LOC102546902	1.25
Hck	1.63	Cyth4	1.39	Prokr2	1.25
Bmp3	1.63	Cd24	1.38	C3ar1	1.25
Fgr	1.62	Pnrc1	1.38	Ugt1a6	1.24
Ifitm1	1.62	Ccl6	1.38	Relt	1.24
Ugdh	1.61	Hmox1	1.38	Klf5	1.23
Clec4d	1.61	Sdk1	1.38	Ifitm2	1.23
Cd274	1.61	Alox5	1.38	Fth1	1.23
Tnfaip6	1.61	Mgst1	1.37	Ackr3	1.22
Fxyd2	1.61	Cd4	1.37	Tagap	1.22
St3gal1	1.59	Ptprk	1.37	Chrdl1	1.22
Dapk1	1.59	Aif1	1.36	Bcl6	1.22
Emilin1	1.58	LOC100360218	1.36	St5	1.21
Bnc2	1.57	Peli1	1.36	Man1a1	1.21
Cd72	1.57	Arhgap24	1.36	Akr1b8	1.21
Il10	1.56	Slc11a2	1.35	Gja1	1.21
F3	1.56	Vstm4	1.35	Cd55	1.20
Slamf8	1.56	C7	1.35	RGD1561113	1.20
Ednrb	1.56	Spi1	1.35	Zfp36l1	1.20
Sh3kbp1	1.56	Col18a1	1.35	Scara5	1.19
Slc15a3	1.55	Cybb	1.35	Tyrobp	1.19
Il1rl1	1.54	Adora2b	1.35	Abca1	1.19
Atp8b4	1.54	Hpgds	1.34	Rftn1	1.19
Zc3h12a	1.54	Nckap1l	1.34	Mmp2	1.19
Mmrn1	1.53	Bag4	1.34	Gnai1	1.18

Cables1	1.18	Slc5a3	1.09	Psip1	-1.01
Tbxas1	1.18	Csf2ra	1.09	Olfml2b	-1.01
Ccl19	1.18	Cxcl13	1.09	Cxcr4	-1.01
Fosl2	1.18	LOC103693634	1.08	Dmpk	-1.01
Rbks	1.18	Ifi47	1.08	Creb3l1	-1.01
Nfkbie	1.18	Ebf3	1.08	Zfp64	-1.01
Phactr2	1.17	Rcan1	1.08	Racgap1	-1.01
Arhgap26	1.17	Laptm5	1.08	Reps2	-1.01
Nlrp3	1.17	Egfr	1.07	Klra1	-1.02
Tnfsf15	1.17	Oasl	1.07	Tns1	-1.02
Fam131b	1.17	Vav1	1.07	Ecm1	-1.02
Hgf	1.17	Fst	1.07	Itm2a	-1.02
Fbln1	1.17	Cyba	1.07	Ptpla	-1.02
Ifngr1	1.17	Nhs	1.06	Afap1	-1.02
Galk2	1.16	Nfkb2	1.06	Pkia	-1.02
Fam213b	1.16	Prg4	1.06	Sh3pxd2a	-1.02
Cygb	1.16	Tlr7	1.06	LOC100359633	-1.03
Slc44a1	1.16	Prr16	1.06	Mmp16	-1.03
Lnx1	1.16	Apobec1	1.06	Gars	-1.03
Sqrdl	1.15	Gpr146	1.05	Crispld2	-1.03
Lst1	1.15	Dgkh	1.05	Nfxl1	-1.03
Prelp	1.15	Tmcc3	1.05	Tnfrsf10b	-1.03
P4ha3	1.15	Fgd6	1.05	Plxnc1	-1.03
Tmem2	1.15	Naprt1	1.05	LOC103694412	-1.04
Adamts3	1.15	P2rx4	1.05	Arhgef2	-1.04
Il6st	1.15	C1rl	1.05	Gdf15	-1.04
Ptgir	1.15	Rarres2	1.04	Pdlim3	-1.04
Egln3	1.15	Rbp1	1.04	Zeb1	-1.04
Slfn3	1.15	Tlr8	1.04	LOC100365921	-1.04
Btg2	1.15	Hpse	1.03	Htr1f	-1.04
Ptpn1	1.14	Timp1	1.03	Plekhb1	-1.04
Hsph1	1.14	LOC314492	1.03	Sgol1	-1.04
Clec14a	1.14	Tifa	1.03	Plxna4a	-1.05
Itgb8	1.14	Ptgs2	1.03	Bub1	-1.05
LOC301748	1.14	Oplah	1.02	Vcpkmt	-1.05
Ucp2	1.13	Cd53	1.02	Etv5	-1.05
Pde4b	1.13	Wt1	1.02	Rnf144a	-1.05
Relb	1.13	Lsm1	1.02	Ldb2	-1.05
Sbno2	1.13	Acvrl1	1.02	Ckap2l	-1.05
Pcsk5	1.13	Lcp2	1.02	Mtfr1	-1.06
Htra4	1.12	Map4k3	1.02	Otub2	-1.06
Plcxd3	1.12	Abcc9	1.02	Hist1h2bl	-1.06
Sept6	1.12	March3	1.01	Il1rap	-1.06
Svep1	1.12	Amigo2	1.01	Plk1	-1.06
Art4	1.11	Crebrf	1.01	Casp12	-1.06
Fam43a	1.11	Olfml3	1.01	Slc3a2	-1.07
LOC102555109	1.11	Aebp1	1.00	Lmod1	-1.07
Ksr1	1.11	Cdh2	1.00	Hist1h2ai	-1.07
Cd244	1.11	Aldh1l2	-1.00	Pde7a	-1.07
Ccl24	1.10	Ehd2	-1.00	NEWGENE_6497336	-1.07
Scin	1.10	Cstf2	-1.00	Lmna	-1.07
Tlr6	1.10	LOC100361180	-1.00	Lama5	-1.07
Rcl1	1.10	Pxdc1	-1.00	Hist1h2ah	-1.08
Pld5	1.10	Hspb6	-1.00	Dusp8	-1.08
Csf1	1.10	LOC366763	-1.00	Uap1l2	-1.08
Gramd4	1.10	Kif2c	-1.00	Tfec	-1.08
Dtnb	1.09	Asb12	-1.01	Syt17	-1.08
Tgm1	1.09	Plat	-1.01	Eps15	-1.08
Ifitm3	1.09	Mpeg1	-1.01	LOC103690838	-1.09

Klf2	-1.09	Slc40a1	-1.22	Kcnv2	-1.42
Hist1h2ac	-1.09	Igfbp6	-1.23	Cenpf	-1.42
Zfp385d	-1.09	Epyc	-1.23	Slc6a9	-1.42
Ccnb1	-1.09	Mical2	-1.24	Hist1h2bf	-1.42
Snrpd2	-1.10	Herpud1	-1.24	Cars	-1.43
Shcbp1	-1.10	Kif23	-1.24	Ackr4	-1.43
Pqlc3	-1.10	Tnc	-1.24	Fbxl7	-1.43
Matn2	-1.10	Pragmin	-1.24	Lyrm1	-1.43
Me1	-1.10	Lars	-1.24	Sphkap	-1.43
Sdc2	-1.10	Unc5b	-1.24	Slc7a3	-1.44
Mthfd1l	-1.11	Trabd2b	-1.25	Shmt2	-1.44
Mars	-1.11	LOC102556004	-1.25	Nrk	-1.44
Hist1h2bcl1	-1.11	Inhba	-1.25	Slc8a1	-1.45
Mir421	-1.11	LOC691984	-1.25	Mrpl42	-1.45
Col4a5	-1.12	Napb	-1.25	LOC103690963	-1.45
Pxdn	-1.12	Xpot	-1.26	Ndc80	-1.46
Aspm	-1.13	Cdh3	-1.26	Cdkl5	-1.46
Zfp469	-1.13	Casc5	-1.26	Dbndd2	-1.47
Lrrc17	-1.14	Ap1s3	-1.27	Mmp28	-1.47
Pdia5	-1.14	Tmeff2	-1.27	Ncam1	-1.48
Mybl1	-1.14	Fndc1	-1.27	Fbln2	-1.48
Pde1a	-1.14	Hmmr	-1.27	Ssbp2	-1.48
Tubb3	-1.14	St8sia2	-1.27	Ddit3	-1.48
Oaf	-1.15	Sesn3	-1.27	LOC103693330	-1.49
Nuf2	-1.15	Psg19	-1.27	Wars	-1.50
RGD1566307	-1.15	Ttk	-1.28	Capn6	-1.51
Ncapg	-1.15	Aars	-1.28	Creb5	-1.51
Kif11	-1.16	Ccdc141	-1.28	Col11a1	-1.52
Cenpn	-1.16	Itga6	-1.28	LOC102554096	-1.52
Ccdc6	-1.16	S100a10	-1.29	Diaph3	-1.52
Nexn	-1.16	LOC100361756	-1.29	Crlf1	-1.52
Pdgfrl	-1.16	Dnajb4	-1.29	Pmepa1	-1.53
Uchl1	-1.17	Mid2	-1.30	Pck2	-1.53
Col3a1	-1.17	Itgb5	-1.30	Ppp1r14a	-1.53
Ccnd2	-1.17	Zmynd19	-1.31	Adamtsl2	-1.54
Plac9	-1.17	Mki67	-1.31	Tfrc	-1.55
Col5a3	-1.17	Hist2h2ab	-1.31	Sipa1l2	-1.55
LOC100360754	-1.18	Nars	-1.31	Stxbp6	-1.56
Eprs	-1.18	Hey2	-1.32	LOC100911253	-1.56
Tubb6	-1.19	Top2a	-1.32	Ppp1r14c	-1.57
Ncaph	-1.19	Ect2	-1.32	Mmp12	-1.58
C1qc	-1.19	Pcdh18	-1.32	Prune2	-1.59
Gata3	-1.19	Cenpe	-1.33	Psph	-1.61
Ccna2	-1.20	Gpr34	-1.33	Pdlim7	-1.61
Arhgap6	-1.20	Bcat1	-1.33	Sdpr	-1.61
Plau	-1.20	Peg10	-1.34	Esco2	-1.62
Fam107b	-1.20	Sesn2	-1.35	Dmd	-1.62
Slc1a4	-1.21	Gpr64	-1.35	Cd74	-1.64
Ifi27l2b	-1.21	Olr1	-1.36	Dysf	-1.65
Cap2	-1.21	Tsc22d3	-1.36	LOC103690836	-1.66
Adam19	-1.21	Igfbp5	-1.37	Nrep	-1.68
Atp2b4	-1.21	Rgs17	-1.38	Rgs4	-1.70
Kif2a	-1.22	Pycr1	-1.39	Aldh1a1	-1.70
Hadhb	-1.22	Depdc1	-1.40	Tubb2a	-1.72
Prrg4	-1.22	Jam2	-1.40	Notch3	-1.73
Sema3d	-1.22	Cth	-1.41	Aoc3	-1.74
LOC499229	-1.22	Bambi	-1.41	Casp4	-1.75
Daam1	-1.22	Anln	-1.41	Jun	-1.75
Rhob	-1.22	LOC103692529	-1.41	Mrgprf	-1.76

Gucy1b3	-1.76
Slc7a1	-1.77
Enpp1	-1.78
Zdhhc2	-1.78
Itgb3	-1.78
Timp3	-1.80
RT1-Da	-1.81
Prss35	-1.81
Cntnap2	-1.81
Adarb1	-1.82
Cthrc1	-1.84
Olr63	-1.85
LOC103690839	-1.86
Plxdc2	-1.87
Mthfd2	-1.88
Asns	-1.88
Loxl2	-1.89
Cnn1	-1.95
Cx3cr1	-1.95
Galnt18	-1.96
Fras1	-1.98
Chac1	-1.99
Fam129a	-2.01
LOC102546963	-2.02
Slc7a5	-2.03
Atf5	-2.09
Ms4a4a	-2.10
LOC103690837	-2.12
Psat1	-2.15
Sox9	-2.17
Itga11	-2.18
Itga4	-2.18
Tgfb3	-2.28
Col6a3	-2.40
Cmklr1	-2.42
Piezo2	-2.45
Serpine2	-2.50
Trib3	-2.57
C1qb	-2.64
Mcam	-2.74
Gucy1a3	-3.00
Eln	-4.08

11 Acknowledgment

I would like to express my gratitude to all of those, whose support and guidance ensured the fulfillment of my thesis project.

First of all, I am grateful to Prof. Dr. Patrick Most for his readiness to take the risk and let me pursue my doctoral thesis in his lab, even though I did not have any previous experience in experimental biology.

I would like to thank my advisor Dr. David Rohde for many discussions and agreements, which finally formed the experimental basis of my thesis. They allowed me to tell a truly fascinating story. I am very grateful for his support during the thesis writing process. I trusted his clear and concise judgements on the weak points and suggestions of possible solutions.

PhD studies are guided also by the thesis advisory committee. I would like to express my deepest gratitude to Prof. Dr. Gudrun Rappold and Prof. Dr. David Hassel for their support and advices on both scientific and organizational matters.

I thank Prof. Dr. Marc Freichel and Dr. Mirko Völkers for agreeing to participate in my examination committee.

The credit for guiding me into the lab life and throughout the labyrinths of establishing experimental settings goes to Dr. Christoph Schön, Nicole Herzog and Dr. Kleopatra Rapti. I thank Nicole for the introduction with all general lab techniques and Christoph for always finding the time to help me with the specific problems of my project. I wish every beginner in the molecular biology had a teacher like Dr. Kleopatra Rapti. Kleo taught me the freedom of experimenting, finding solutions and accepting mistakes as inevitable and even necessary companions in the process of the establishment of new experimental models.

I would like to thank our collaborators Dr. Melanie Börries and Prof. Dr. Hauke Busch for my good-looking transcriptome section. Their invaluable input in data processing and visualization helped me to reveal one of the key facts of my dissertation.

My thesis wouldn’t be possible without Dr. Thomas Ruppert and Dr. Bernd Heßling. I thank Dr. Ruppert for his guidance through the establishment of the secretome experiment. I truly enjoyed and appreciated the work or, more precise, learning process together with Dr. Heßling. If there is any question related to mass spectrometry data processing or statistics, Bernd will clarify it better than Google. His advices and tutoring on how to better present data allowed me to tell the secretome part of my thesis story.

Acknowledgement

As a very important part of my thesis project I consider my really educational time in between experiments. Priceless input in my German knowledge was given by Jasmin Hoffmann, Anne Marie Volkert, Jasmin Köhler and during my final months also Andrea Schneider. Moreover, they always explained to me how and why things in Germany function like they do, and, more important, how Germans function and what they mean by saying something. Among the people who have enriched my education besides direct experimental work, I want to name also Dr. Mauro Siragusa. I enjoyed those conversations about the structure of science and shared experience in living and working abroad. A special thanks goes to Tamara Kantzos-Marinkovic, who magically ensured that all administrative issues were solved unnoticeably.

A very special contribution to my thesis project has been given by Dr. Henrike Tscheschner and Dr. to be Nuttarak Sasipong, also known as Pete. Their constant support and more or less discreet push forced me to pull myself together and stop whining and start doing.

The whole journey of doing my doctorate was possible thanks to two organizations. I thank DAAD that trusted me and awarded with a stipend for 3 years and HBIGS for outstanding training program and especially Dr. Rolf Lutz for excellent support on various organizational issues.

Finally, I owe my deepest thanks to Juris, who has stood by my side from the very first crazy idea of PhD. His support through all my science crises and practical advises have made my thesis possible. I believed and followed his “you can do it!” even when there was no rational reason to think like this.